This dissertation has been
microfilmed exactly as received 68-14,194

TSAI, Yih-Wan, 1940-
RADIATIVE TRANSPORT PROPERTIES OF FLAMES.

The University of Oklahoma, Ph.D., 1968
Engineering, mechanical

University Microfilms, Inc., Ann Arbor, Michigan

Downloaded from SHAREOK. Persistent Handle URL: https://hdl.handle.net/11244/2380

THE UNIVERSITY OF OKLAHOMA

GRADUATE COLLEGE

RADIATIVE TRANSPORT PROPERTIES OF FLAMES

A DISSERTATION

SUBMITTED TO THE GRADUATE FACULTY

in partial fulfillment of the requirements for the

degree of

DOCTOR OF PHILOSOPHY

BY

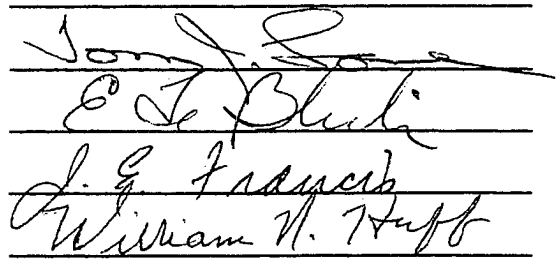
YIH-WAN TSAI

Norman, Oklahoma

1968

RADIATIVE TRANSPORT PROPERTIES OF FLAMES

APPROVED BY



DISSERTATION COMMITTEE

ABSTRACT

The aim of this work is to provide a method to predict the total heat flux from a flame which has specific size and geometry. The transport equation was used to determine the volume emission coefficient, J_λ, and the volume extinction coefficient, β_λ, based on the laboratory measurements. J_λ and β_λ were obtained on the assumption that average values could be used, and the average values were measured by viewing the outer cone of the flame. A new and improved technique was used in which the flame size was varied during the experiments. Data for methanol, natural gas, acetone, n-hexane, cyclohexane, and benzene were provided.

Total heat fluxes from large fires predicted by using the J_λ and β_λ values from small laminar flames were compared to radiometer readings. Atmospheric absorption and the transmittance of the quartz window of the radiometer were taken into consideration in the total predicted heat flux integration. The measured and calculated heat fluxes showed good agreement.

ACKNOWLEDGMENTS

The author wishes to express his sincere appreciation to Dr. T. J. Love, Jr. for his guidance, patience, constant supply of personal library materials, and assistance in various ways.

The appreciation is also extended to Dr. J. E. Francis, for many helpful discussions and to the other members of the author's graduate committee, Dr. E. F. Blick and Dr. W. N. Huff.

A special thanks is given to Dr. J. R. Welker for the helpful discussions and assistance in preparing the manuscript. Mr. D. B. Pfenning's help is also appreciated.

In addition, the author would like to extend his gratitude to the many graduate students and friends, for their assistance in various ways and to Mrs. Joyce Meyer, for typing the manuscript.

The financial support furnished by the U.S. Army Physical Research Laboratory at Edgewood Arsenal is gratefully acknowledged.

TABLE OF CONTENTS

		Page
LIST OF TABLES		vi
LIST OF FIGURES		vii
Chapter		
I.	INTRODUCTION	1
II.	EQUIPMENT AND PROCEDURE Equipment Calibration Procedure	10
III.	ATMOSPHERIC ABSORPTION	29
IV.	ANALYSIS OF DATA	37
V.	CONCLUSIONS	75
NOMENCLATURE		78
BIBLIOGRAPHY		80
APPENDICES		
A.	RADIATIVE TRANSPORT PROPERTIES OF METHANOL, NATURAL GAS, ACETONE, N-HEXANE, CYCLOHEXANE AND BENZENE FLAMES	85
B.	MONOCHROMATIC TRANSMITTANCE OF QUARTZ	111
C.	COMPUTER PROGRAMS FOR THE CALCULATION OF RADIATIVE TRANSPORT PROPERTIES AND TOTAL FLUX INTEGRATION FROM A CYLINDRICAL FLAME	113

LIST OF TABLES

Table		Page
1.	Wavelength Versus Spectral Slit Width.	14
2.	Drum Setting Versus Wavelength	21
3.	Monochromatic Transmittance in the Atmosphere (91.5 cm separation from source to monochromator).	34
4.	Monochromatic Transmittance in the Atmosphere (300 cm separation from flame to target) . .	36
5.	Transport Properties of Methanol Flame.	86
6.	Transport Properties of Natural Gas Flame. . .	88
7.	Transport Properties of Acetone Flame.	91
8.	Transport Properties of N-Hexane Flame	99
9.	Transport Properties of Cyclohexane Flame. . .	103
10.	Transport Properties of Benzene Flame.	107
11.	Monochromatic Transmittance of Quartz.	112

LIST OF FIGURES

Figure		Page
1.	Boundary Conditions for Flame.	7
2.	Graph of $f(\beta_\lambda)$	9
3.	Monochromator Internal Optics.	11
4.	External Optical System.	15
5.	Schematic Diagram of the Heating System. . . .	17
6.	Schematic Diagram of Precipitator.	19
7.	Acetone Flames	27
8.	Spectrograph of Acetone Flame.	28
9.	Sketch of Globar Spectrograph over 2.7μ and 4.3μ Absorption Bands	32
10.	Monochromatic Volume Emission Coefficient of Methanol Flame.	39
11.	Monochromatic Volume Extinction Coefficient of Methanol Flame.	40
12.	Monochromatic Volume Emission Coefficient of Natural Gas	42
13.	Monochromatic Volume Extinction Coefficient of Natural Gas	43
14.	Monochromatic Volume Emission Coefficient of Acetone Flame	44
15.	Monochromatic Volume Extinction Coefficient of Acetone Flame	45

Figure Page

16. Monochromatic Volume Emission Coefficient of N-Hexane Flame. 46

17. Monochromatic Volume Extinction Coefficient of N-Hexane Flame 47

18. Monochromatic Volume Emission Coefficient of Cyclohexane Flame 48

19. Monochromatic Volume Extinction Coefficient of Cyclohexane Flame 49

20. Monochromatic Volume Emission Coefficient of Benzene Flame 50

21. Monochromatic Volume Extinction Coefficient of Benzene Flame. 51

22. J_λ/β_λ of Methanol Flame. 52

23. J_λ/β_λ of Natural Gas 53

24. J_λ/β_λ of Acetone Flame 54

25. J_λ/β_λ of N-Hexane Flame. 55

26. J_λ/β_λ of Cyclohexane Flame 56

27. J_λ/β_λ of Benzene Flame 57

28. Acetone, Methanol, and Acetone-Methanol Flames. 59

29. Flame Extrapolation. 60

30. Geometry for Cylindrical Flame 63

31. Schematic Diagram of Flame Merging Table . . . 66

32. Comparison of Flux for a Merged Acetone Flame 68

33. Comparison of Flux for a Merged Acetone Flame 69

34. Comparison of Flux for a Merged Acetone Flame 70

Figure Page

35. Comparison of Flux for a Merged N-Hexane Flame 71

36. Comparison of Flux for a Merged N-Hexane Flame 72

37. Comparison of Flux for a Merged N-Hexane Flame 73

38. Comparison of Flux for a Merged Cyclohexane Flame 74

RADIATIVE TRANSPORT PROPERTIES OF FLAMES

CHAPTER I

INTRODUCTION

Fires and fire behavior have been the object of research for hundreds of years. Greek philosopher Heraclitus (500 B.C.) postulated that flame was one of the fundamental substances. This probably is the first scientific thinking about fires. This idea was generally accepted until the Renaissance, when Francis Bacon (1600) took an important step in the study of fire by studing the structure of a candle flame (17). Then, the so-called "phlogiston theory" was originated by Becher and Stall (17), in the seventeenth century. They theorized that flames were caused by imponderable substances. However, in the middle of the eighteenth century Black, Scheele, Laviosier and other workers (17) made quantitative chemical observations and discovered a number of elements and gases, thereby providing groundwork for modern chemistry. Several famous chemists, including Volta, Berthelot, and Dalton (17), worked on combustion in the early ninetheenth century. Wallaston (50) studied a candle flame in his experiments in which a slit was first

used with a spectroscope. Sir Humphrey Davy (18) did the next systematic work by investigating the problem of mine explosions for the Royal Society and devising the safety lamp. In 1823 Herschel (50) noted the yellow emission characteristic of sodium compounds in flames and the red colors produced by strontium compounds. The new elements cesium and rubidium were discovered between 1800 and 1864, following the observation of their resonance lines in flame spectra. This led gradually to the use of flames and spectra for identifying the presence of elements by Talbot, Kirchhoff, and Bunsen (17). Bunsen is best known for the burner used in every chemical laboratory. He was also the first to study flame temperatures. In the period between World Wars I and II, the number of workers in flames steadily increased. Kurlbaum (30) used flame pyrometry based on the visible light spectrum to measure the flame temperature in 1902. Infrared pyrometry was next used by Coblentz (13) and Schmidt (46) in 1905 and 1909, respectively. Their use of infrared pyrometry was based on thermodynamic considerations. Since then, a number of investigators (33, 42, 45, 51) have worked on flame temperature determination tc enable computation of the radiant flux from a flame. Tourin (52) further determined the emissivities of the hot gas from infrared absorption spectra of gas samples heated under controlled conditions. Almost all the work relevant to the radiation from flames in the past has been confined to flame temperature

determination from laboratory measurements. However, a different way of predicting the radiant flux from flames was developed by Love, Hood, and co-workers (34), who used the transport equation to compute the monochromatic volume absorption and emission coefficients from measurements made on small laboratory flames.

The aim of this study is to extend Hood's work, but at the same time to employ a new and improved technique. The flames used for the measurements are diffusion flames, in which a combustible vapor burns in the surrounding air. The flame can approximately be classified into two zones, the inner cone and the outer cone. The inner cone is primarily a reaction zone where the combustible vapor is broken and oxidized to products including hydrogen, carbon monoxide, water vapor, etc. The combustion phenomena and chemical reactions in this zone are very complex. Above the inner cone is a luminous region where these products further burn in a secondary combustion zone of the red-orange color typical of a candle flame forming carbon dioxide and more water vapor. As pointed out by Hollander (24), "The concentrations of the major stable flame species when leaving the reaction zone are not much different from their equilibrium values. But the radicals leave this zone with concentrations exceeding markedly their equilibrium. Above the reaction zone these radicals recombine into stable molecules and consequently the flame-gas mixture gradually

approaches complete chemical equilibrium.---In the flame no general thermodynamic equilibrium exists."

The advantage of using the transport equation is that it needs no assumption of the thermodynamic equilibrium. Since complete chemical equilibrium is achieved above the reaction zone, it can be considered that it is fairly homogeneous in the outer cone of the flame. The assumption was made that the average values of monochromatic volume absorption and emission coefficients can be obtained.

The equation for the intensity of radiation transfer in an absorbing and emitting medium is

$$\frac{dI_\lambda(x)}{dx} = -\beta_\lambda I_\lambda(x) + J_\lambda \qquad (1)$$

where

$I_\lambda(x)$ = monochromatic intensity along path length, $\frac{\text{watts}}{\text{cm}^2\text{-cm-steradian}}$

x = path length, cm

β_λ = monochromatic volume extinction coefficient, cm^{-1}

J_λ = monochromatic volume emission coefficient, $\frac{\text{watts}}{\text{cm}^3\text{-cm-steradian}}$

The solution to equation (1) for constant J_λ and β_λ is

$$I_\lambda(x) = Ae^{-\beta_\lambda x} + \frac{J_\lambda}{\beta_\lambda} \qquad (2)$$

If there is no source outside the flame path length, the intensity at the flame boundary is zero. The boundary condition for equation (2) at $x = 0$ is $I_\lambda = 0$. Hence A is found to be

$$A = - \frac{J_\lambda}{\beta_\lambda} \tag{3}$$

Upon substituting these results into equation (2) the intensity emitted by a flame having a path length x is found to be

$$I_\lambda(x) = \frac{J_\lambda}{\beta_\lambda} (1 - e^{-\beta_\lambda x}) \tag{4}$$

Because of the difficulties Hood (26) encountered in maintaining sufficient accuracy in his measurements, a second method of measuring J_λ and β_λ was devised for this work. The new method uses two flames and involves the simultaneous solution of two equations. Hood (28) handled equation (4) by introducing a globar source to illuminate through the flame. The intensity observed was the sum of the globar intensity after it passed the flame and the intensity emitted by the flame. Hence

$$I_\lambda \text{ (Globar + Flame)} = I_\lambda \text{(Globar, attenuated)} + I_\lambda \text{ (Flame)} \tag{5}$$

Lambert's law states

$$I_\lambda \text{(Globar, attenuated)} = I_\lambda \text{ (Globar)} e^{-\beta_\lambda x} \tag{6}$$

where

β_λ = monochromatic volume extinction coefficient, cm^{-1}

x = path length, cm

Thus Hood obtained

$$I_\lambda \text{ (Globar + Flame)} = I_\lambda \text{ (Globar)} e^{-\beta_\lambda x} + I_\lambda \text{ (Flame)} \quad (7)$$

or

$$e^{-\beta_\lambda x} = \frac{I_\lambda \text{(Globar + Flame)} - I_\lambda \text{(Flame)}}{I_\lambda \text{(Globar)}} \quad (8)$$

He then solved for β_λ and J_λ from equations (8) and (4), using experimental data for the respective intensities. However, the monochromatic intensity of the globar was very susceptible to voltage fluctuation.

Multiplying equation (4) by the solid angle and cos θ of the incident radiation, the energy from the flame which enters the monochromator can be written as follows

$$q_\lambda(x) = \frac{J_\lambda}{\beta_\lambda} (1-e^{-\beta_\lambda x}) (\omega \cos \theta) \quad (9)$$

where

$q_\lambda(x)$ = energy incident onto the monochromator, $\frac{\text{watts}}{cm^2\text{-cm}}$

θ = angle between the normal to the surface and the central direction of the solid angle, degree

$\cos \theta = 1$ (because the angle θ is zero)

ω = solid angle of incident radiation, steradian

$q_\lambda(x)$ is a function of the path length x. Equation (9) suggests that J_λ and β_λ can be obtained by solving two simultaneous equations obtained by measurements made at two different path lengths through the flame. Since the region in the outer cone of a flame is fairly homogeneous, this can be accomplished by varying the size of the flame. Hence, the heat fluxes from two flames having two different path lengths are (see Figure 1)

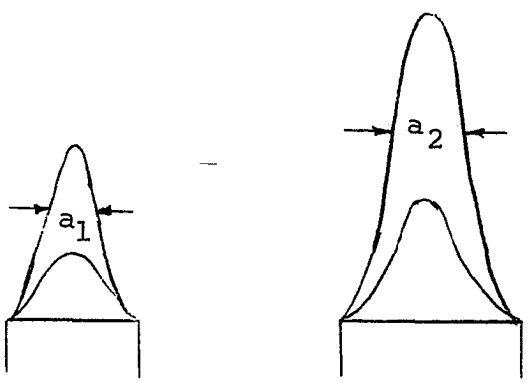


Figure 1. Boundary Conditions for Flame.

for $x = a_1$

$$q_\lambda(a_1)_{\text{recorded}} = \frac{J_\lambda}{\beta_\lambda} (1 - e^{-\beta_\lambda a_1}) . \omega \qquad (10)$$

for $x = a_2$

$$q_\lambda(a_2)_{\text{recorded}} = \frac{J_\lambda}{\beta_\lambda}\left(1 - e^{-\beta_\lambda a_2}\right).\omega \qquad (11)$$

From equations (10) and (11), one obtains

$$f(\beta_\lambda) = q_\lambda(a_1)e^{-\beta_\lambda a_2} - q_\lambda(a_2)e^{-\beta_\lambda a_1} - q_\lambda(a_1) + q_\lambda(a_2) = 0 \qquad (12)$$

$q_\lambda(a_1)$ and $q_\lambda(a_2)$ can be recorded as the monochromator scans over the emission spectrum for each path length. The only unknown in equation (12) is β_λ. However, because a closed form solution for β_λ cannot be obtained, a Newton-Raphson iterative equation was used. This equation is

$$(\beta_\lambda)_{n+1} = (\beta_\lambda)_n - \frac{f(\beta_\lambda)_n}{f'(\beta_\lambda)_n} \qquad (13)$$

The value of β_λ at each wavelength in equation (12) is different. An arbitrary first guess of β_λ for equation (13) will ordinarily end in divergence. However, the curve represented by equation (12) as shown in Figure 2 suggests that a very good first guess for β_λ at every wavelength can be obtained as follows. First, compute $\beta_{\lambda,c}$ at point C by setting the derivative of $f(\beta_\lambda)$ with respect to β_λ equal to zero.

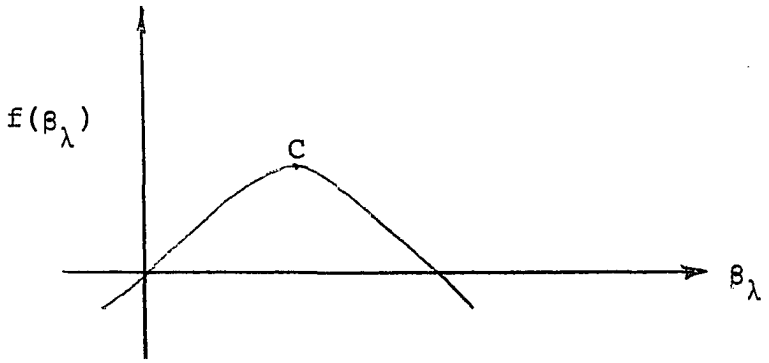


Figure 2. Graph of $f(\beta_\lambda)$

$$f'(\beta_\lambda) = a_2 q_\lambda(a_1) e^{-\beta_\lambda a_2} - a_1 q_\lambda(a_2) e^{-\beta_\lambda a_1} = 0 \text{ or}$$

$$\beta_{\lambda,c} = \frac{1}{a_2 - a_1} \ln\left(\frac{a_2 q_\lambda(a_1)}{a_1 q_\lambda(a_2)}\right) \tag{14}$$

and then add 1/2 $\beta_{\lambda,c}$ to $\beta_{\lambda,c}$ as the first guess. Thus

$$(\beta_\lambda)_1 = \beta_{\lambda,c} + 1/2\ \beta_{\lambda,c} \tag{15}$$

The scheme introduced proved to be very effective and time saving. After having found β_λ, J_λ was computed from equation (11).

CHAPTER II

EQUIPMENT AND PROCEDURE

Equipment

The equipment used is essentially that described in Hood's work (26). Additions include a second boiler and its fuel line, two flowmeters, and a precipitator. The addition of a second boiler allows the spectroscopic flame study for binary fuel mixture. The equipment used is briefly described as follows:

Monochromator and external optical system

The monochromator used was a Perkin Elmer Model 12-C which is a single pass instrument with an external chopper. A globar source is used for intensity calibrations. A sodium chloride prism and thermocouple detector were used for the spectral region from 0.74μ to 5.79μ, which is the only region that every fuel in this study emits its energy. The schematic diagram of the monochromator is shown in Figure 3.

An external optical system is used to focus the image of the radiation source onto the plane of the entrance slit of the monochromator. The slit is formed between two metal jaws, one of which is fixed while the other is moved

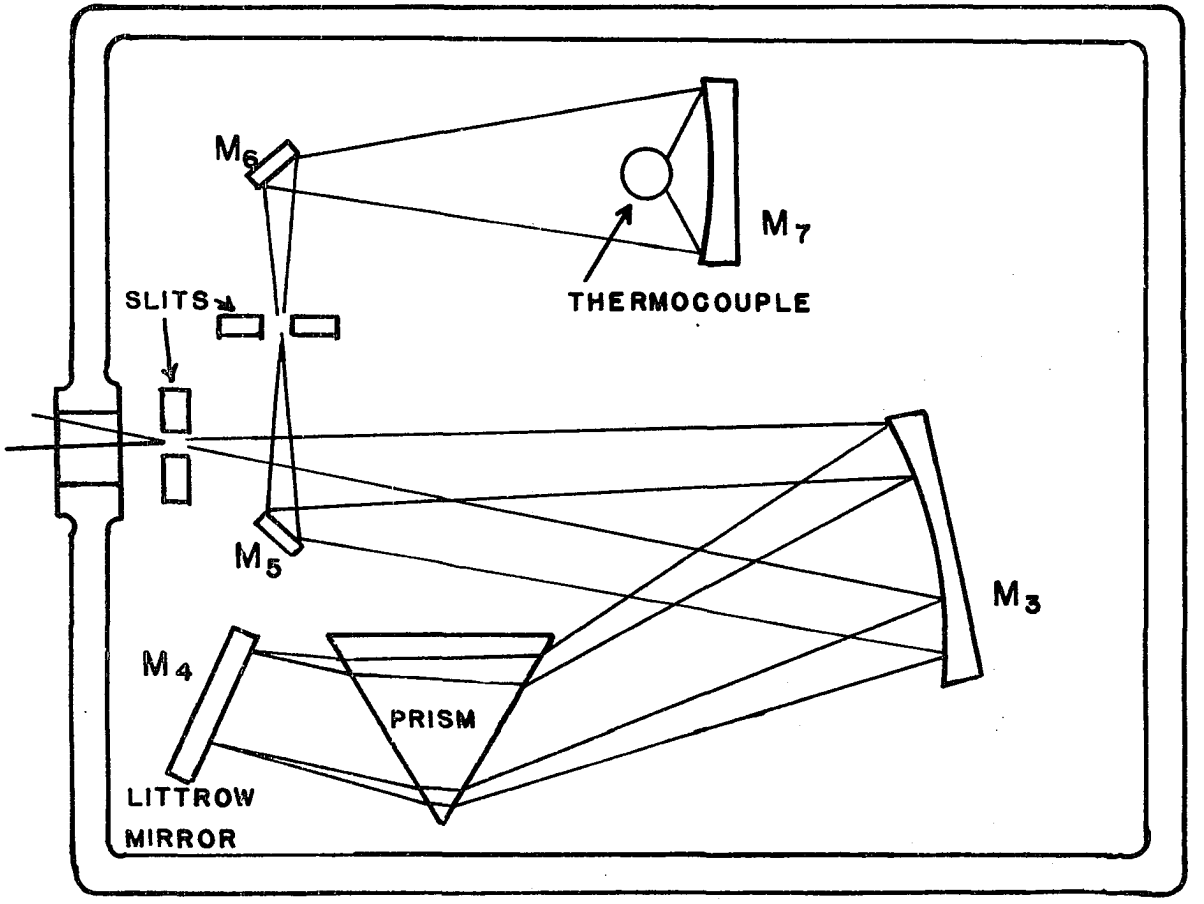


Figure 3. Monochromator Internal Optics

by a fine-pitched screw, which enables the width of the opening between the jaws to be accurately adjusted. Diffraction, resolving power, and spectral purity are all related to the opening of the slit. The bending of light around an obstacle is known as diffraction. The diffracted light is not distributed uniformly but appears as fringes or bands which are separated by intervals of darkness. This can be caused by both the width and height of the aperture. The resolving power is the ratio between the mean wavelength of a pair of lines that can just be resolved by the spectroscope and the difference in wavelength between the two components of the pair. This refers strictly to an infinitely narrow slit, a condition that does not occur in actual practice. The resolving power has to be considered when the slit is given a definite width. A finite width slit increases the amount of light available, and at the same time decreases the resolving power. The slit opening should be the best balance between resolving power and light available for the object being viewed. In order to select the best balance, spectral purity is introduced. It is a measure of the efficiency of an instrument with wide slits, while the resolving power measures the efficiency with infinitely narrow slits. For narrow slits, the purity is proportional to the resolving power, but is also depends on the width of the slit. A datailed discussion is given by Rossi (44). An entrance slit 0.1 millimeter wide and 5 millimeters long was

computed by Hood (26) to make diffraction negligible and to provide good resolving power and spectral purity.

The spectral slit width of the exit slit is the sum of the dispersion of the prism and optical system and the resolving power. The details of the computation of spectral slit width are discussed in (3,26). Values of the wavelength and its corresponding spectral slit width are tabulated in Table 1.

The external optical system is shown schematically in Figure 4. This system focuses a small area of flame or source onto the entrance slit of the monochromator. M_2 and M_3 are spherical mirrors with diameters of 4 1/2 inches. Mirrors M_1 and M_4 are plane first surface mirrors. The object distance and the image distance of M_2 are both 18 inches. This provides a magnification factor equal to unity. Therefore, the area of the flame viewed by the monochromator is equal to the area of the entrance slit opening. The solid angle is the area of M_2 divided by the square of the object distance. That is

$$\omega = \frac{\pi R^2}{(S_2)^2} = \frac{3.14 \times 2.25^2}{18^2} = 0.04909 \qquad (16)$$

The object distance S_3 and M_3 is 28.29 inches and the image distance S_3' is 18 inches. This gives a magnification factor of 0.636. The solid angle which is focused on the entrance slit of the monochromator is thus

TABLE 1

WAVELENGTH VERSUS SPECTRAL SLIT WIDTH

Wavelengths (microns)	Spectral Slit Width (microns)	Wavelengths (microns)	Spectral Slit Width (microns)
0.743	0.00275	2.690	0.06160
0.850	0.00580	2.710	0.06170
0.862	0.00610	2.740	0.06180
0.874	0.00625	2.780	0.06190
0.886	0.00650	2.820	0.06200
0.899	0.00685	2.860	0.06210
0.911	0.00712	2.880	0.06210
0.924	0.00740	2.950	0.06230
0.938	0.00765	2.990	0.06230
0.915	0.00800	3.080	0.06210
0.964	0.00830	3.170	0.06180
0.980	0.00890	3.270	0.06140
0.990	0.00930	3.310	0.06130
1.040	0.01080	3.390	0.06090
1.080	0.01220	3.430	0.06060
1.130	0.01350	3.510	0.06020
1.180	0.01450	3.590	0.05960
1.230	0.01700	3.720	0.05860
1.290	0.01950	4.020	0.05620
1.360	0.02200	4.160	0.05520
1.420	0.02260	4.180	0.05100
1.500	0.02790	4.200	0.05000
1.650	0.03530	4.220	0.05480
1.720	0.03820	4.240	0.05460
1.780	0.04070	4.260	0.05450
1.850	0.04390	4.290	0.05420
1.950	0.04700	4.330	0.05390
2.020	0.04950	4.350	0.05370
2.060	0.05040	4.370	0.05360
2.140	0.05280	4.390	0.05350
2.210	0.05440	4.410	0.05340
2.280	0.05600	4.430	0.05330
2.360	0.05730	4.460	0.05290
2.410	0.05810	4.500	0.05270
2.450	0.05890	4.550	0.05230
2.490	0.05950	4.600	0.05190
2.500	0.05970	4.650	0.05160
2.520	0.05990	4.710	0.05130
2.540	0.06020	4.830	0.05040
2.610	0.06090	4.990	0.04940
2.630	0.06110	5.220	0.04790
2.670	0.06150	5.790	0.04300

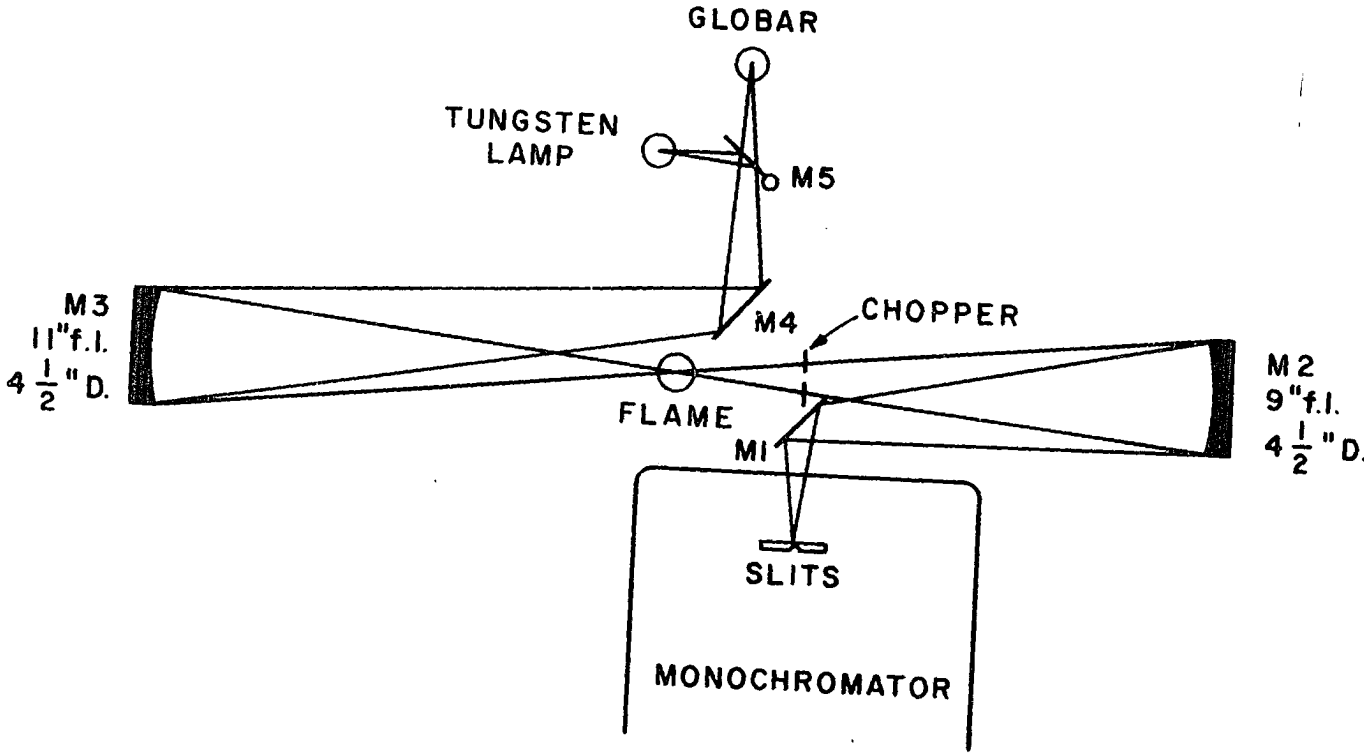


Figure 4. External Optical System

$$\omega' = \frac{\pi r^2}{(S_3)^2} = \frac{3.14 \times 2.25^2}{(28.29)^2} = 0.01988 \qquad (17)$$

The above arrangement is to be able to keep the aberrations at a minimum. Aberrations in an optical system destroy the point to point correspondence between the object and image. A detailed discussion is given by Jenkins (29) and Monk (38).

Boiler, pipeline and burner.

A stable flame is needed for spectral analysis. A boiler system was constructed to provide uniform fuel flow to the burner. The boiler was made by welding a 3-inch ID copper pipe to copper plates. Twenty gauge heating wiring sandwiched between layers of electrical resisting cement and asbestos was used for heating. The fuel in the boiler was heated to a gauge pressure of approximately 10 psi. A heated fuel line and a flow-meter were connected to the boiler. The vapor was passed from each boiler through its fuel line and flow-meter to the burner (see Figure 5). A 2 1/2-inch tall burner was made from a piece of 3/4-inch ID copper tubing. Three stainless steel screens were placed in the circular burner to straighten the flow and produce a steady laminar flow. To provide a different path length, a brass plate of 7/8-inch diameter with a 3/8-inch diameter copper tube inserted in the middle was made, so that the plate can be put on the top of the burner to reduce the flame diameter. A

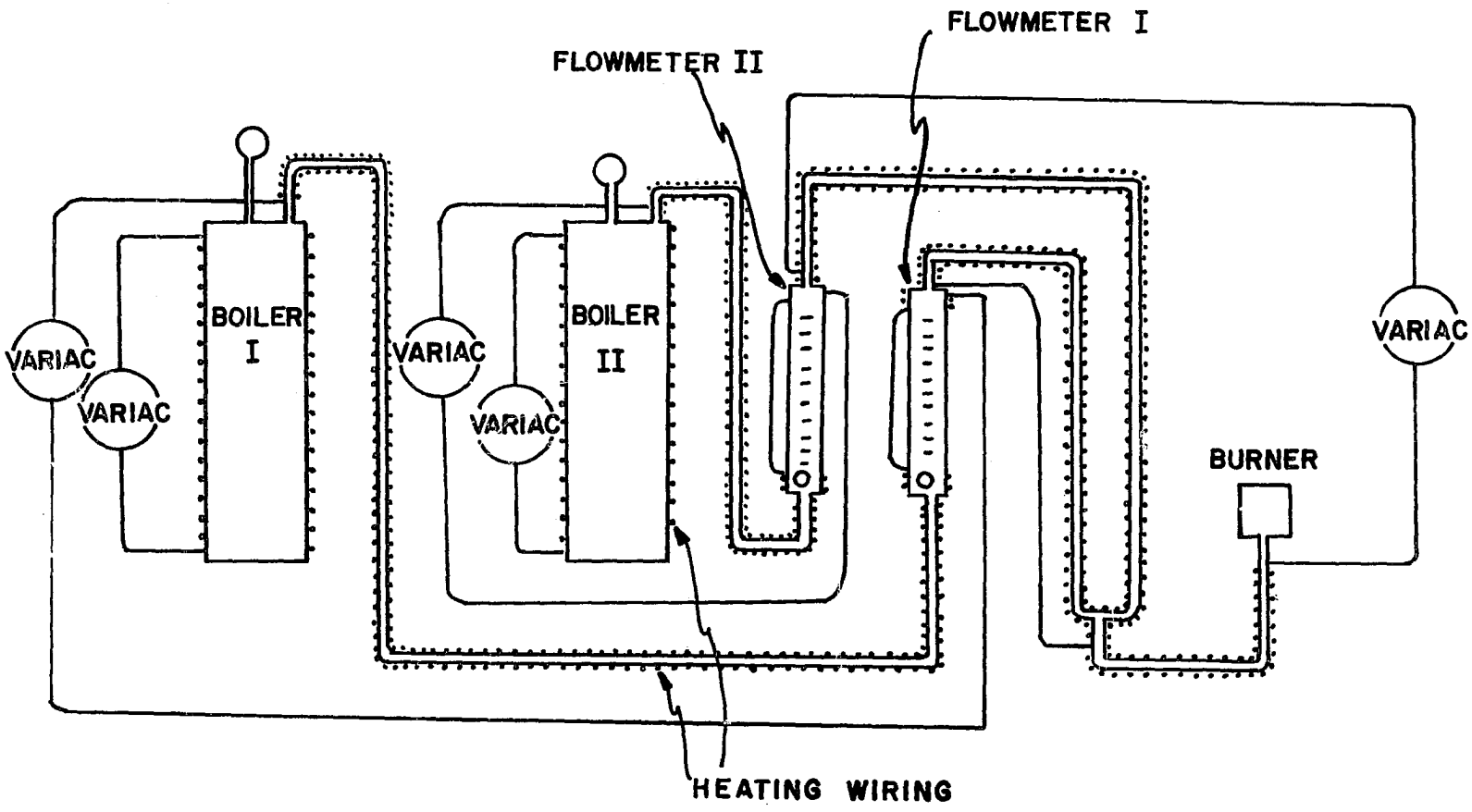


Figure 5. Schematic Diagram of Heating System

number of holes were drilled around the flame holder and a cylindrical screen was placed around the burner to straighten the free convection pattern. A square hole was cut on the screen, so that the monochromator can "see" through the screen. The flame holder was mounted on a mechanism which allowed it to be moved in two dimensions. This allows the monochromator to be able to "see" different locations on the flame. Figure 5 is a schematic diagram of the heating system. A cabinet surrounds the external optical system and the burner to prevent eddy currents disturbing the flame. A precipitator was constructed to collect the smoke and soot from the fires (see Figure 6). The precipitator, which was able to provide a maximum voltage of 20 kv, was used for some smoky fuels such as benzene. Because the carbon dioxide accumulation seriously affects the reading in the 4.3μ region, the chimney was connected to a vacuum cleaner. Prior to the spectral recording at 4.3μ, the vacuum cleaner was turned on for several minutes to clear the carbon dioxide accumulation inside the cabinet. The system was able to produce a steady flame of constant size for several hours.

Calibration

Drum setting calibration provides the relationship between drum reading and wavelength. The monochromator scans the spectrum continuously by rotating the Littrow mirror which is driven by a shaft or drum. The relationship between the drum setting and its corresponding

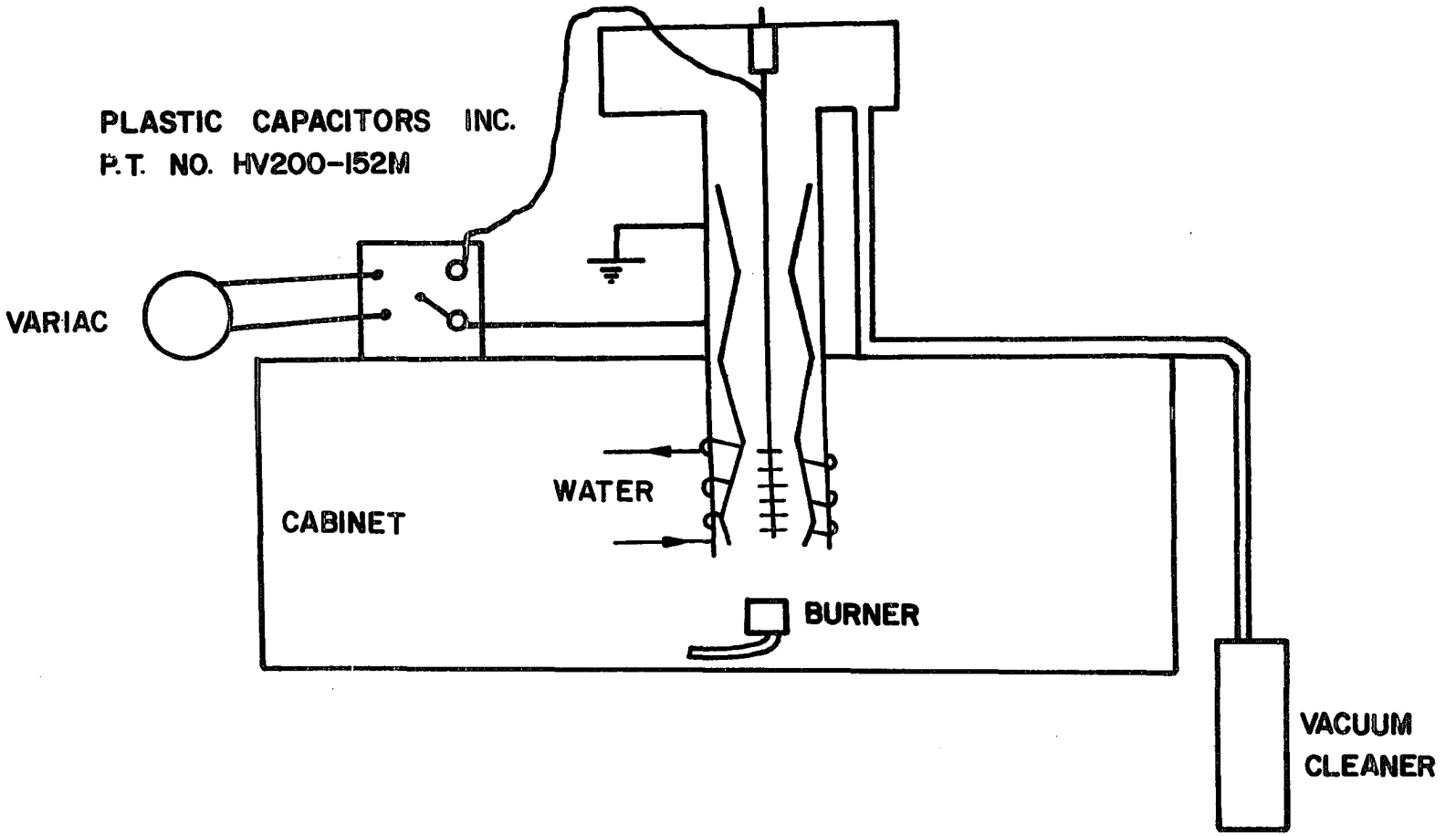


Figure 6. Schematic Diagram of Precipitator

wavelength is identified by some of the known specific absorption peaks through some materials. Trichlorobenzene, toluene, polystyrene, and didymium glass are materials which can be used for drum setting calibration. Due to its easy handling, a Perkin Elmer 0.07 mm polystyrene film was used for this purpose. Several absorption peaks were identified from the film to determine the relationship between the wavelength and the drum setting. The relationship is tabulated in Table 2. The drum setting was checked prior to each series of runs. This can be done by taking a spectrograph having a polystyrene film in front of the entrance slit. If the spectrograph did not check with the wavelength calibration curve, a fine adjustment of the Littrow mirror was performed until agreement was obtained. Throughout the experiment, it was found that the drum setting stayed fairly constant.

Absolute intensity calibration relates the energy incident on the monochromator to the output of the radiation detector on the spectrograph. The radiation source used for the calibration was a globar which was purchased from the Perkin Elmer Corporation. It is a silicon carbide rod 3/16 inch in diameter and 2 inches long with silver film on both ends to provide a good electrical contact. It can be electrically heated to 2000°K, and is a practical approximation of a gray body obeying Wien's displacement law; that is, the position of the wavelength peak or maximum of radiation depends on the temperature of the radiator by the

TABLE 2

DRUM SETTING VERSUS WAVELENGTH

Drum Setting	Wavelength (microns)	Drum Setting	Wavelength (microns)
2050	.743	1834	2.69
2000	.850	1833	2.71
1995	.862	1832	2.74
1990	.874	1830	2.78
1985	.886	1828	2.82
1980	.899	1826	2.86
1975	.911	1825	2.88
1970	.924	1822	2.95
1965	.938	1820	2.99
1960	.951	1816	3.08
1955	.964	1812	3.17
1950	.980	1808	3.27
1945	.990	1806	3.31
1940	1.04	1802	3.39
1935	1.08	1800	3.43
1930	1.13	1797	3.51
1925	1.18	1793	3.59
1920	1.23	1785	3.72
1915	1.29	1770	4.02
1910	1.36	1762	4.16
1905	1.42	1760	4.18
1900	1.50	1759	4.20
1890	1.65	1759	4.22
1886	1.72	1758	4.24
1882	1.78	1757	4.26
1878	1.85	1755	4.29
1872	1.95	1753	4.33
1868	2.02	1752	4.35
1866	2.06	1751	4.37
1862	2.14	1750	4.39
1858	2.21	1749	4.41
1854	2.28	1748	4.43
1850	2.36	1746	4.46
1848	2.41	1744	4.50
1846	2.45	1741	4.55
1844	2.49	1738	4.60
1843	2.50	1735	4.65
1842	2.52	1732	4.71
1841	2.54	1725	4.83
1838	2.61	1715	4.99
1837	2.63	1700	5.22
1835	2.67	1659	5.79

following equation

$$\lambda_m T = C \tag{18}$$

where

λ_m = peak wavelength, micron

T = temperature, °K

C = constant

No detailed information concerning the emittance of a globar over a wide temperature range is available. However, Silverman (48) and Morris (39) provided the monochromatic emittance of the globar at temperature of 1375°K, and at temperature of 395°K respectively. The intensity calibration involved in this work is in the range of 800°F to 1300°F. The emittance of the globar at this range is lacking. However, Silverman (48) and Morris (39) showed that the average emittance of globar is 0.94 at 1375°K and 0.92 at 395°K. Since the globar temperature used in the intensity calibration was in the between, an average emittance of 0.93 was assumed. A V-groove 40/64 inches long, 3/64 inches wide, and 3/64 inches deep was made on the globar. It was used to improve the emittance of the globar. The apparent emittance of the globar is estimated by the following equation

$$\epsilon_{app} = \frac{\epsilon_c \sigma T_c^4}{A_H \sigma T_c^4 \left[\frac{1-\epsilon_c}{A_c} + \frac{\epsilon_c}{A_c F_{c-H}}\right]} \tag{19}$$

where

σ = Stephan-Boltzmann Constant = 5.6699×10^{-5} erg-sec cm^2 $°K^4$

A_H = area of the opening = 0.0293 in^2

A_c = area of the cavity = 0.063 in^2

ϵ_c = emissivity of globar

F_{c-H} = configuration factor of the cavity to the opening

T_c = temperature of the cavity

Knowing $A_c F_{c-H} = A_H F_{H-C}$, and $F_{H-C} = 1$, equation (19) can be rewritten as

$$\epsilon_{app} = \frac{1}{1 + \frac{1-\epsilon_c}{\epsilon_c} \left(\frac{A_H}{A_C}\right)} \tag{20}$$

Hence, the apparent emittance was obtained

$$\epsilon_{app} = .966 \tag{21}$$

A hole of 0.052 inch diameter and 0.875 inch deep was drilled 0.025 inch above the V-groove. A Chromel-Alumel thermocouple was inserted into the hole. Sausereisen Electric Resistor Cement No. 78 was used to seal around the thermocouple to prevent convective heat transfer loss. The thermocouple leads were connected to a Leeds and Northrup Co. millivolt potentiometer Cat. No. 8686, so that the globar temperature could be read from the potentiometer. At the same time, the corresponding intensity was recorded on a chart. The equation used for the intensity calibration is as follows:

$$E_\lambda = \frac{\epsilon_\lambda A\omega\Delta\lambda\ C_1}{\lambda^5} \left(\frac{1}{e^{C_2/\lambda T}-1}\right) \qquad (22)$$

where $C_1 = 1.77 \times 10^{-12}$ watts cm^2, $C_2 = 2.5776$ cm degree Rankin; λ is the wavelength in cm; ϵ_λ is the apparent emittance of the globar source, and was computed from equation (16) to be equal to 0.966; A is the area of the source observed which is equal to 1.23×10^{-2} cm^2; ω is the solid angle focussed onto the monochromator, and was computed from equation (17) to be equal to 1.988×10^{-2} steradians; $\Delta\lambda$ is the wavelength interval being observed.

The intensity calibrations were made by simultaneously taking a spectrograph of the globar source and reading the globar temperature. A Perkin Elmer Model 12-C monochromator, a recorder, and a potentiometer were used for this purpose. Blackbody intensity was computed from the globar temperature. The apparent emittance was multiplied by the blackbody intensity to give the energy which was incident on the monochromator for wavelengths of 2.18μ, 3.82μ, 4.65μ. These three wavelengths were chosen as they are outside the regions of atmospheric absorption. These intensities were divided by the corresponding pen deflections at each wavelength recorded on the spectrograph to give the full scale intensity for the recorder. The average value was obtained from the three absolute intensity calibrations at the three wavelengths. It

was found that the deviation of the three absolute intensity calibrations was within a few percent.

Procedure

The Boiler was electrically heated so that the fuel vapor pressure was built up to about 10 psig. Fuel vapor was heated above saturation in the fuel line to assure that no vapor would condense on the tube wall. Electrical heating of the boiler, flowmeter, and fuel lines was adjusted until the flame was stabilized. Proper gain settings were determined. A spectrograph was taken with the monochromator viewing the outer cone of the flame. Because carbon dioxide absorption causes a serious effect of the spectrograph reading in the 4.3μ region, just prior to that region the cabinet door was opened and the vacuum cleaner was turned on for several minutes to clean out the carbon dioxide accumulation. The scanning was then resumed until the region was reached where the intensity was negligible. A plate into which a 3/8 inch copper tube 1/8 inch high had been inserted was put on the top of the burner, and the flowrate was adjusted to reduce the flame size. The flame holder was also adjusted, so that the monochromator viewed the outer cone of the flame again. Then, a second spectrograph was taken.

During each run, several pictures were taken. The film used was Polaroid type 57 (ASA 3000). A pin hole

camera was used to take pictures. The exposure was about 50 seconds. Typical pictures of the flames are shown in Figure 7. Figure 8 shows some of the spectrographs. It can be seen from the spectrographs that the pen deflection is fairly smooth, indicating the stability of the laminar flow. Pen deflections corresponding to each wavelength were read from both spectrographs. These data were then fed into a computer program based on equation (18) to compute J_λ and β_λ.

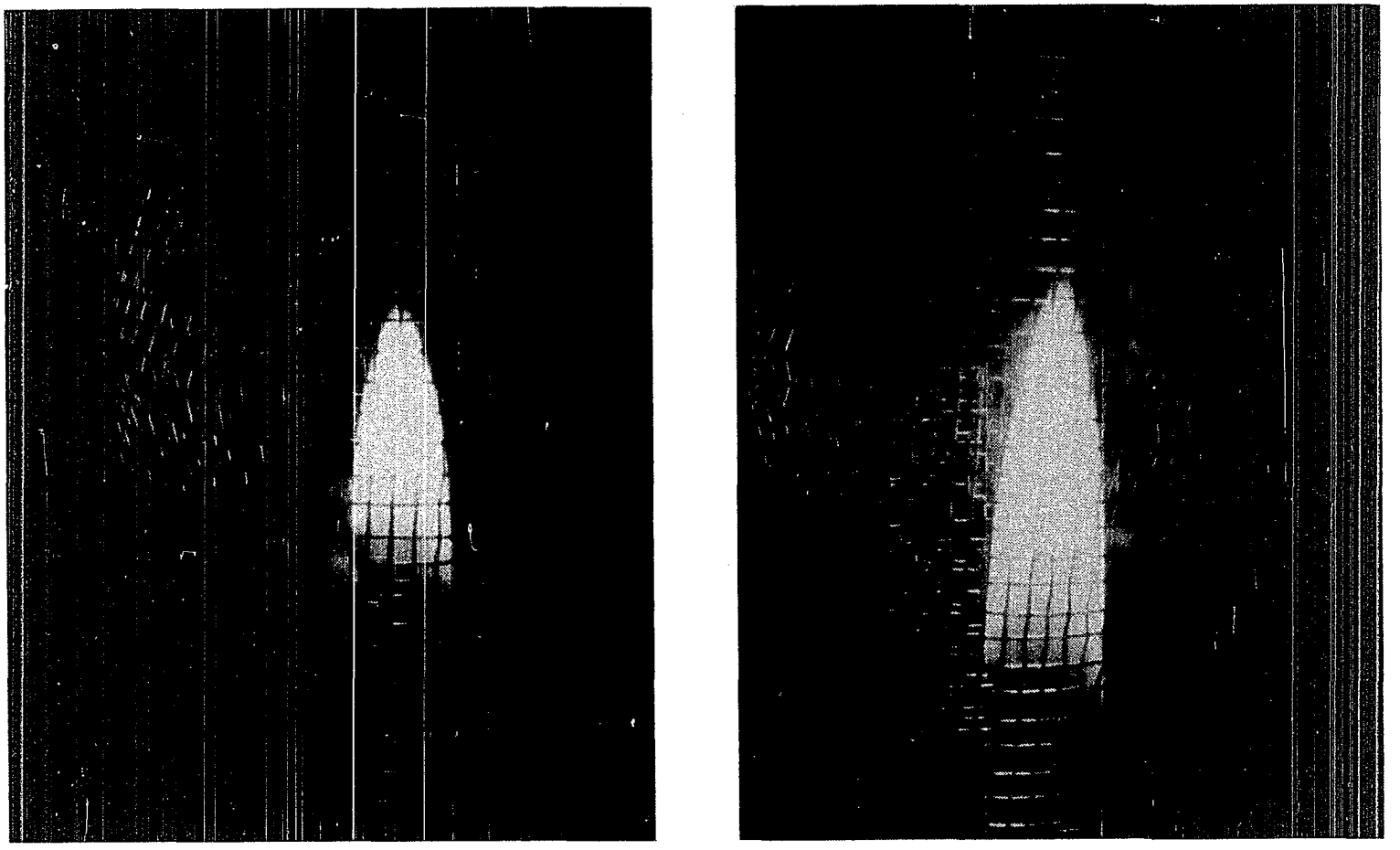


Figure 7. Acetone Flames

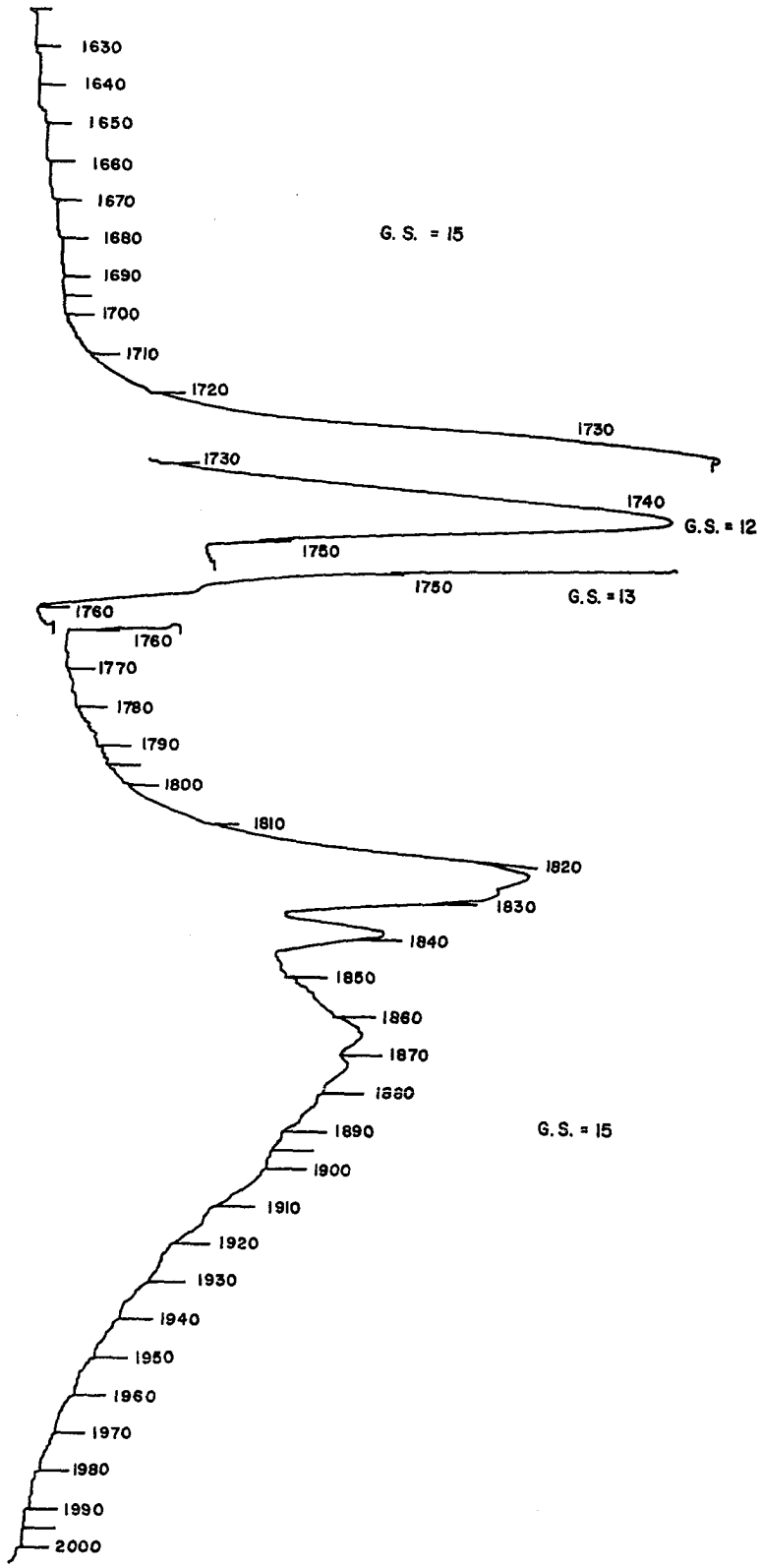


Figure 8. Spectrograph of Acetone Flame

CHAPTER III

ATMOSPHERIC ABSORPTION

Energy may be transmitted from one body to another by means of electromagnetic waves. From the view of quantum mechanics, each electron circling the nucleus in its particular orbit inside the atom has a certain amount of energy. This energy is related to the frequency by the expression

$$E = h\nu \tag{23}$$

where E = energy, erg

h = Planck's constant, 6.624×10^{-27} erg-sec

ν = frequency, sec^{-1}

An electron can elevate to a larger orbit if a certain specific amount of energy corresponding to a certain frequency is supplied to the electron. If a beam of radiation consisting of a continuous range of frequencies and energies travels through the absorbing medium, a quantum of radiation may come very close to an orbital electron of the medium. If the energy of that quantum is just equal to that needed by the electron to elevate it to a higher permitted orbit, the electron may absorb this radiant energy and jump to the higher orbit; otherwise, no absorption will occur and the energy will be transmitted. Since there are many atoms in the medium

containing electrons which are at some given energy level, there will be many "captures" of quanta of the specific energy to raise these electrons to a higher orbit. Consequently, the radiation beam will suffer a selective depletion of the quanta of this specific energy. This is the selective absorption at the frequency corresponding to the energy for the electronic transition. However, the electronic transition is not the only possible one. A polyatomic molecule may absorb a certain specific amount of energy as a result of accelerating its vibration of the component atoms or as a result of accelerating its rotation of the molecule. These vibrational and rotational energies must also be thought of as being quantized. That is, the permitted levels of vibration and rotation are also separated by a specific amount of energy, and the elevation from one level to another needs an absorption of correct frequency.

A radiation beam will attenuate in the atmosphere due to some of its constituents. Most of the absorption is due to molecules of water vapor and carbon dioxide in the atmosphere. The amount of the absorption is proportional to the path length and the concentration. The three other most common atmospheric gases, nitrogen, oxygen, and argon, have only negligible absorption bands in the infrared region of interest in flame radiation. They can be considered as completely transparent gases in the infrared region.

The fraction of the energy in an infrared beam which is transmitted through the atmosphere between two fixed points fluctuates with time as meteorological conditions change. Carbon dioxide is more nearly uniformly mixed in the atmosphere while water vapor may vary considerably. However, in an air conditioned laboratory where the apparatus was located, it was assumed that carbon dioxide and water vapor are fairly constant in the atmosphere. The amount of carbon dioxide and water vapor in the laboratory was not analyzed. However, the amount of flame radiation energy absorbed by the carbon dioxide and water vapor during its path to the monochromator was obtained by using another apparatus which consists of a Perkin-Elmer Model 112 U double pass monochromator, a recorder, a globar source, two plane first surface mirrors, and two spherical mirrors with diameter D = 4½ inch and the aperture ratio, f = 4.0. This apparatus was originally used for the determination of the reflection coefficient of metal surfaces or the determination of the scattering coefficient of particles. This set-up was temporarily adjusted so that the distance from the globar source to the monchromator was exactly the same as the distance from the flame to the monochromator in the set-up used for the flame spectral analysis. The selective absorption of the atmosphere mainly occurs in the 2.7μ band and 4.3μ band. The temperature of the globar was adjusted to shift the gray body curve such that the absorption bands were not located on the peak. Spectrographs were

taken corresponding to the 2.7μ region and the 4.3μ region. A smooth curve was drawn over the absorption band on the spectrograph as shown in Figure 9.

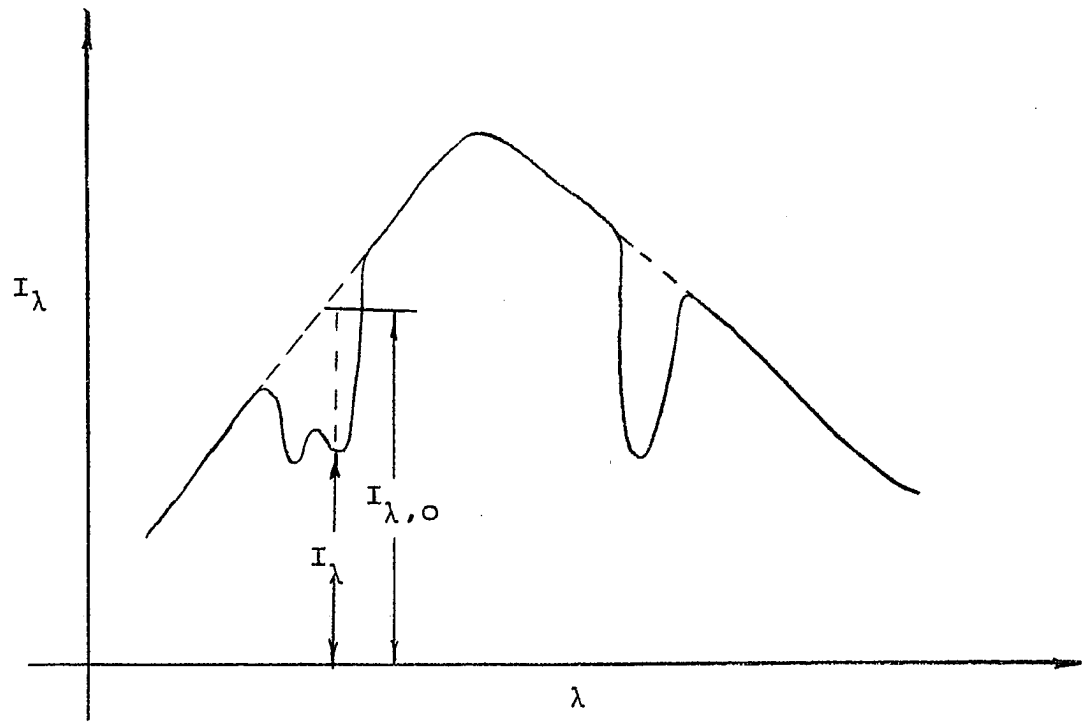


Figure 9. Sketch of Globar Spectrograph over 2.7μ and 4.3μ Absorption Bands.

I_λ (See Figure 9) is the intensity received by the monochromator, $I_{\lambda,o}$ is the intensity the monochromator would receive if there were no absorption. The relation between I_λ and $I_{\lambda,o}$ is expressed by Lambert's law which states

$$I_\lambda = I_{\lambda,o} e^{-K_\lambda X}$$

$$\text{or} \qquad \alpha_\lambda = e^{-K_\lambda X} = \frac{I_\lambda}{I_{\lambda,o}} \tag{24}$$

where $I_{\lambda,o}$ is the original intensity of the beam, K_λ the monochromatic volume extinction coefficient of the atmospheric constituents, X is the path length from source to monochromator, and α_λ is defined as the monochromatic transmittance of the atmosphere. This is the ratio of energy which will be transmitted in the atmosphere from the source to the monochromator in the set-up. The monochromatic transmittance of the atmosphere was computed by taking the ratio of $I_\lambda/I_{\lambda,o}$ at each specific wavelength throughout the absorption bands and was tabulated in Table 3. The intensity of the flame read from the flame spectrograph in these bands was divided by its corresponding monochromatic transmittance to give the original intensity in the J_λ and β_λ calculation.

A correction for atmospheric absorption of the flux from a flame to a target which is several hundred centimeters away in the atmosphere (as in Chapter IV) was made. The monochromatic transmittance of the atmosphere in the 2.7μ region and 4.3μ region were taken from the data of Burch, France, and Williams (11). In their work the monochromatic transmittance for the 4.3μ and 2.7μ carbon dioxide and 2.7μ

TABLE 3

MONOCHROMATIC TRANSMITTANCE IN THE ATMOSPHERE
(91.5 centimeter separation from source to monochromator)

Wavelength (microns)	Monochromatic Transmittance	Wavelength (microns)	Monochromatic Transmittance
2.61	.900	4.24	.983
2.63	.795	4.26	.930
2.67	.620	4.29	.568
2.69	.610	4.33	.264
2.71	.634	4.35	.256
2.74	.623	4.37	.263
2.78	.590	4.39	.333
2.82	.638	4.41	.467
2.86	.708	4.43	.595
2.88	.770	4.46	.840
2.95	.940	4.50	.900
2.99	1.000	4.55	.960

water vapor band are plotted against the equivalent pressure P_E and optical path length u.

An equivalent pressure was defined as follows

$$P_E = P_{N_2} + 1.3P_s \tag{25}$$

where P_{N_2} = Partial pressure of Nitrogen

P_s = Partial pressure of specimen (either carbon dioxide or water vapor)

Then, optical path length u was computed as

$$u = \rho x \tag{26}$$

where

ρ = density of absorbing gas

x = path length

The partial pressures of nitrogen and carbon dioxide in the atmosphere are 0.871 and .00033 respectively. Although the partial pressure of the water vapor may vary from time to time, an average value of 0.02 was assumed for computations. These two computed values served as parameters in monochromatic transmittance determinations.

In the 2.7μ region, both carbon dioxide and water vapor attenuate infrared intensity. The monochromatic transmittance was obtained by multiplying two attenuations together. For a distance of 300 centimeters away, which is the average distance from flame to the target as in Chapter IV, the monochromatic transmittance in 2.7μ and 4.3μ regions were read and tabulated in Table 4. These monochromatic transmittances were then multiplied by the corresponding monochromatic flux during the total flux integration.

TABLE 4

MONOCHROMATIC TRANSMITTANCE IN THE ATMOSPHERE
(300 centimeter separation from flame to target)

Wavelength (microns)	Monochromatic Transmittance	Wavelength (microns)	Monochromatic Transmittance
1.78	.98	2.99	.98
1.85	.78	4.18	.98
1.95	.98	4.20	.50
2.50	.98	4.22	.00
2.52	.92	4.24	.00
2.61	.80	4.26	.00
2.63	.45	4.29	.05
2.67	.60	4.33	.30
2.69	.37	4.35	.37
2.71	.32	4.37	.45
2.74	.31	4.39	.65
2.78	.52	4.41	.70
2.82	.67	4.46	.90
2.86	.87	4.50	.92
2.88	.95	4.55	.96
2.95	.98	4.60	1.00

CHAPTER IV

ANALYSIS OF DATA

Drum setting calibration was performed regularly and it was found that it stayed very constant. Full scale intensity for each amplifier gain was determined and calibrated prior to each run. A spectrogram was taken corresponding to each path length. The data reduction was just a matter of taking the readings from the spectrographs. These readings together with the values of intensity calibration for each gain and path length were fed into a computer program to perform the computations indicated by equations (11) and (12) to obtain values for J_λ and β_λ. Throughout the entire emission spectrum from 0.74μ to 5.79μ, eighty-four (84) specific wavelengths were picked for this purpose. These wavelengths were picked mainly based on the slope of the emission curve. More points were chosen in the regions where the emission curve rises sharply.

Computed values of J_λ and β_λ for every fuel throughout the entire emission region were scattered. This scatter is due to a small flicker of the flame. A smooth curve was drawn through the points based on judgment of the

calculated values and the behavior of the original recordings of emission from the flames.

A three-flame method was used for methanol. This was done by rebuilding a larger burner which was made of a 1 1/8 inch ID copper tube. Two brass plates having a 3/4 inch hole and a 3/8 inch hole in the middle respectively were made, so that either of the plates could be put on the top of the burner to reduce the flame size. Three spectrographs were obtained corresponding to each path length. Readings were taken and submitted for computation to obtain three values for J_λ and β_λ at each specific wavelength. The luminous flames were not stable on the big burner, and the three flame method could not be used for them. However, the more stable methanol flame was tried. The methanol flame is dim and more than 95 percent of its emission concentrates in the 2.7μ band and 4.3μ band. It was found that all three of the values of β_λ and J_λ obtained by the three-flame method for methanol checked fairly well in these regions. (See Appendix A). The average values of three J_λ and β_λ values for methanol flame at each wavelength are shown in Figures 10 and 11.

Natural gas burns in a pale-orange color in its outer cone region. It looks more like an acetone flame; however, its emission characteristic is very similar to a methanol flame. The 2.7μ band and 4.3μ band are almost the

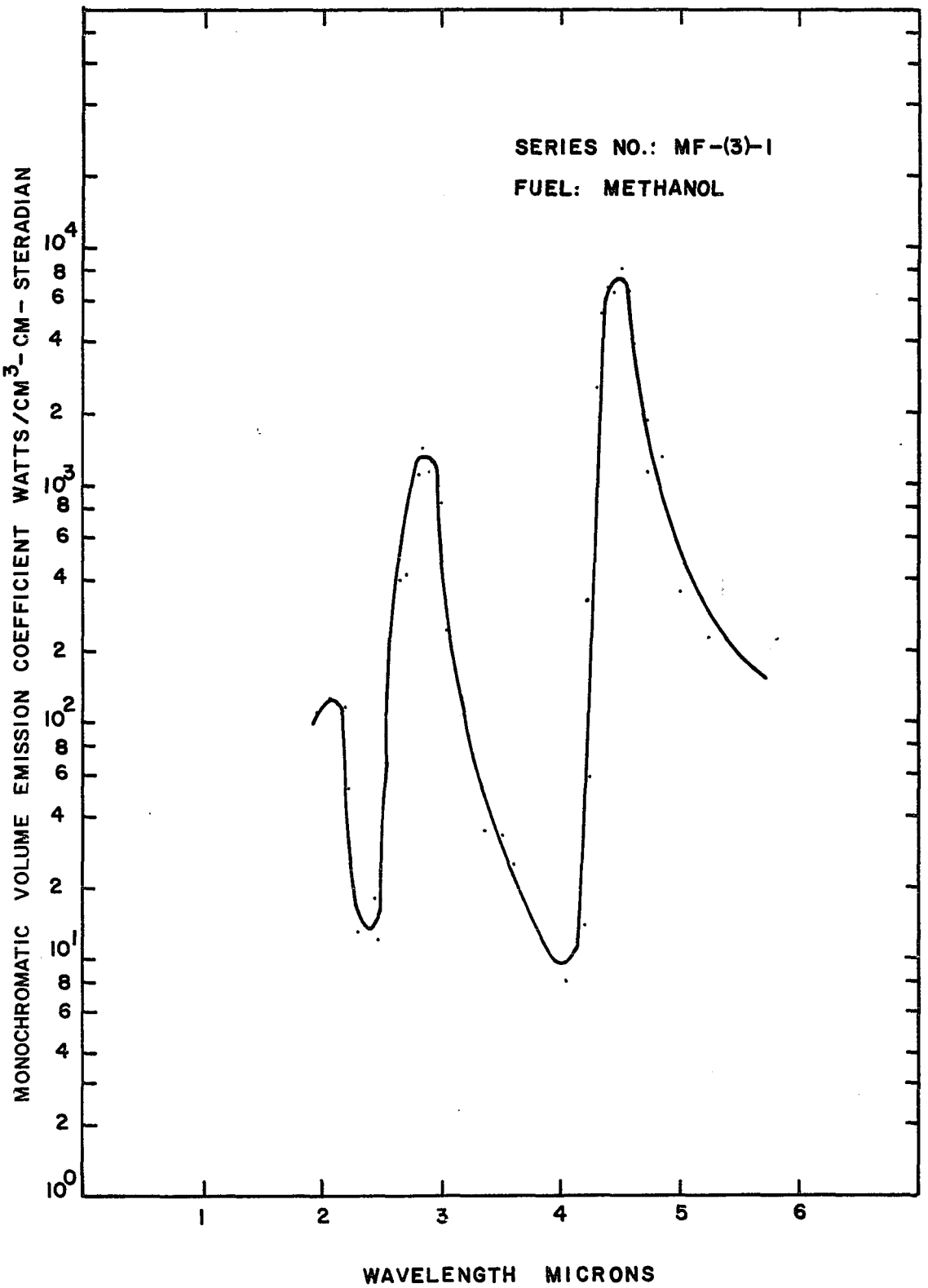


Figure 10. Monochromatic Volume Emission Coefficient of Methanol Flame

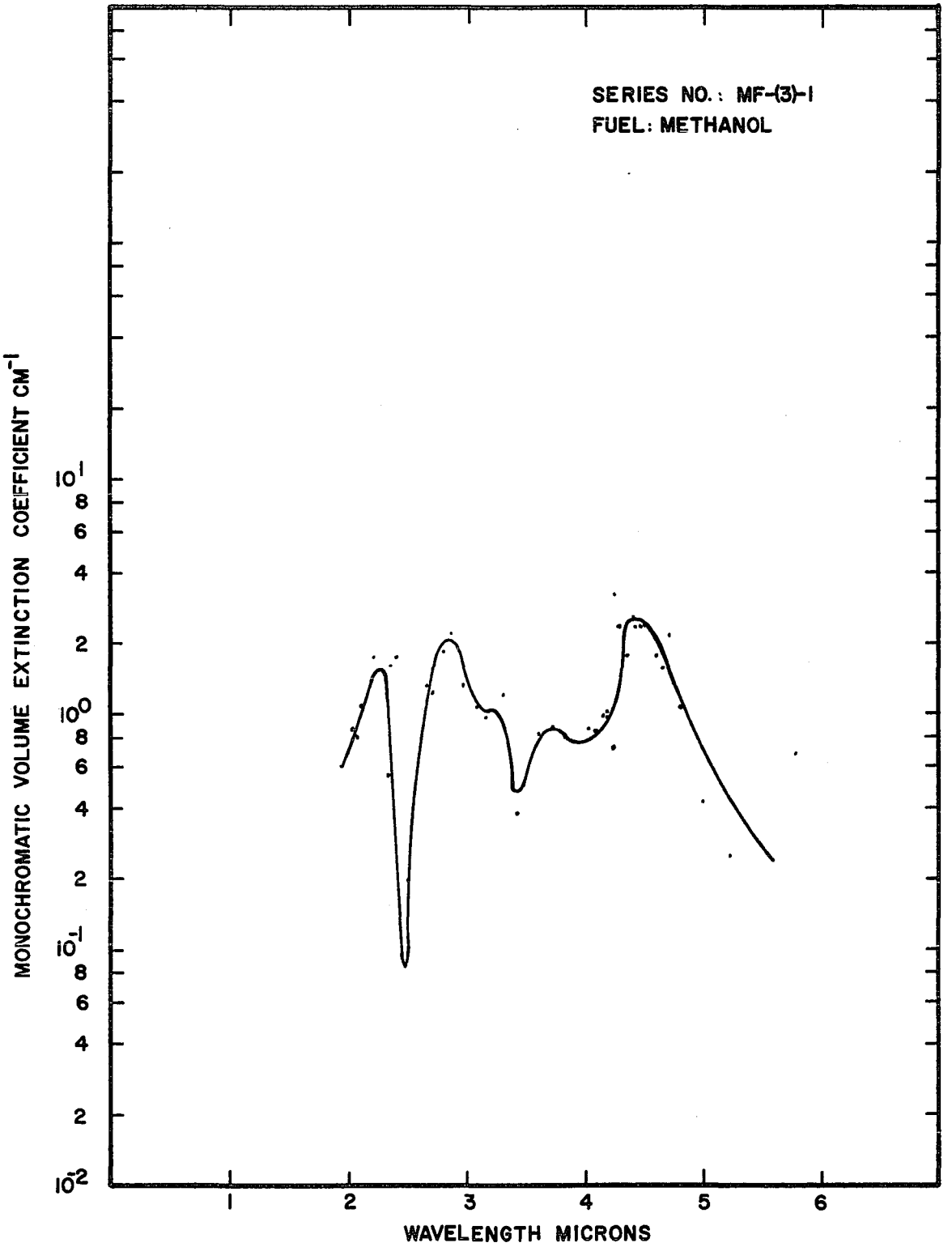


Figure 11. Monochromatic Volume Extinction Coefficient of Methanol Flame

entire emission source as shown in Figures 12 and 13. The acetone flame has a small continuum throughout the entire emission spectrum. However, the 2.7μ band and the 4.3μ band emission are the main emission sources. The acetone emission and extinction coefficients are shown in Figures 14 and 15. Figures 16 through 21 are J_λ and β_λ plots for n-hexane, cyclohexane, and benzene. The emission spectra for these flames are rather continuous throughout the entire region. The emission in the 2.7μ band and 4.3μ band are overshadowed by the continuum emission. It is interesting to note that the 4.3μ band emission is about the same for every fuel except acetone which is somewhat higher. It is the continuum emission that makes n-hexane, cyclohexane, and benzene give off considerable more total radiant energy than methanol, natural gas, and acetone.

Figures 22 through 27 are plots of J_λ/β_λ versus wavelength for the several fuels. For an opaque fire, J_λ/β_λ is the monochromatic flux per steradian at the given wavelength. Methanol, natural gas, and acetone flames emit mainly from the 2.7μ band and the 4.3μ band. As these fires get thicker, the 4.3μ band still provides the highest emission value. The emission spectra of n-hexane, cyclohexane, and benzene flames are very continuous. For thin fires the 4.3μ band has the highest emission value, however, as the fires get thicker, the highest emission value shifts to lower wavelength regions.

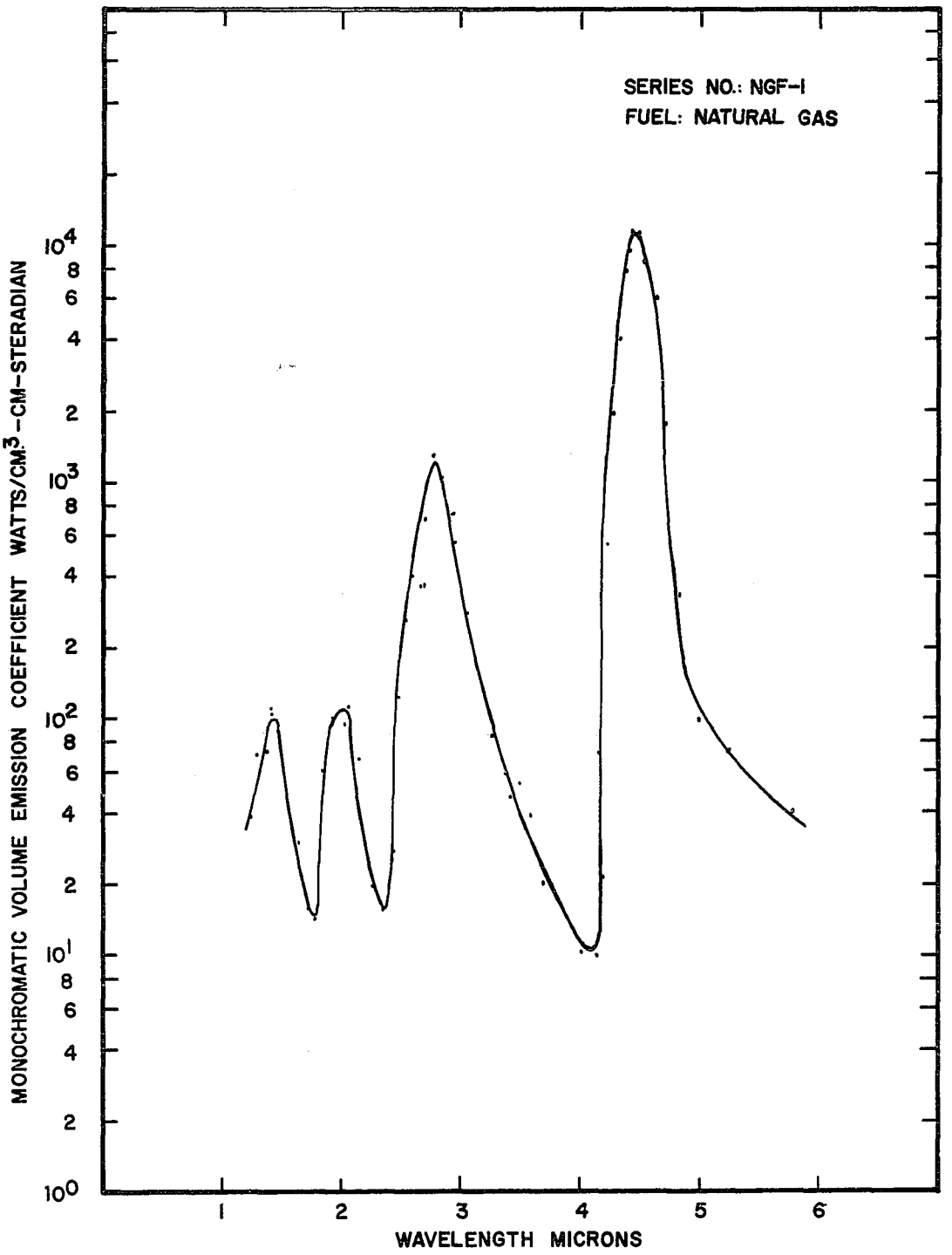


Figure 12. Monochromatic Volume Emission Coefficient of Natural Gas

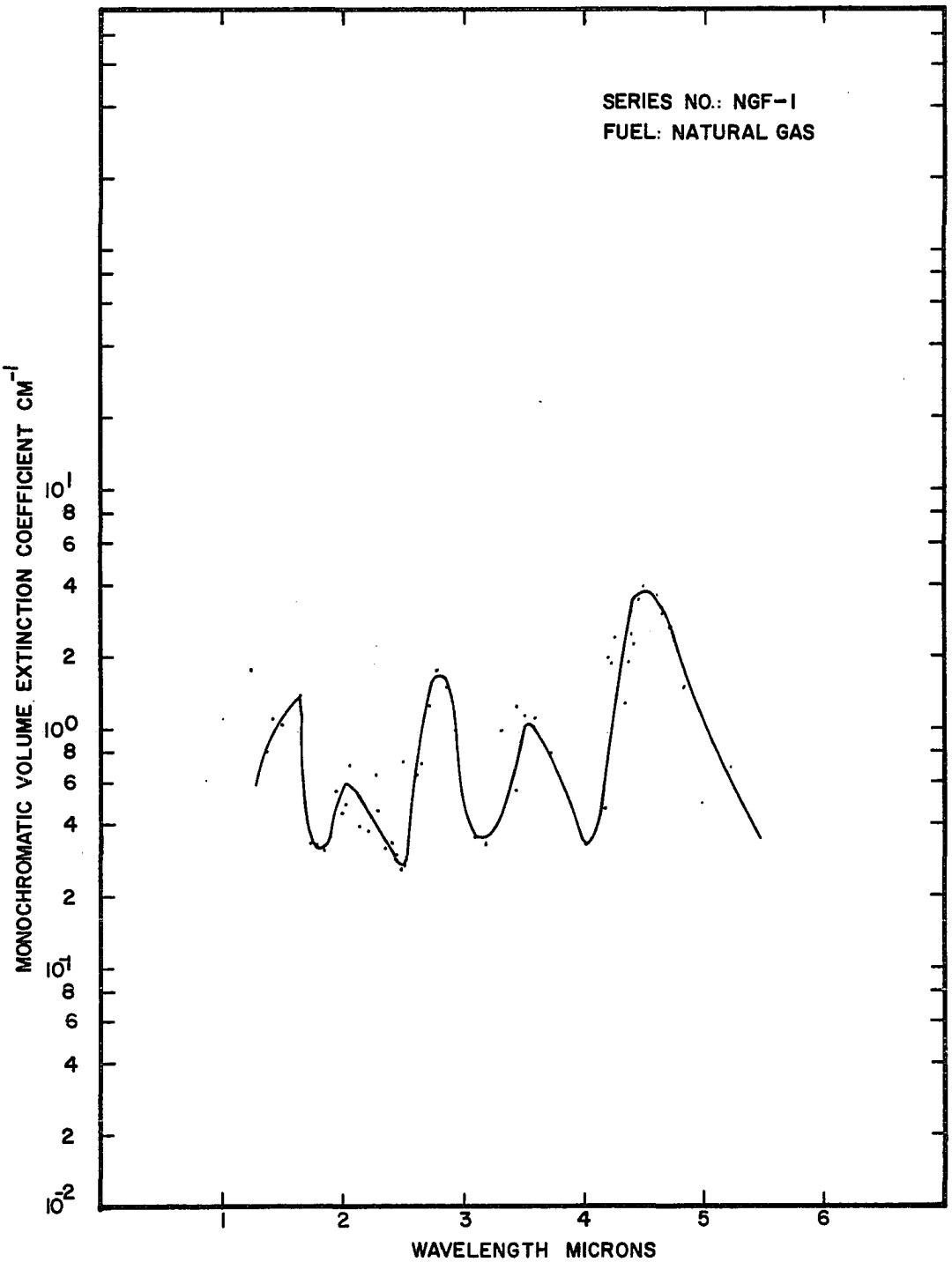


Figure 13. Monochromatic Volume Extinction Coefficient of Natural Gas

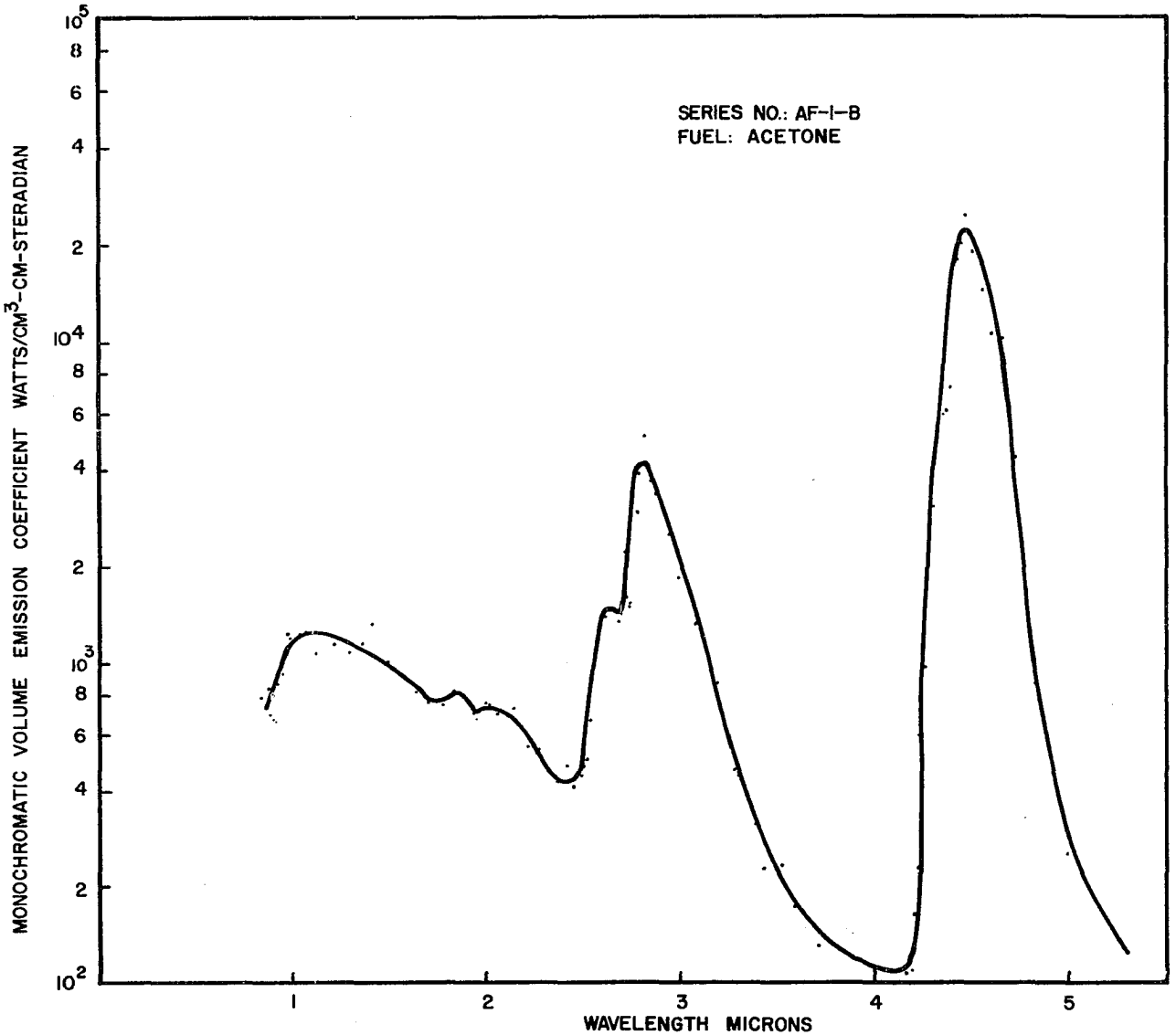


Figure 14. Monochromatic Volume Emission Coefficient of Acetone Flame

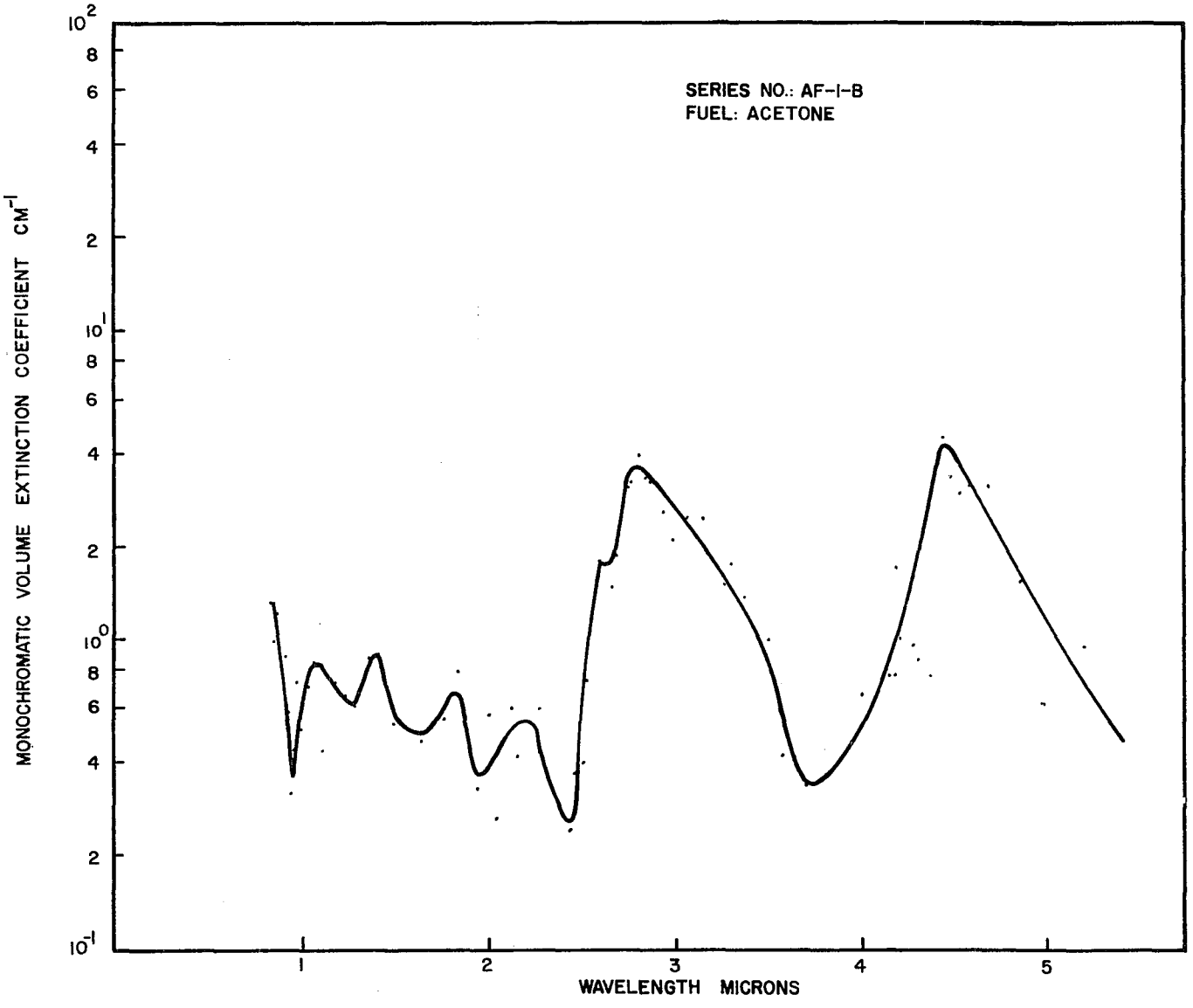


Figure 15. Monochromatic Volume Extinction Coefficient of Acetone Flame

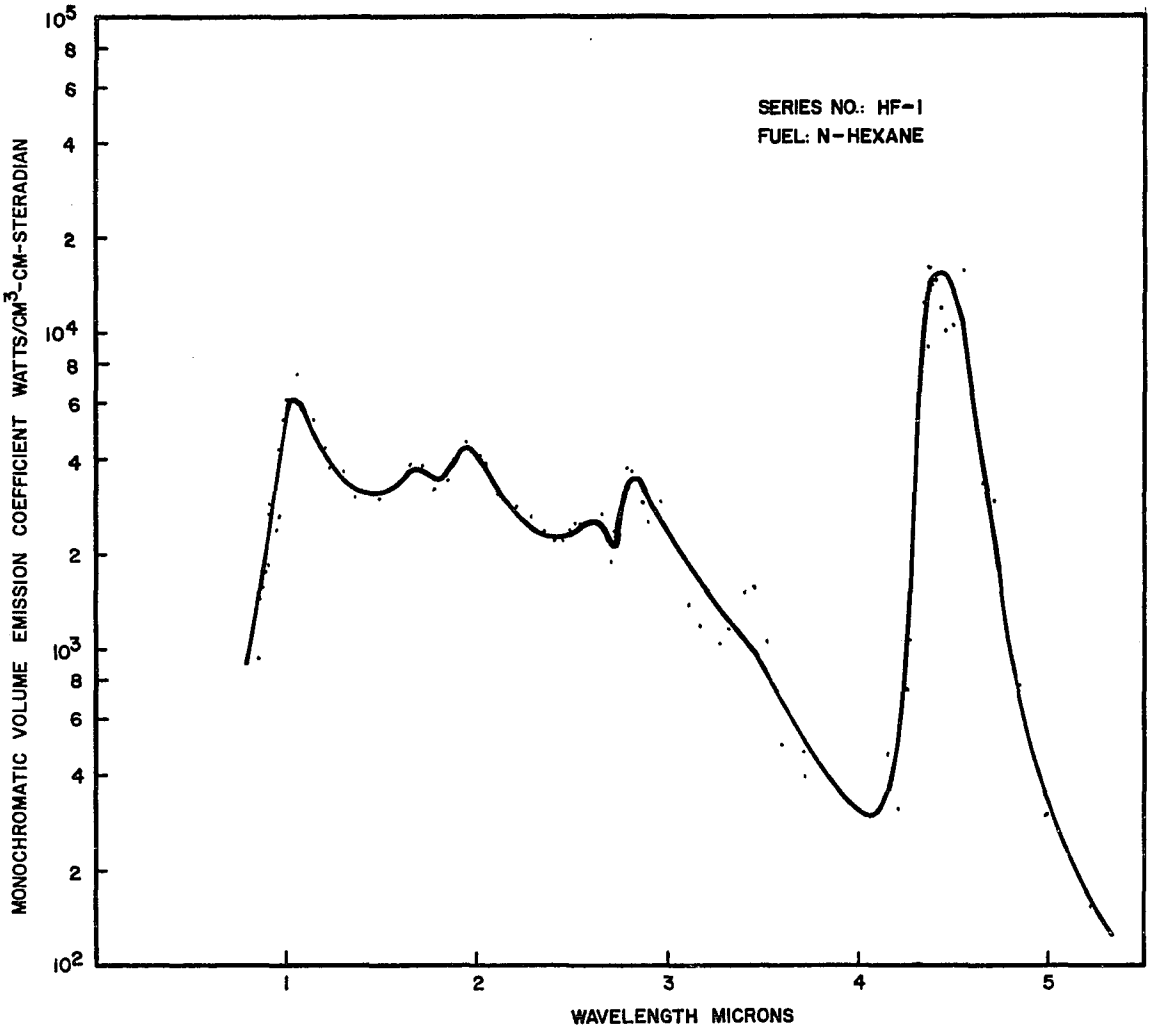


Figure 16. Monochromatic Volume Emission Coefficient of N-Hexane Flame

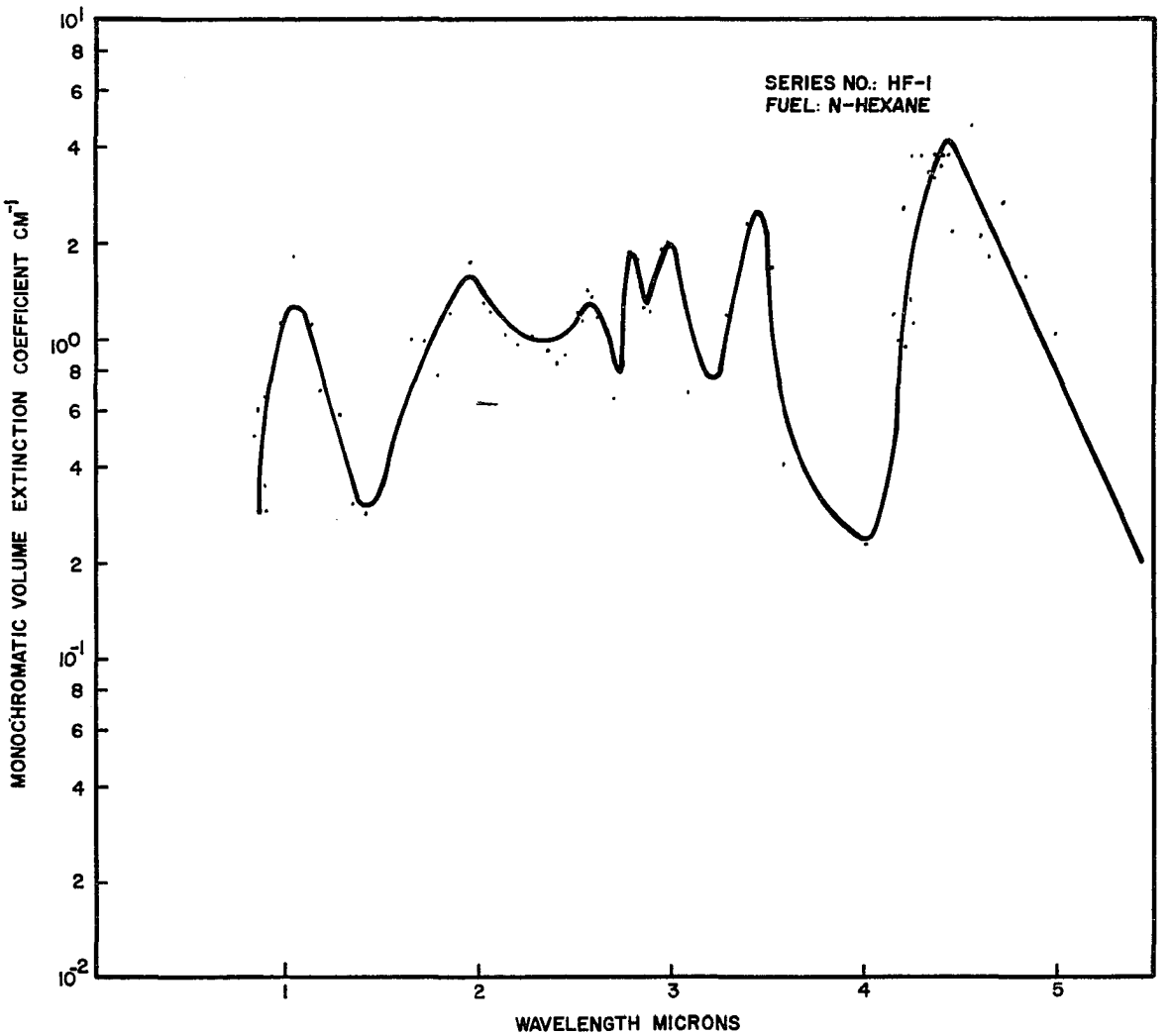


Figure 17. Monochromatic Volume Extinction Coefficient of N-Hexane Flame

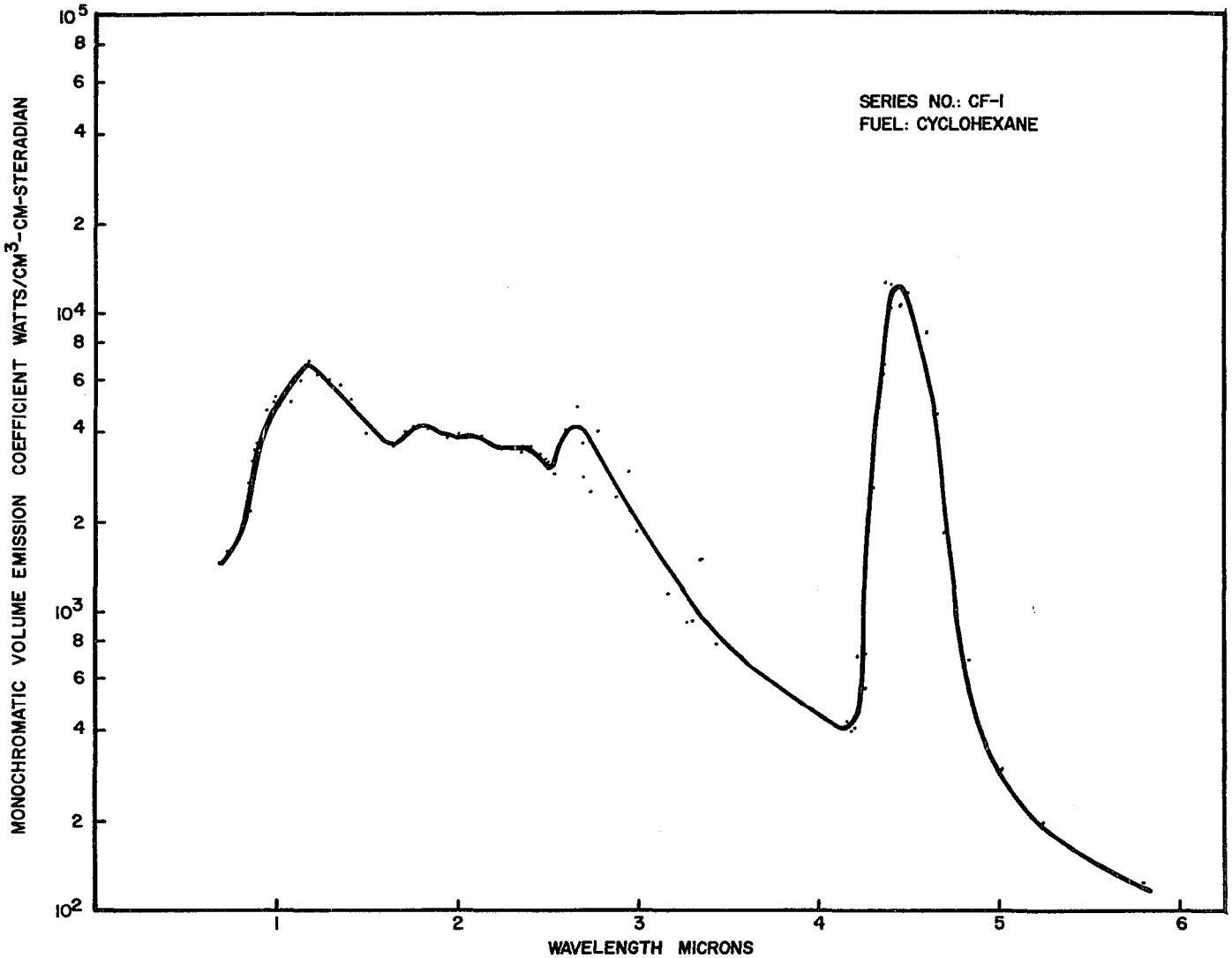


Figure 18. Monochromatic Volume Emission Coefficient of Cyclohexane Flame

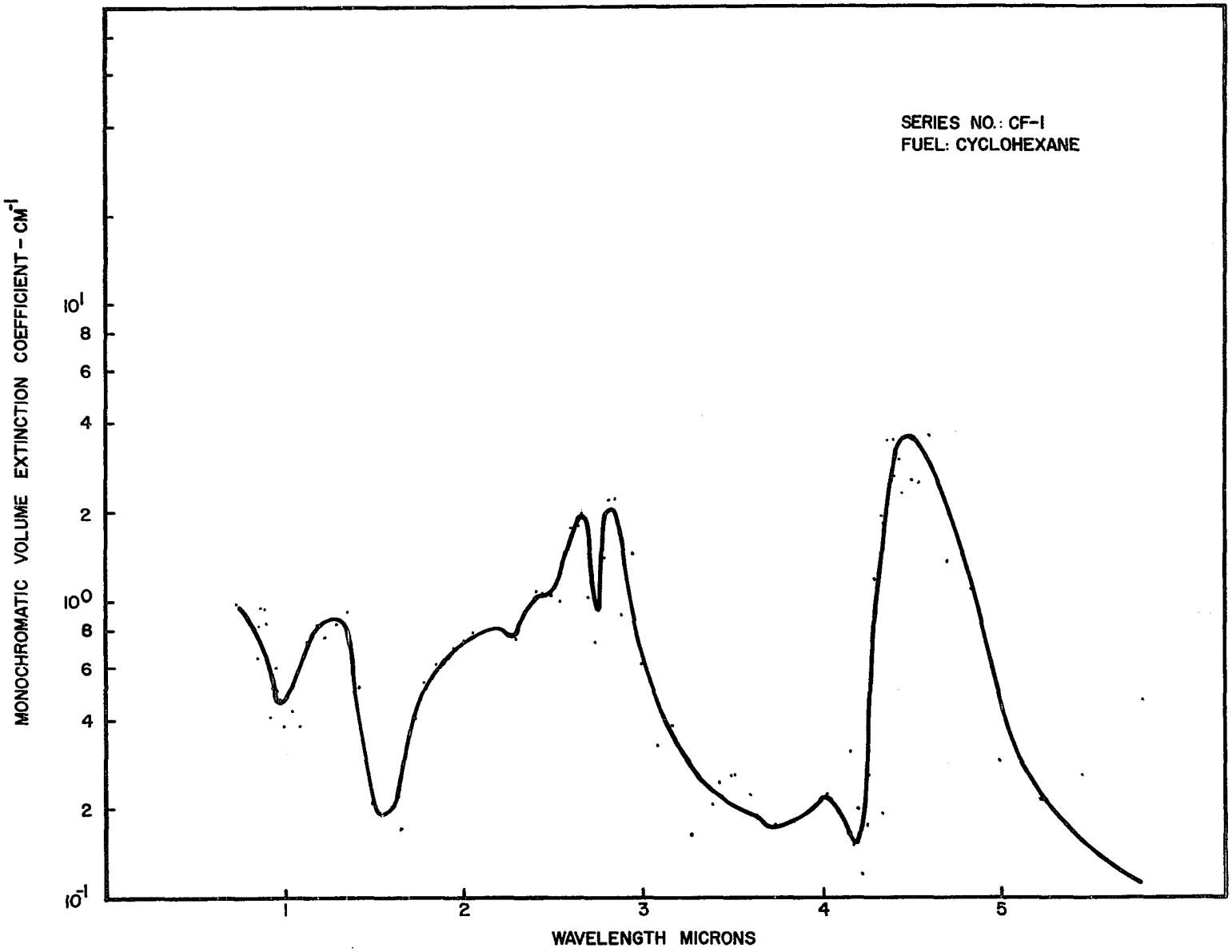


Figure 19. Monochromatic Volume Extinction Coefficient of Cyclohexane Flame

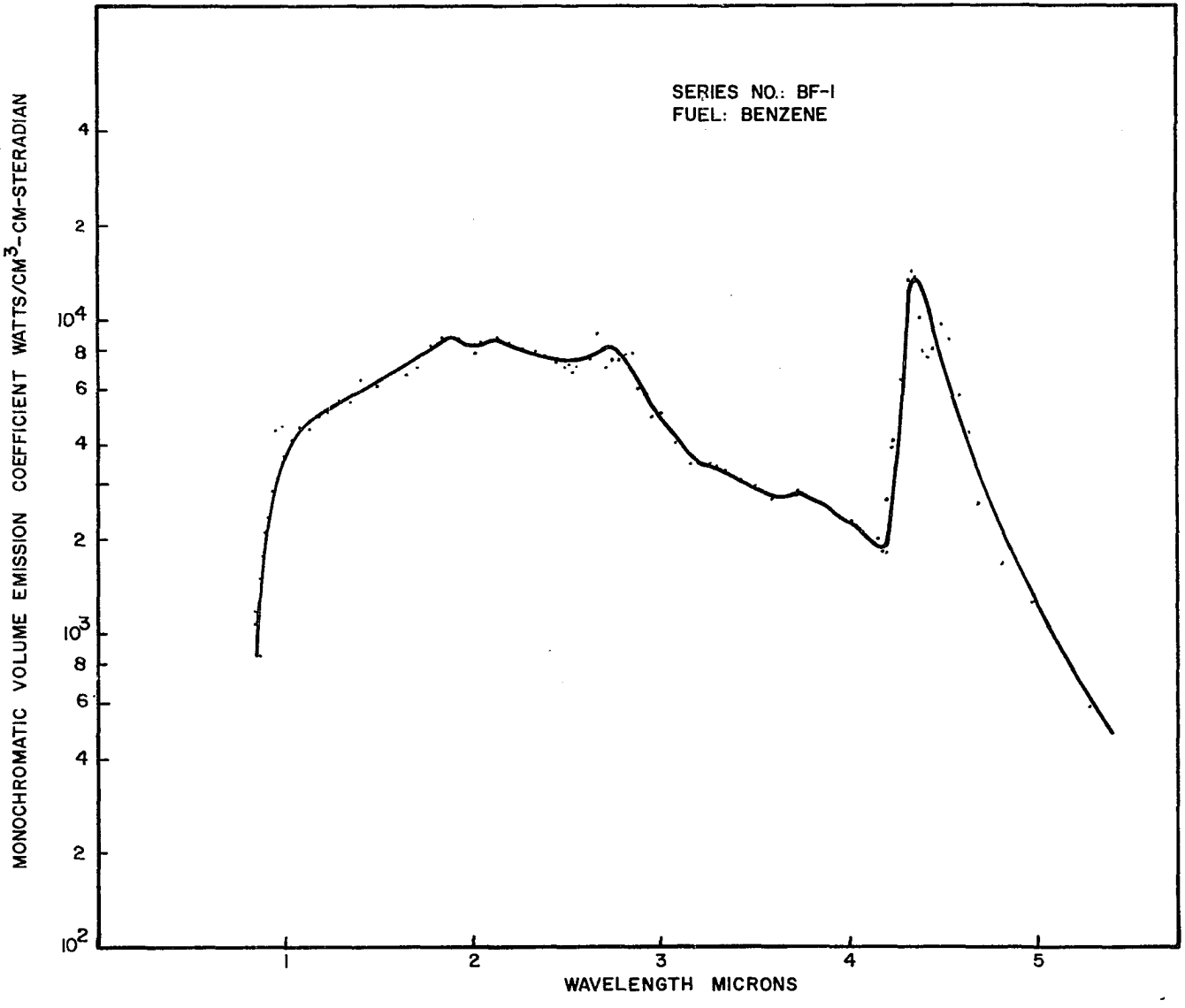


Figure 20. Monochromatic Volume Emission Coefficient of Benzene Flame

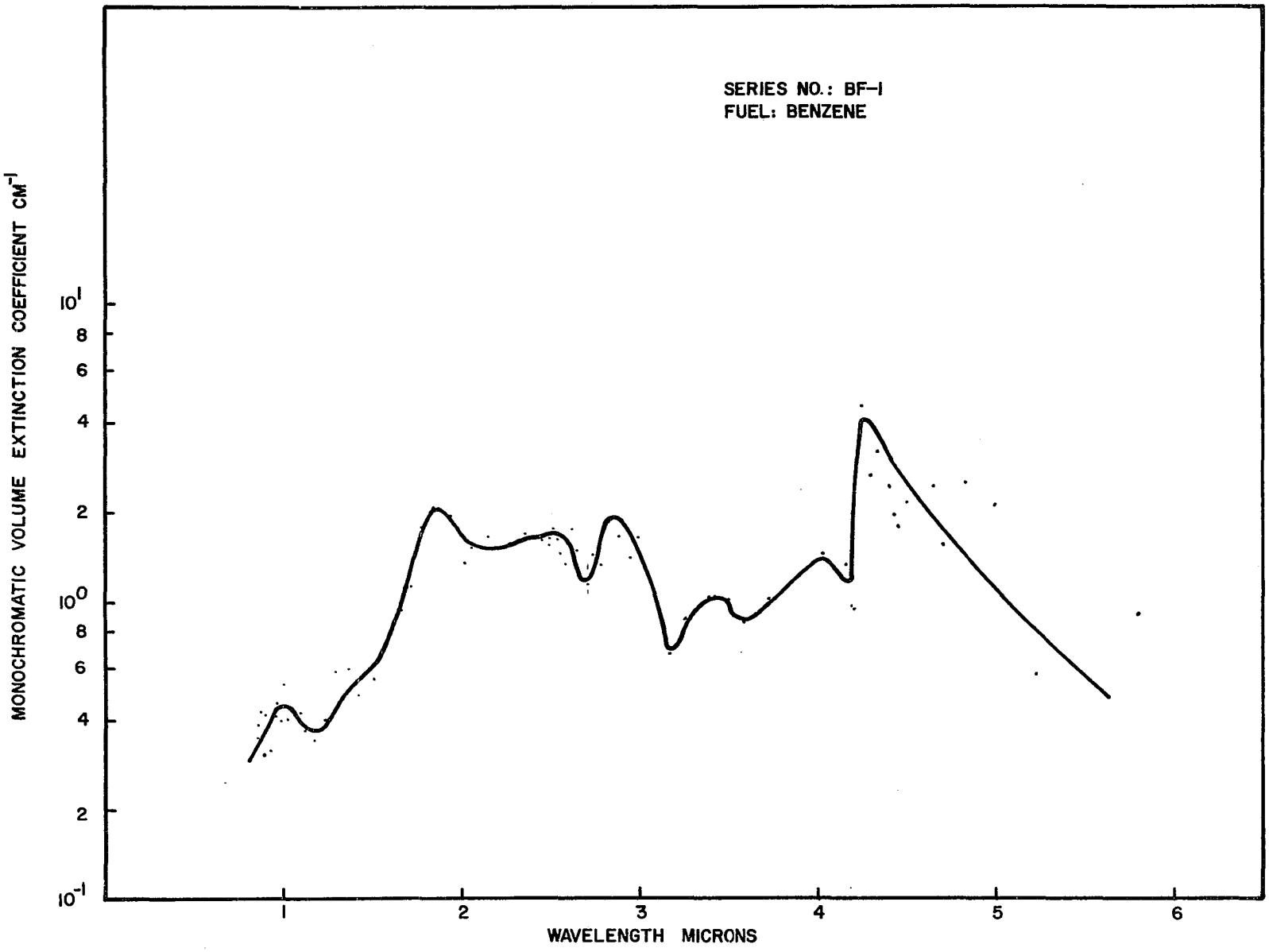


Figure 21. Monochromatic Volume Extinction Coefficient of Benzene Flame

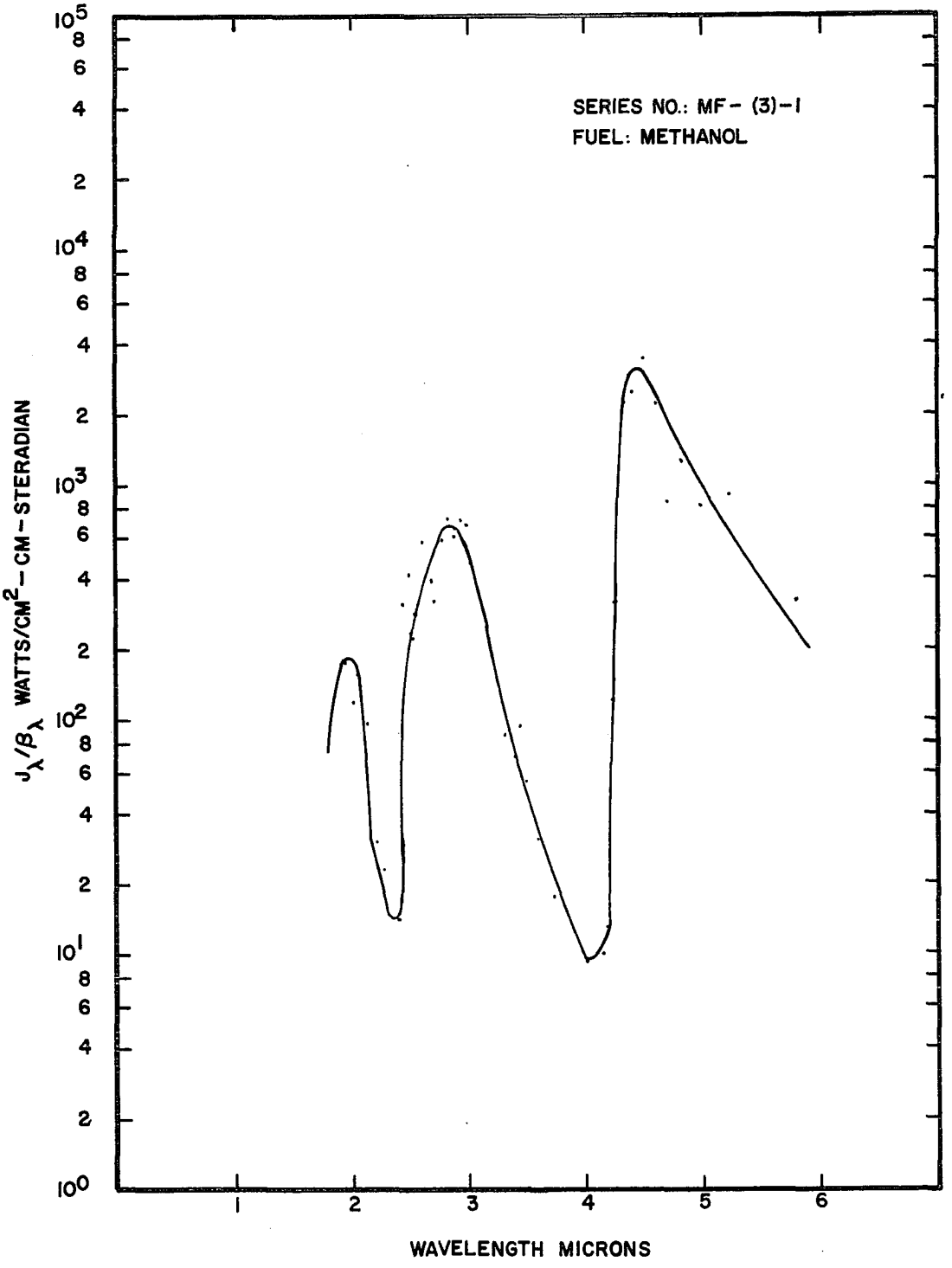


Figure 22. J_λ/β_λ of Methanol Flame

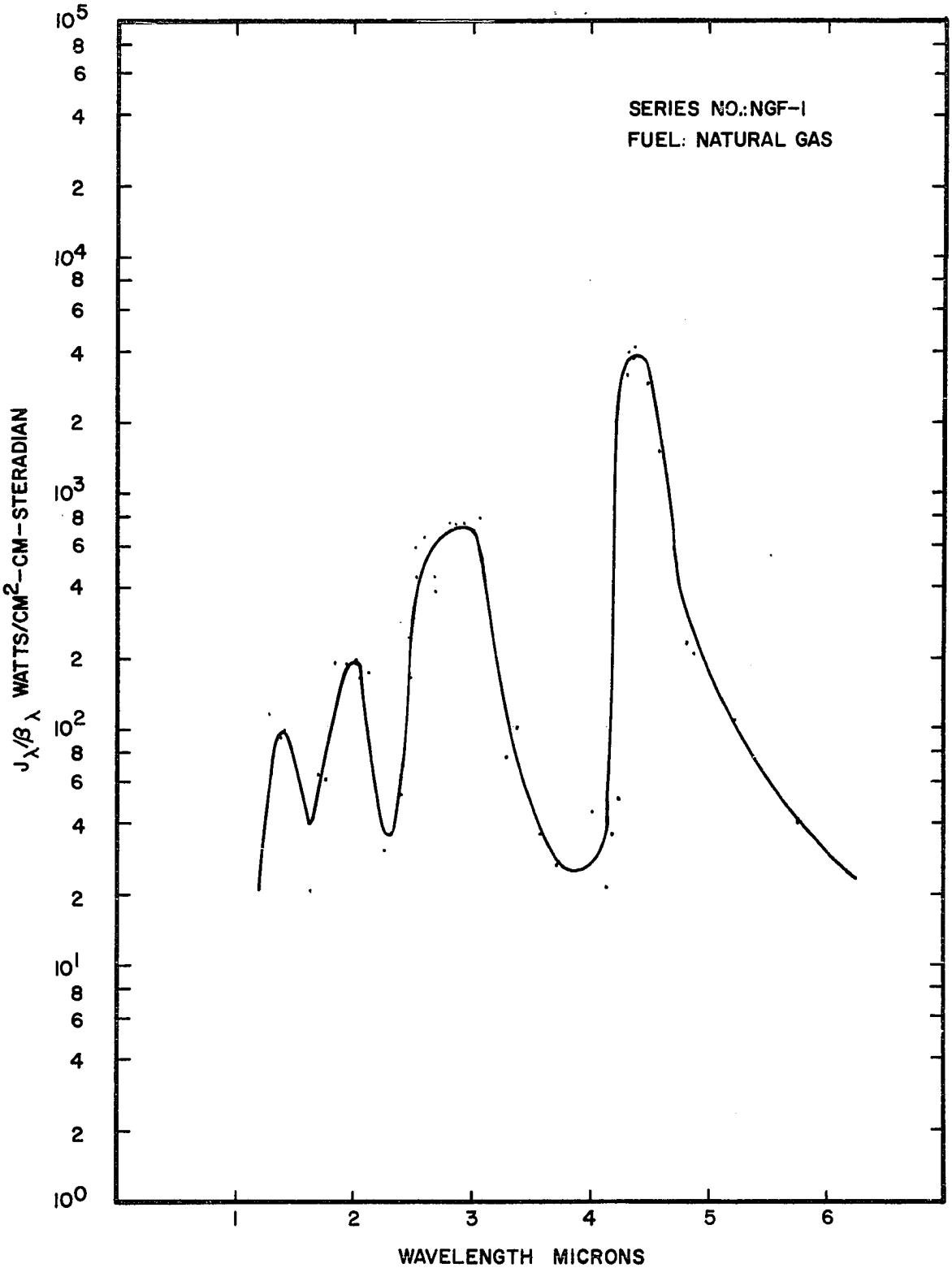


Figure 23. J_λ/β_λ of Natural Gas

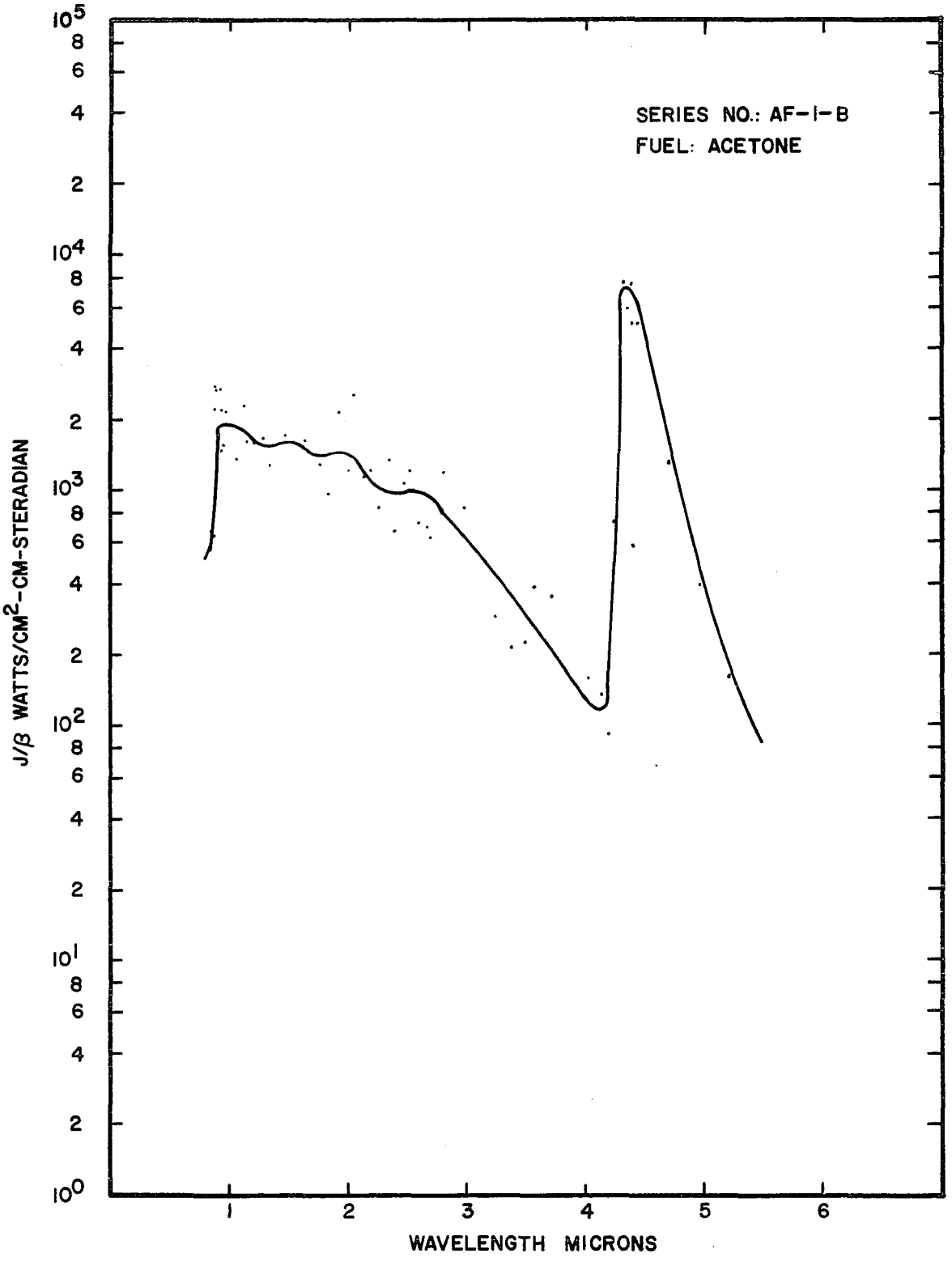


Figure 24. J_λ/β_λ of Acetone Flame

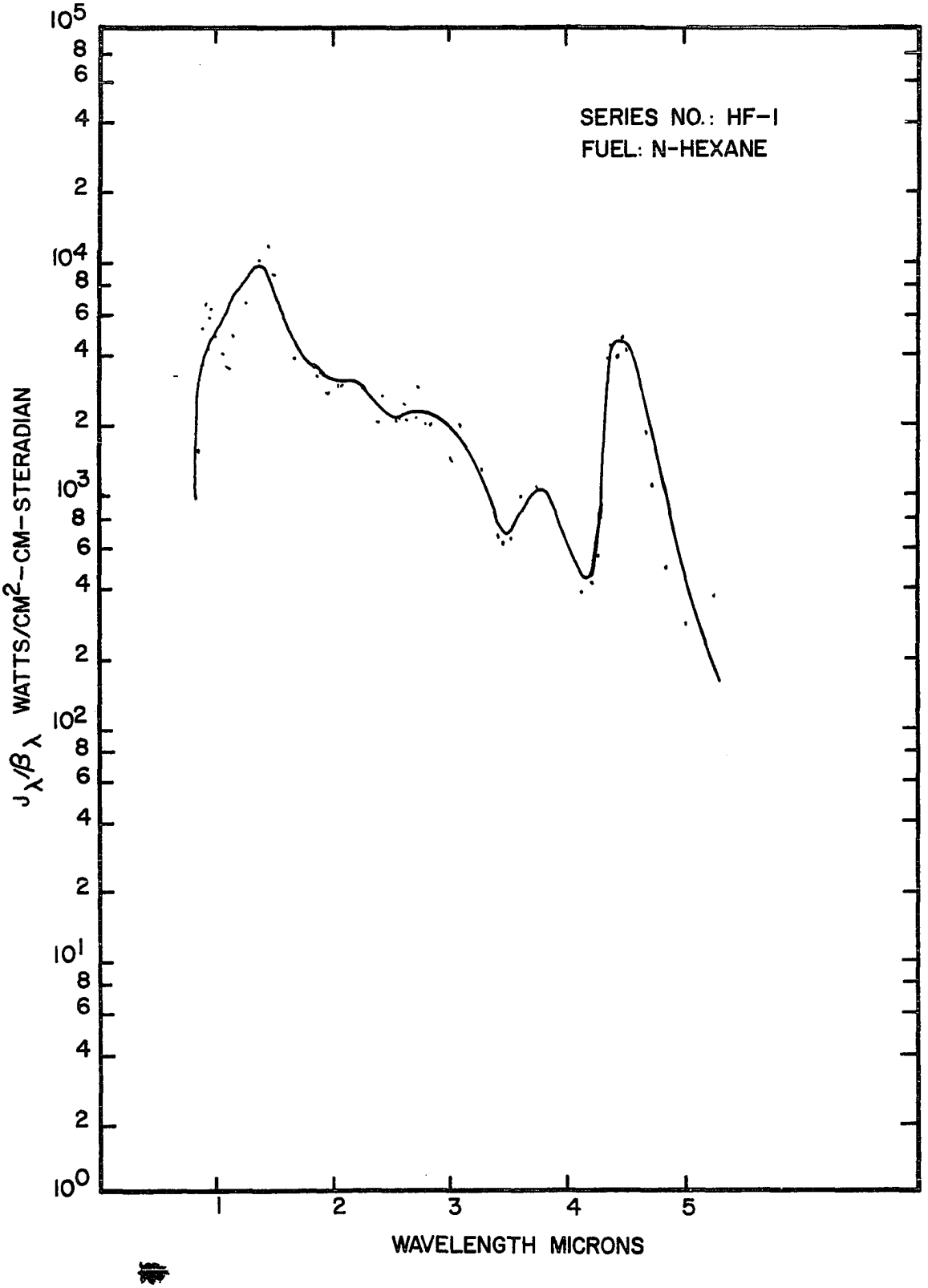


Figure 25. J_λ/β_λ of N-Hexane Flame

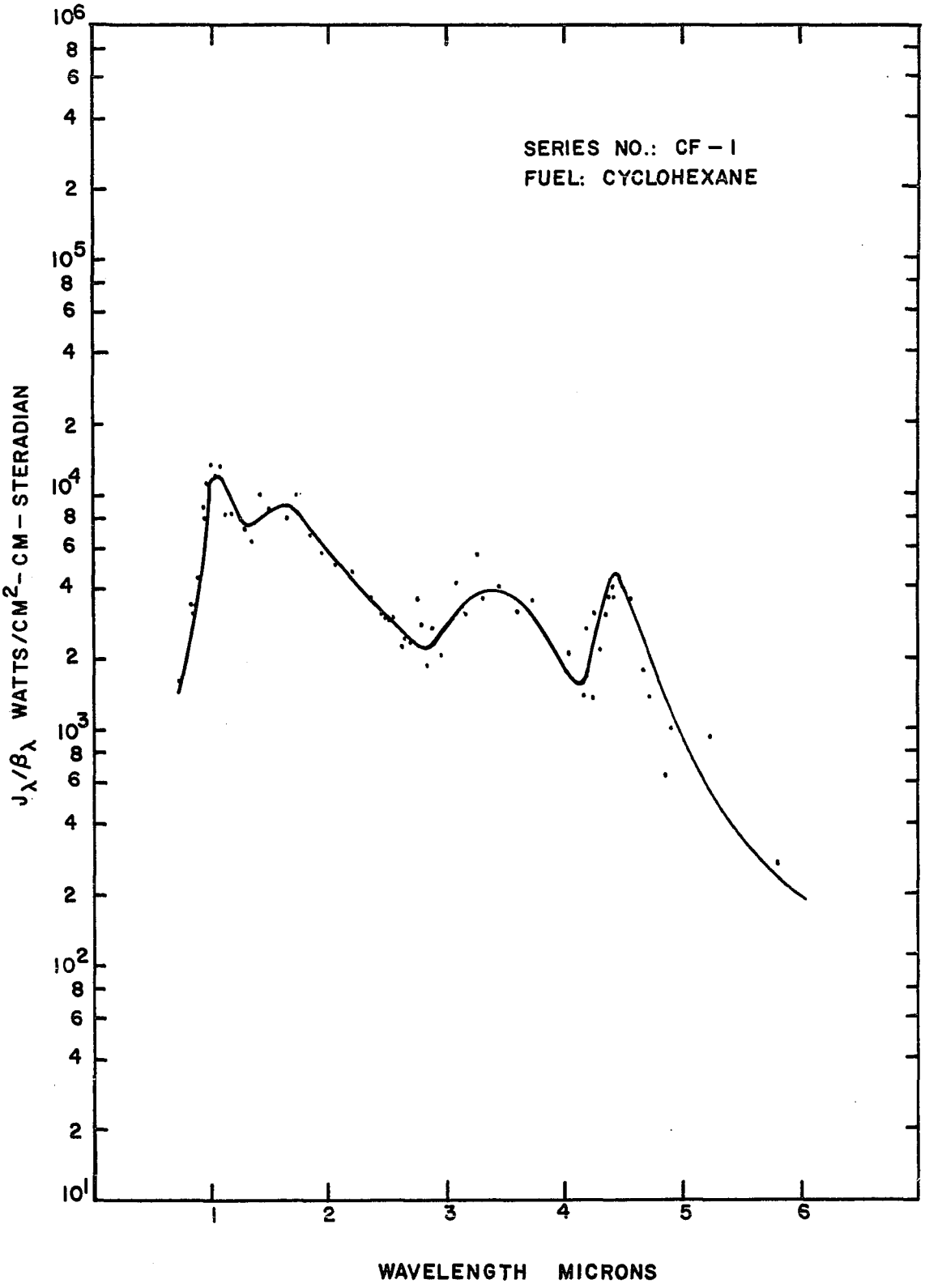


Figure 26. J_λ/β_λ of Cyclohexane Flame

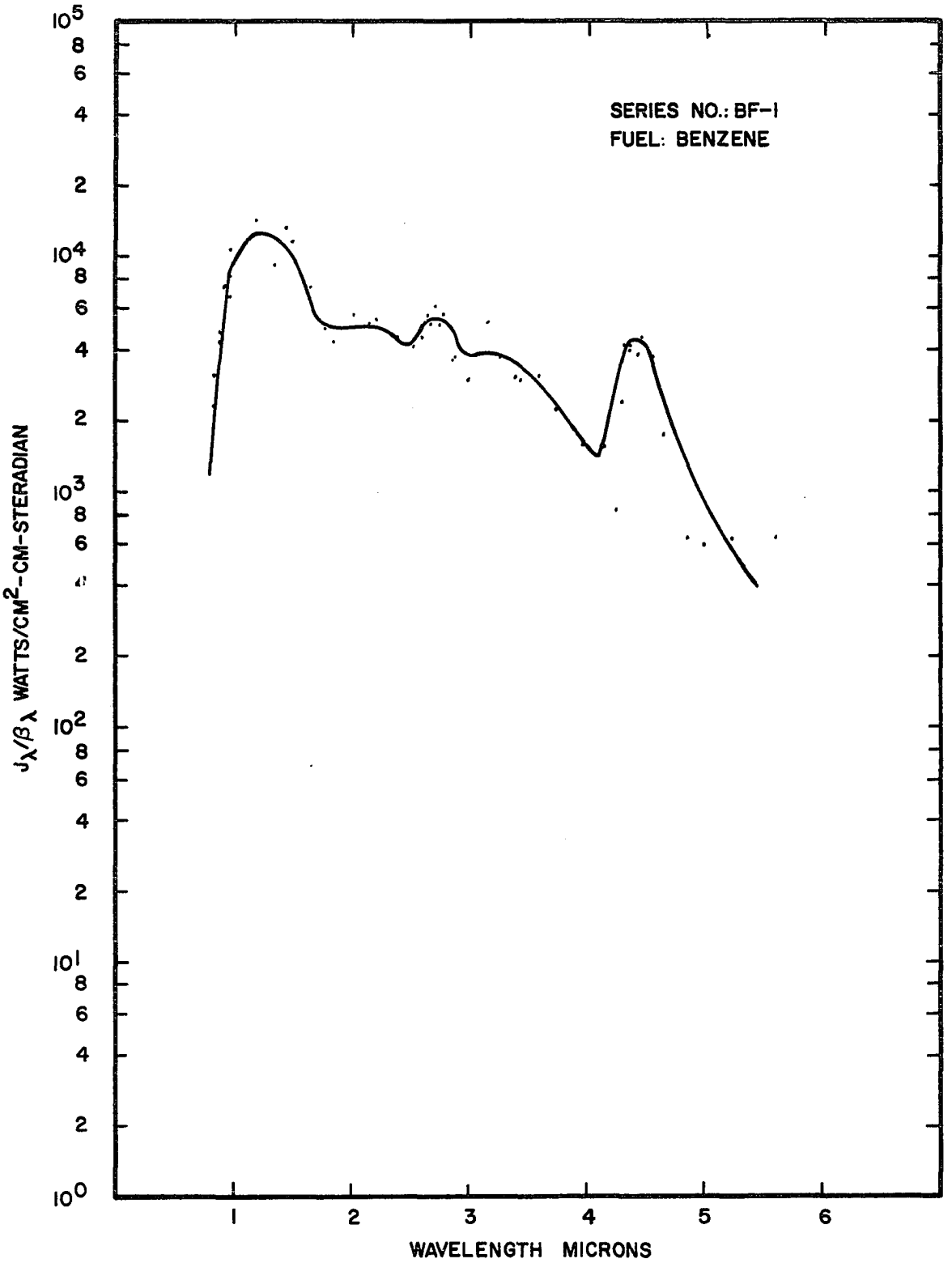


Figure 27. J_λ/β_λ of Benzene Flame

The radiative parameters J_λ and β_λ for fuel mixture are difficult to obtain, for different flames do not seem to mix. Figure 28 shows photographs of acetone, methanol, and acetone-methanol flames. It is interesting to note that the luminous acetone flame stays inside the dim methanol flame in the mixed flame, even though the fuels were thoroughly mixed before the combustion zone was reached. Data for fuel mixtures were not obtained.

Radiant flux per steradian versus path length was plotted for several fuels as shown in Figure 29. As seen from the figure, once a certain path length is reached, each fuel emits essentially independent of the path length. This is expected because the flame gets optically thick and begins to emit effectively as a surface source rather than a volume source. It is found from Figure 29 that every fuel except natural gas gets optically thick at about the same distance. For prediction of radiant flux from a hemispherical flame, the values of Figure 29 must be multiplied by π steradians.

Hood (26) used a different approach to compute J_λ and β_λ (see Chapter I). The procedure he introduced was to obtain the measured values of I_λ (Globar + Flame), I_λ (Flame), and I_λ (Globar) as follows. "First a spectrogram was taken of the sum of the intensity emitted by the flame and that portion of the intensity emitted by the globar which was transmitted through the flame. A shutter was then placed

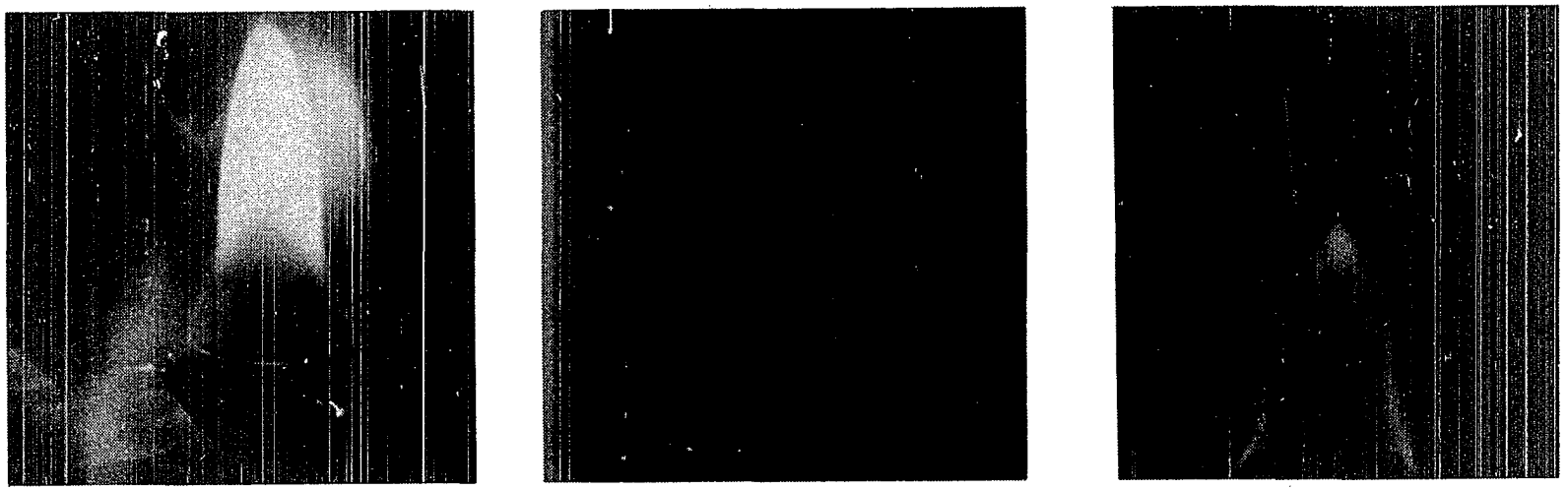


Figure 28. Acetone, Methanol and Acetone-Methanol Flames

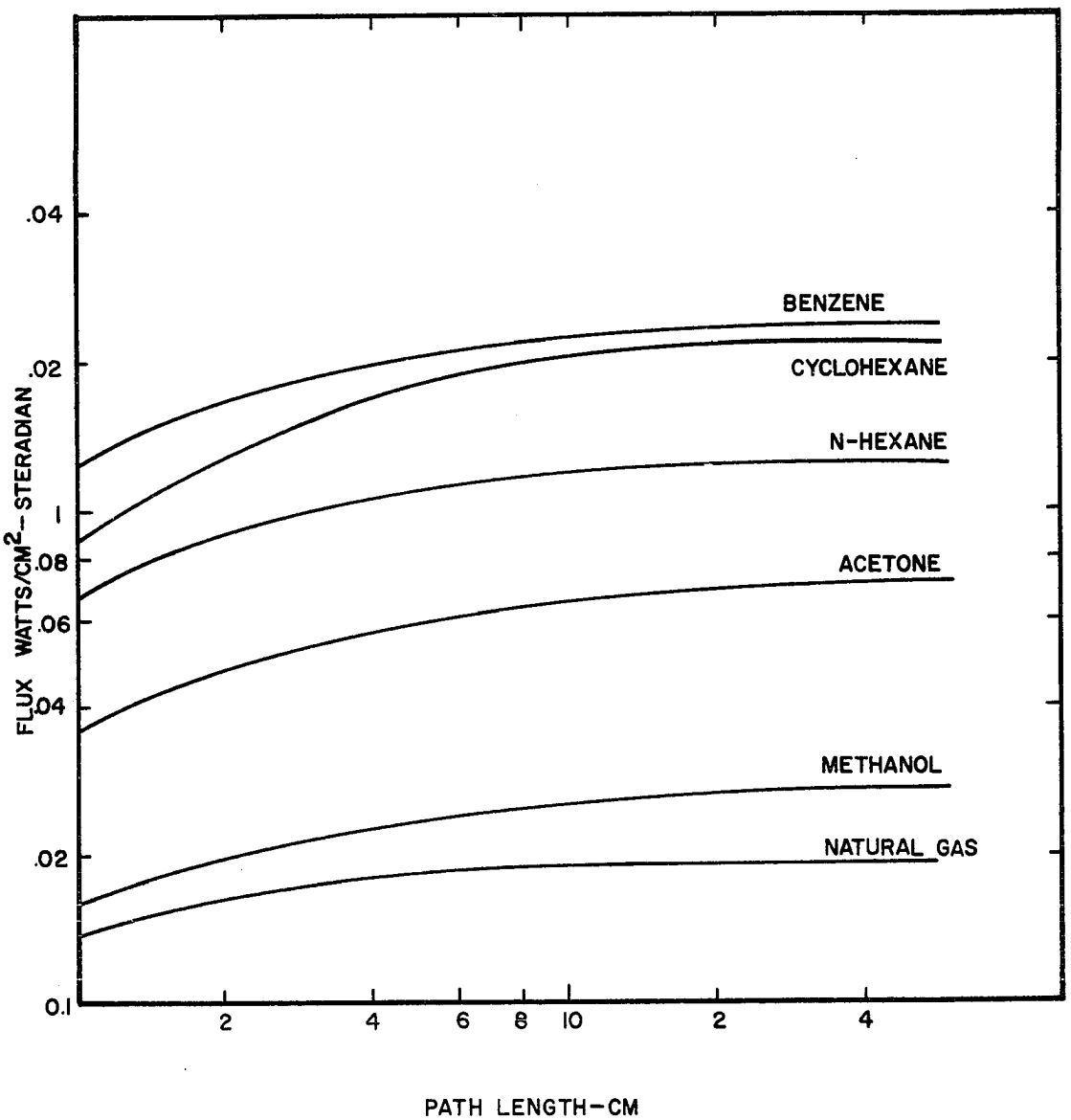


Figure 29. Flame Extrapolation

in front of the globar and a spectrogram of the intensity emitted by the flame was taken. The temperature of the globar was recorded throughout the first spectrogram. Since the output of the spectrometer had been calibrated in terms of intensity, $I_{\lambda a}$ (Globar + Flame) could be determined from the first spectrogram and $I_{\lambda b}$ (Flame) could be determined from the second spectrogram." This was a good method as long as the temperature of the globar stays constant or the monochromatic emittance of the globar at every temperature is known. However, the temperature of the globar is very susceptible to fluctuations in voltage. One volt deviation of the electrical power supply will cause about 60°F difference in the globar temperature. So far there is no way to keep voltage fluctuation within a very small range, so that the globar temperature will not be affected appreciably. Besides, the information about the monochromatic emissivity of the globar at the temperature range of 800°F - 1300°F which was used in the work is lacking. Furthermore, the emission spectrum of the globar source will not cover the entire emission spectra of flames. At near visible range, a tungsten lamp has to be used. Again, the monochromatic emittance of the tungsten lamp is unknown and the temperature is difficult to determine. Thus it is difficult to obtain a reliable value for source intensity for the calculations.

The drawback of the two flame methods used in this work is that J_λ and β_λ cannot be obtained in the inner cone of the flame. However, due to its lacking of oxygen in this region, presumably, there is no appreciable emission. The spectroscopy of the inner cone region by having the monochromator viewed through it indicated that the emission very likely comes from the surrounding thin luminous layer.

An extrapolation program to determine the radiative heat transfer from flame to a target was first worked out by Shahrokhi (47), and was later clarified (55). Flames were classified to be cylindrical, conical, or sheet. A cylindrical flame or conical flame is obtained from a circular burner. Careful judgment needs to be made to determine whether the flame is cylindrical or conical.

For a cylindrical flame, the flame is considered to occupy a cylindrical volume by having a mean diameter and height. The flame sub-division is made by M horizontal planes and N vertical planes, as shown in Figure 30.

Thus (55)

$$H_m = \frac{H}{M} \tag{27}$$

$$R_m = \frac{R}{N} \tag{28}$$

The area of element mn on the midsection of the flame projected normal to γ_{mn} is

$$A_{mn} = R_n H_m \text{ Cos } \delta_{mn} \text{ Cos } \varphi_{mn} \tag{29}$$

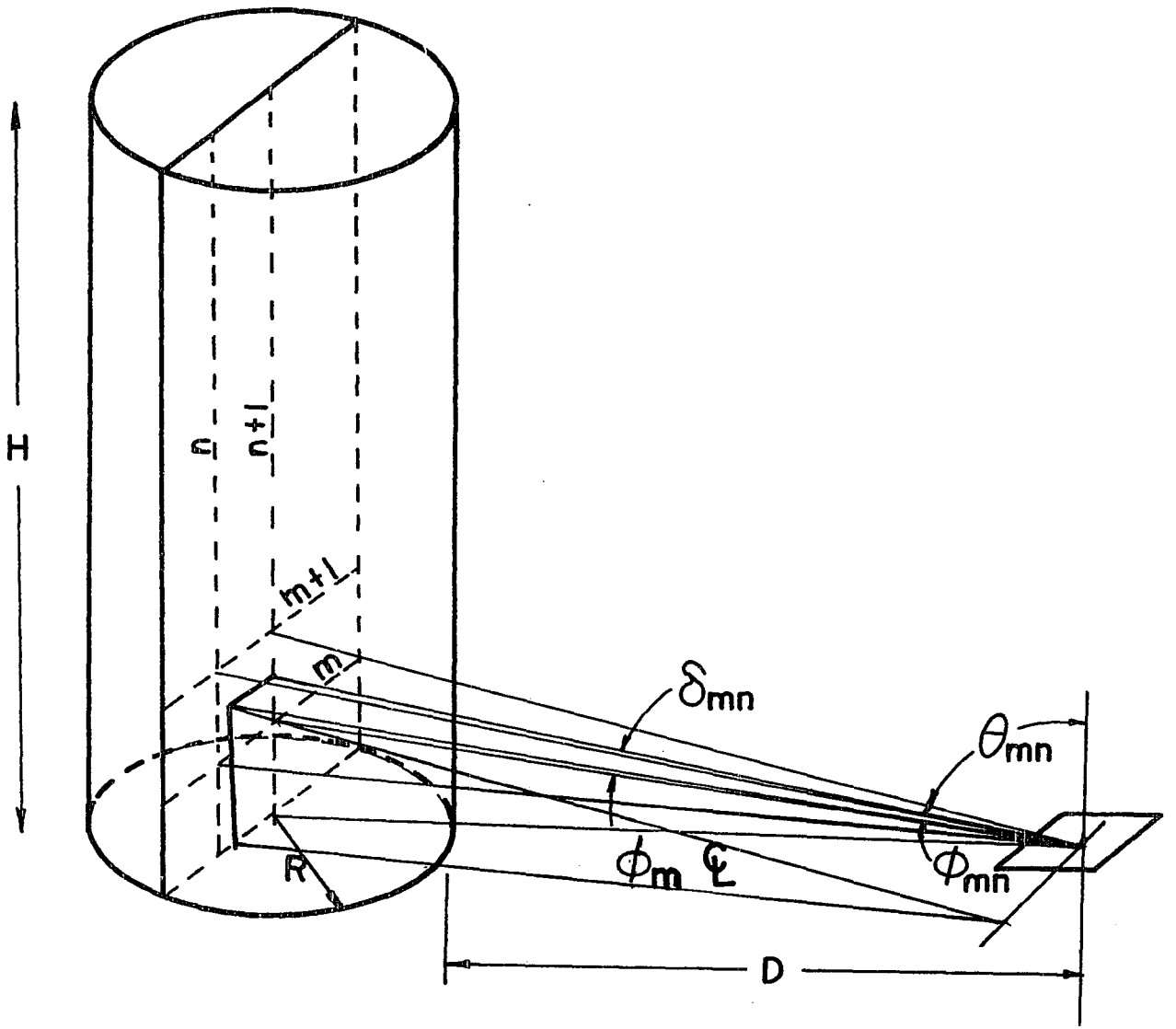


Figure 30. Geometry for Cylindrical Flame

Other geometric relations are:

$$\tan \varphi_{m\mathfrak{L}} = \frac{(m - \tfrac{1}{2}) H_m}{D + R} \tag{30}$$

$$\tan \delta_{mn} = \frac{R - (N - \tfrac{1}{2}) R_n}{\left[(D+R)^2 + [(m-\tfrac{1}{2}) H_m]^2\right]^{\frac{1}{2}}} \tag{31}$$

$$\operatorname{Cos} \delta_{mn} = \frac{\operatorname{Sin} \delta_{mn}}{\tan \delta_{mn}} = \frac{R - R_n(n - \tfrac{1}{2})}{r_{mn} \tan \delta_{mn}} \tag{32}$$

$$\operatorname{Sin} \varphi_{mn} = \frac{(m - \tfrac{1}{2}) H_m}{\left[[(m - \tfrac{1}{2}) H_m]^2 + (R + D)^2 + [R - (n - \tfrac{1}{2}) R_n]^2\right]^{\frac{1}{2}}} \tag{33}$$

Optical Depth $$a_{mn} = \frac{2R}{\operatorname{Cos} \varphi_{mn}} \left(1 - \operatorname{Sin}^2 \gamma\right)^{\frac{1}{2}} \tag{34}$$

where $$\operatorname{Sin} \gamma = \frac{(R + D) \operatorname{Sin} \delta}{R} \tag{35}$$

and $$\operatorname{Sin} \delta = \frac{[R - (n - \tfrac{1}{2}) R_n]}{\left[(D + R)^2 + [R - (n - \tfrac{1}{2}) R_n]^2\right]^{\frac{1}{2}}} \tag{36}$$

$$\Omega_{mn} = \frac{A_{mn}}{r^2_{mn}} = \frac{R_n H_m \operatorname{Cos} \delta_{mn} \operatorname{Cos} \varphi_{m\mathfrak{L}}}{(R + D)^2 + [R - (n - \tfrac{1}{2}) R_n]^2 + [(m - \tfrac{1}{2}) H_m]^2} \tag{37}$$

$$\theta_{mn} = \frac{\pi}{2} - \varphi_{mn} \tag{38}$$

The incident monochromatic flux at the target is

$$Q_\lambda = 2 \frac{J_\lambda}{\beta_\lambda} \sum_{m=1}^{M} \sum_{n=1}^{N} \left[1 - \exp(-\beta_\lambda a_{mn})\right] \Omega_{mn} \operatorname{Cos} \theta_{mn} \tag{39}$$

The total flux reaching the target was obtained by numerical integration over the entire emission region.

$$Q = \int_{\lambda_1}^{\lambda_2} Q_\lambda \, d\lambda \qquad (40)$$

Since 0.743μ to 5.79μ is the only region where every fuel in this work emits, these two values are used for the limits.

It is obvious that radiation from diffusion flames depends largely on its surrounding conditions. A comparatively big region of inner cone will result in an environment of insufficient oxygen, while a fuel pool burning in the open air with wind blowing will decrease the inner cone region and consequently will give off more radiation. Big fires are very turbulent. It is difficult to determine a suitable flame size for big fires. Schemes and rules for flame size determination need to be developed. Inner cone volume, which presumably contributes the least emission, needs to be evaluated. For very large fires, the effect of the deviation of the fire dimensions could be smaller than for moderate size fires. However, the radiometer reading from a big fire could be appreciably affected by its elevation. This effect is caused mainly by two factors; first, the geometry configuration Cos θ as shown in equation (39); second, at which zone the radiometer directly faces. A radiometer placed at the same level as the fuel pool will face the inner cone region directly and apparently will

collect less radiation. An extensive study of these factors is necessary to permit determination of a suitable flame dimension for flux computation.

Huffman (27) made an investigation of flame interaction and merging. In his work, nine (9) pools were arranged as shown in Figure 31. It appears that merging flames are more stable than a single pool flame, and therefore their geometry can be found more easily.

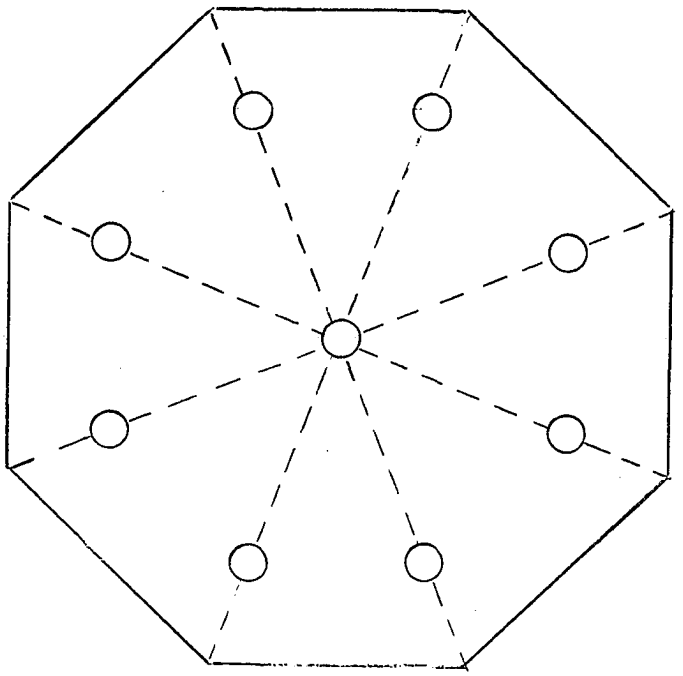


Figure 31. Schematic Diagram of Flame Merging Table.

Because there are distances between the individual pools, it is obvious that this set-up will enable more air to mix with fuel vapor. Consequently, comparatively small inner cones will result. Huffman measured the radiant flux using a radiometer with a quartz window at a certain elevation at various distances. Pictures were taken. A planimeter was used to determine the projected area of the flame from the picture. Diameters at the base, 1/4 flame height, 1/2 flame height, 3/4 flame height, and at the top were measured. The mean diameter was obtained by averaging the measurements at different heights. The mean height of the cylindrical flame was obtained by dividing the projected area by the mean diameter. These dimensions, together with the monochromatic transmittance of the quartz window, the monochromatic transmittance of the atmosphere, and the measured J_λ and β_λ from the laboratory were submitted to a computer program (See Appendix C) based on equations (39) and (40). Figures 32 through 38 show the comparisons between the experimental values and the predicted values for acetone, n-hexane, and cyclohexane. It is found that in most cases, the predicted values are higher. This is because the volume occupied by the inner cone region is not excluded from the flame size determination and because of the air entrained into the turbulent flames during combustion. The regions occupied by the inner cone and the entrained air do not radiate as effectively as the outer cone.

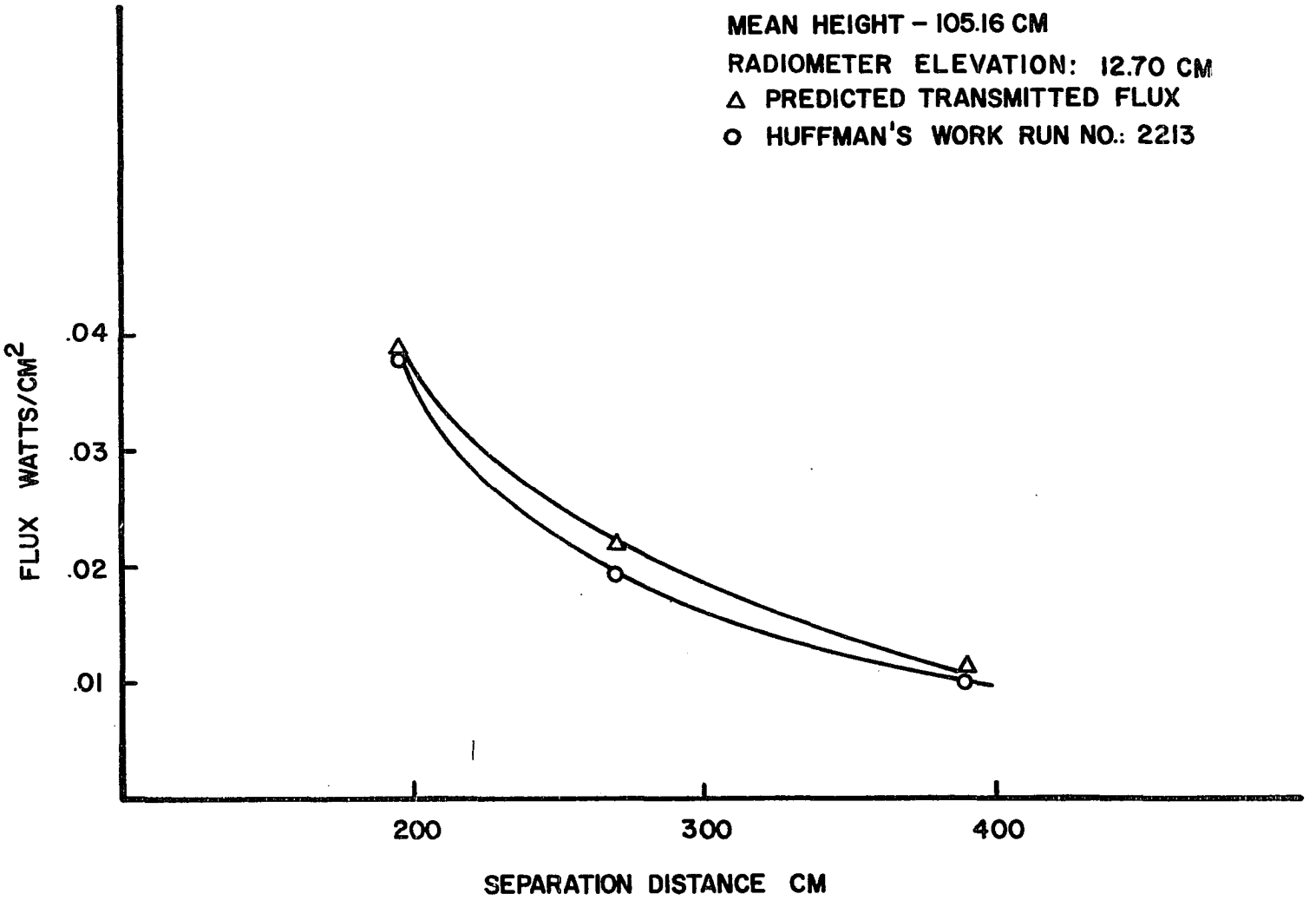


Figure 32. Comparison of Flux for a Merged Acetone Flame

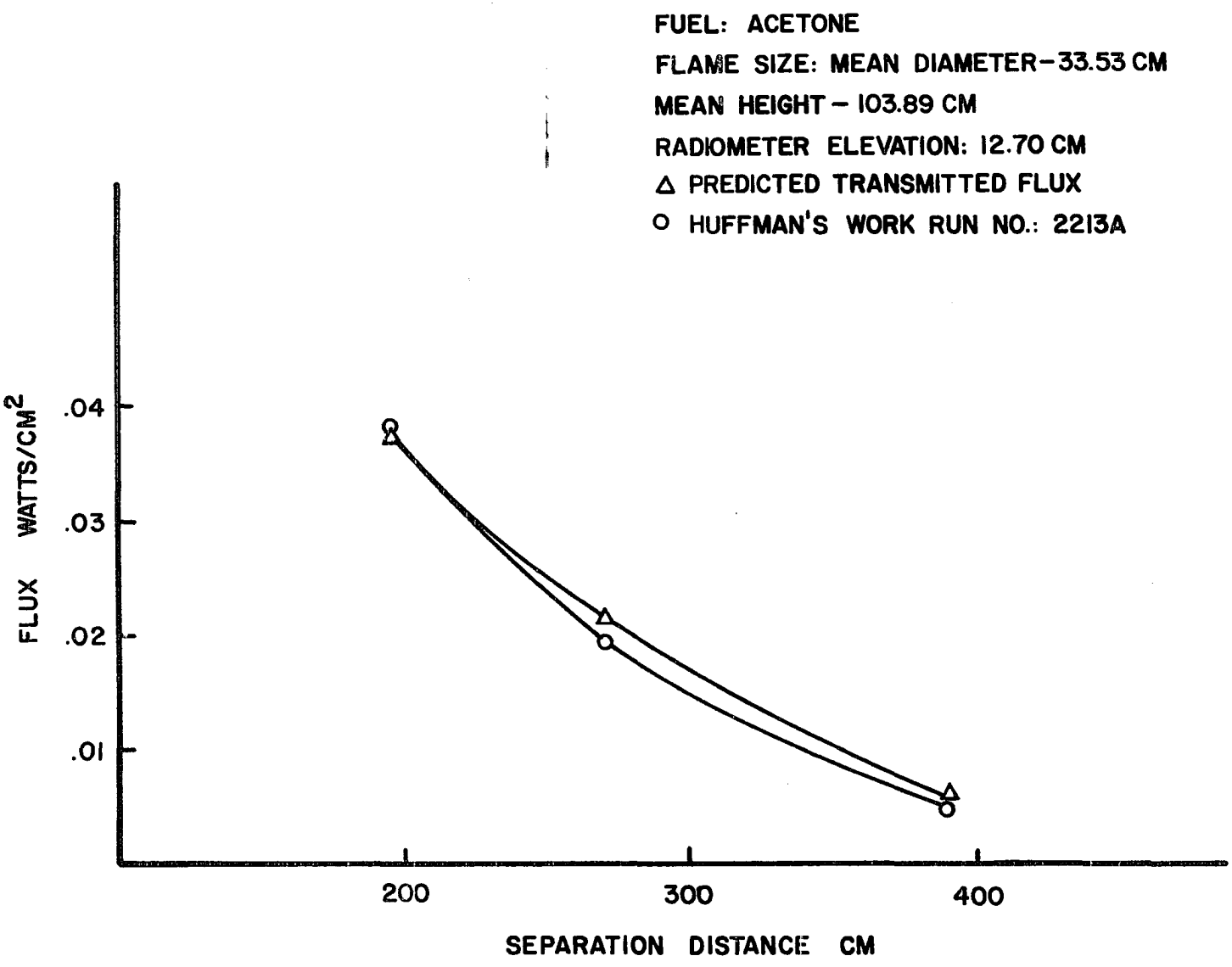


Figure 33. Comparison of Flux for a Merged Acetone Flame

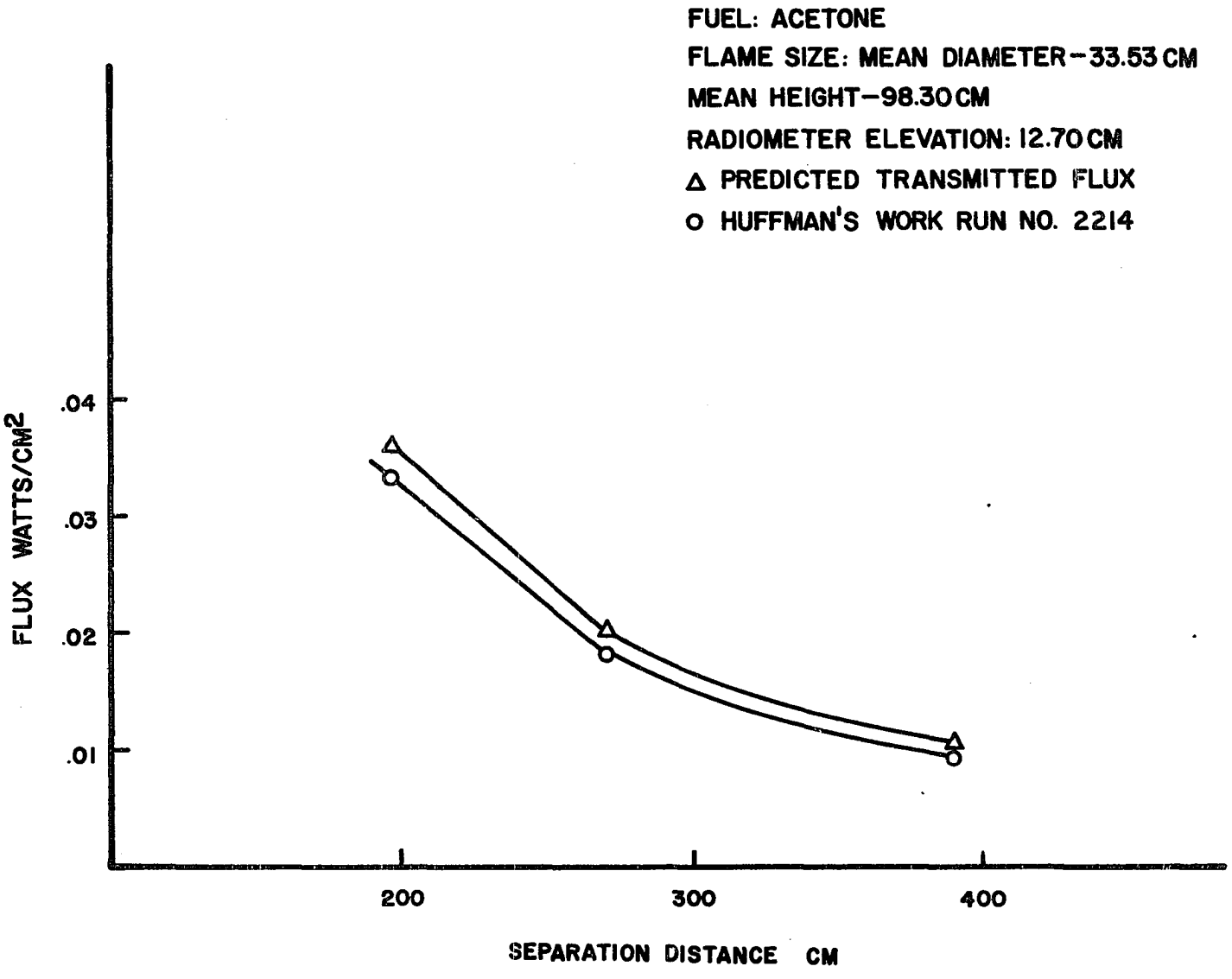


Figure 34. Comparison of Flux for a Merged Acetone Flame

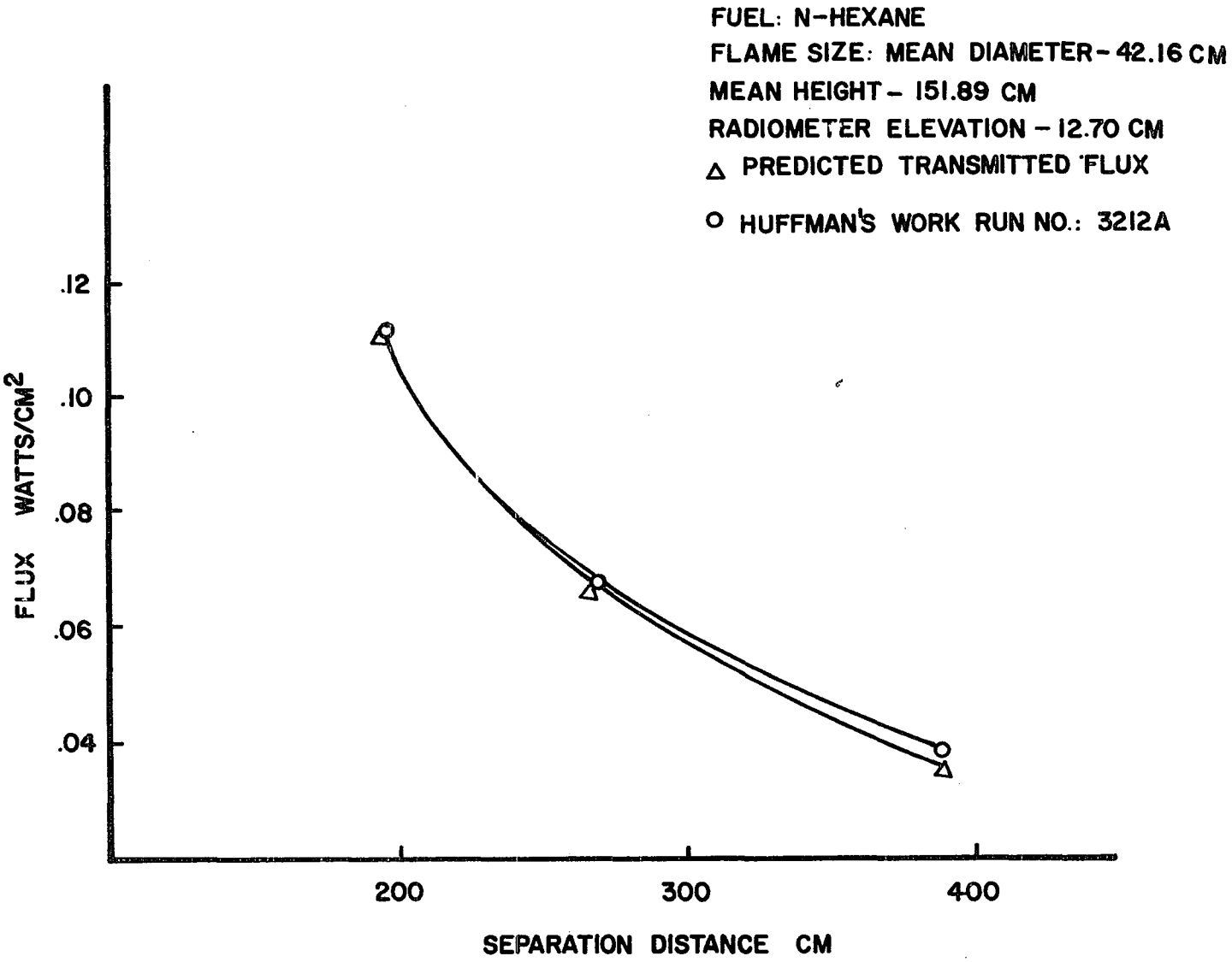


Figure 35. Comparison of Flux for a Merged N-Hexane Flame

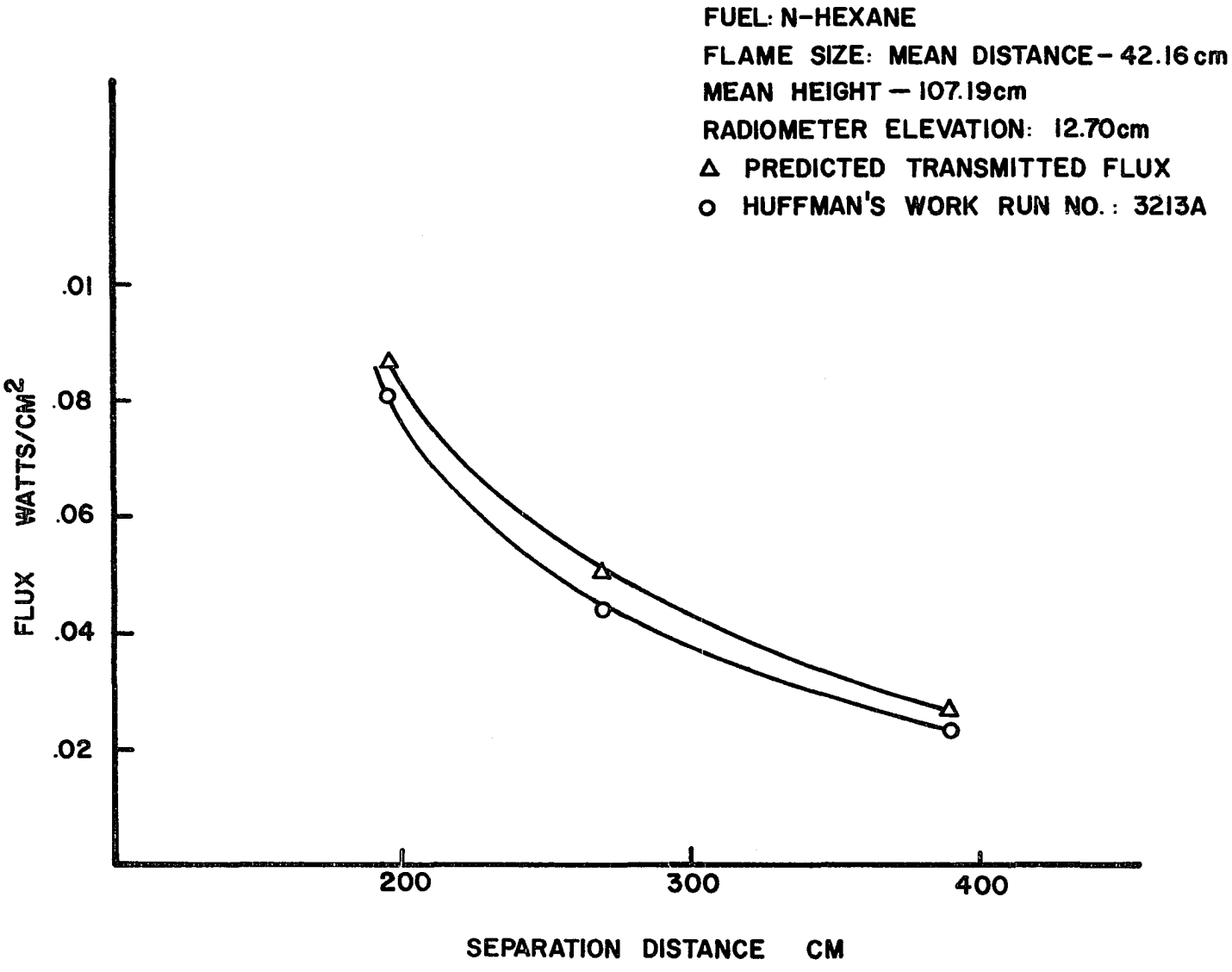


Figure 36. Comparison of Flux for a Merged N-Hexane Flame

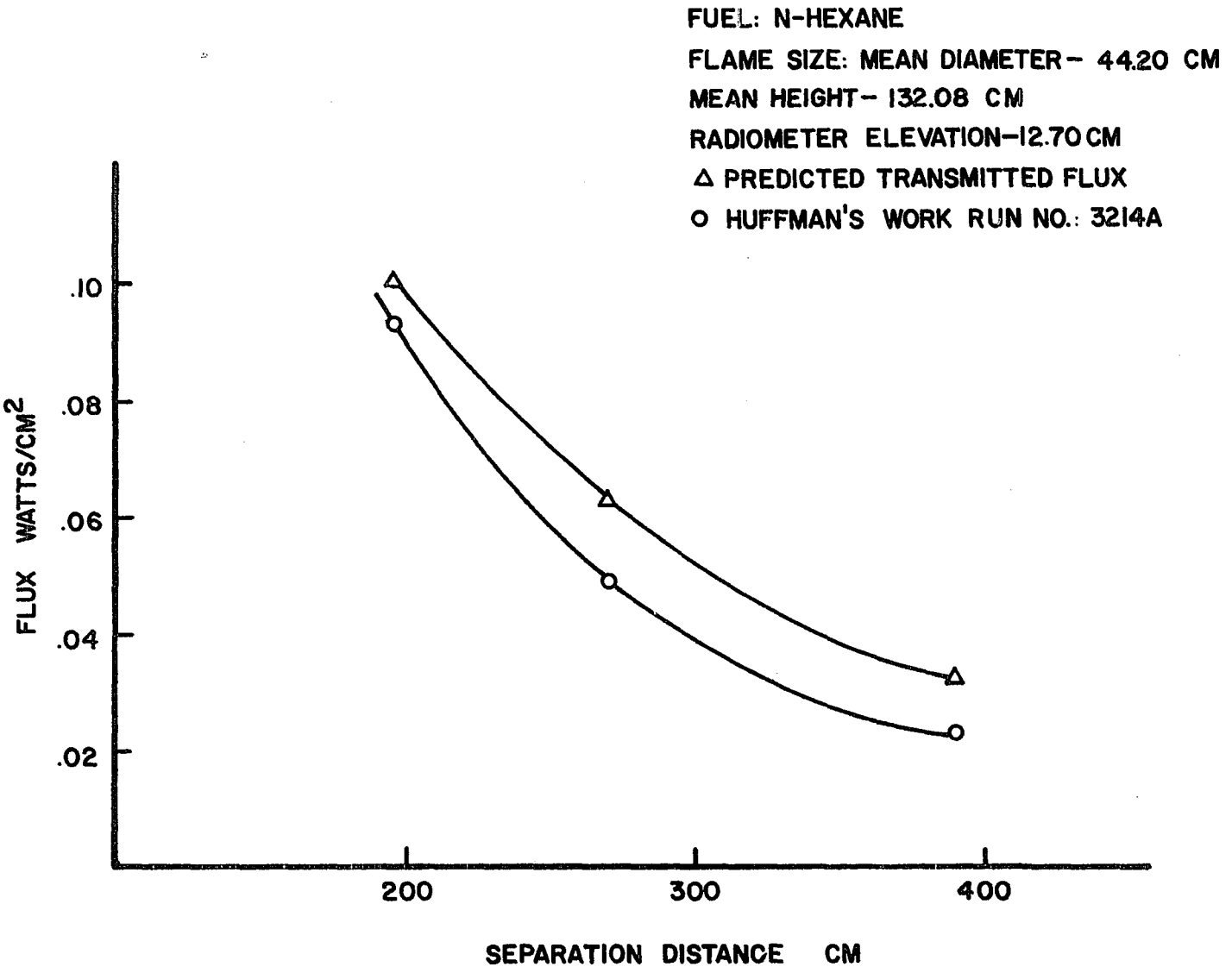


Figure 37. Comparison of Flux for a Merged N-Hexane Flame

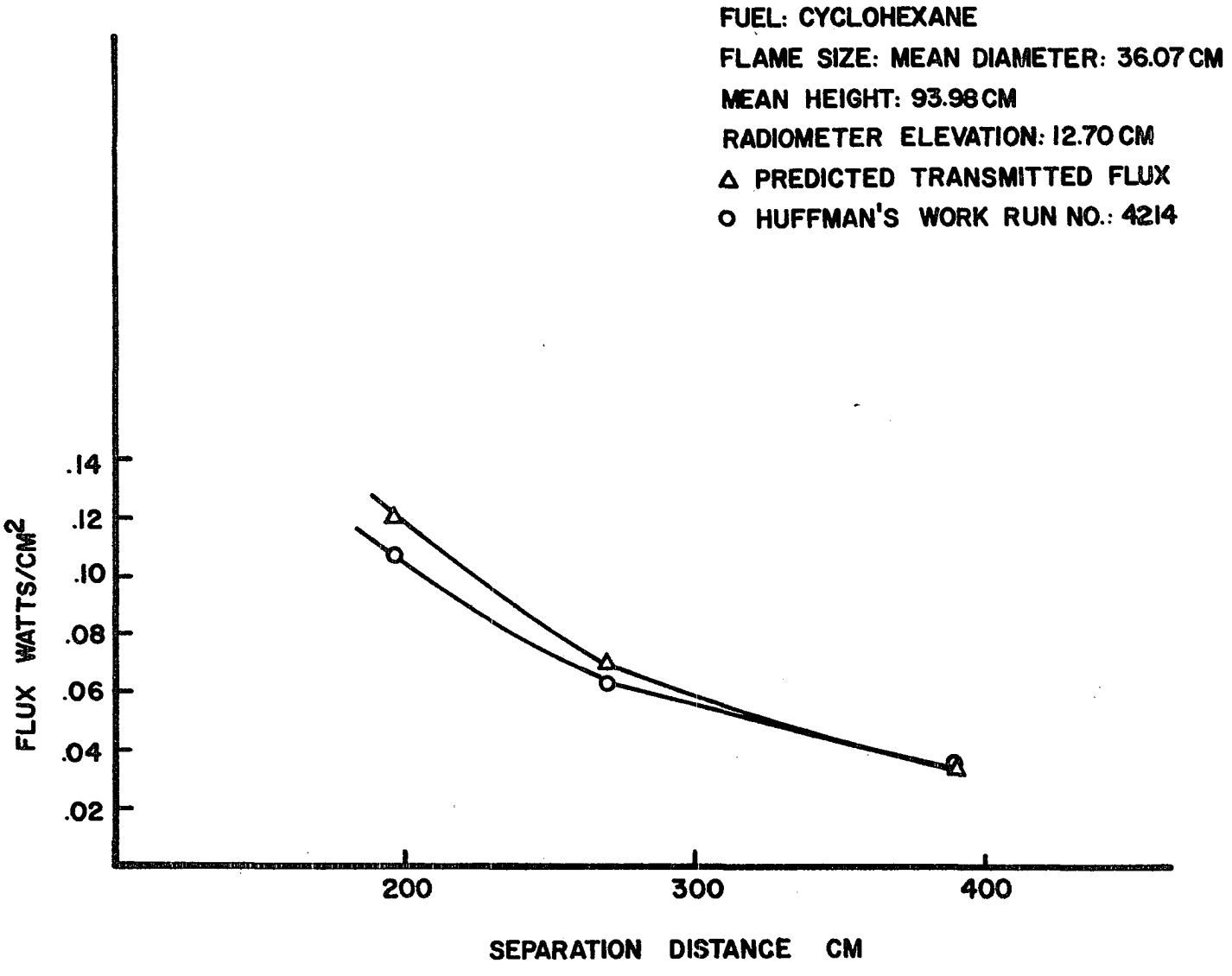


Figure 38. Comparison of Flux for a Merged Cyclohexane Flame

CHAPTER V

CONCLUSIONS

Flame is a form of hot gas which contains heated solid particles. It is obvious that radiative flux prediction from flames based on the transport equation is more fundamental than any other established technique. The conventional way of heat flux prediction from flames by measuring the flame 'temperature' is inaccurate, because the flame generally is not in thermodynamic equilibrium and the flame 'temperature' measurement is a very strong function of the measuring technique, as pointed out by Broida (9). So far, methods of practical flame 'temperature' measurements have not yet been developed. A slight deviation in measured 'temperature' will introduce a significant error in flux computation.

There are usually air bubbles, of different sizes inside a large turbulent fire. These bubbles, although they are heated to a certain 'temperature', will not radiate appreciatively, for the 'temperature' of the bubbles is moderate as compared to the flame 'temperature'. Also, the emission characteristic of the bubbles at high temperature is low as compared to carbon dioxide or water vapor. The presence of

these air bubbles inside large fires has only negligible effect on the heat flux prediction, as long as the 'solid' fire diameter, that is after excluding what is occupied by the air bubbles, is greater than the optically thick path length. For small size fires, although the fire diameter may be greater than the optically thick path length from the picture, its 'solid' fire diameter may not be the case. This may result in some deviation in the heat flux prediction. In general, air bubbles generate and move rapidly inside the fire. The effect of turbulent factors in heat flux prediction needs to be studied.

The inner cone of fire presumably does not radiate significantly. The volume occupied by this region needs to be excluded. Big fires flicker randomly from time to time. The exposure time in fire photography needs to be studied. In general, rules for fire size determination need to be developed.

The consideration of atmospheric absorption in radiative heat transfer prediction from fires to targets in the atmosphere is important, especially for methanol, natural gas, and acetone. The emission of these fuels is restricted mainly to the atmospheric absorption bands, 2.7μ and 4.3μ. A short separation distance from fire to target (say 400 cm) may result in a fairly high loss of radiant energy due to the atmospheric absorption. The effect of the atmospheric absorption for n-hexane, cyclohexane and benzene is comparatively

less due to its continuum through out the entire emission spectrum.

The results of this work have provided:

1. A new, improved two flame method of obtaining J_λ and β_λ
2. The average J_λ and β_λ for methanol, natural gas, acetone, n-hexane, cyclohexane, and benzene fuels.
3. The comparison of measured and predicted heat flux which showed good agreement for big fires.
4. An extensive discussion on the applicability of using the transport equation in radiative heat flux prediction from fires.

NOMENCLATURE

A = constant; area, cm^2

a_1 = finite path length, cm

a_2 = finite path length, cm

C = constant

C_1 = dimensional constant in the Planck Equation, 1.177×10^{-12} watts cm^2

C_2 = dimensional constant in the Planck Equation, 2.5776 cm °K

D = distance from flame to target, cm

E = energy, watts/cm^2

$f(\beta_\lambda)$ = function defined by equation (12)

H = mean height of a cylindrical flame, cm

h = Planck's constant, 6.624×10^{-27} erg-sec

I = intensity, watts/cm^2-steradian

J_λ = monochromatic volume emission coefficient, watts/cm^3-cm-steradian

K_λ = monochromatic volume extinction coefficient of the atmospheric constituants, cm^{-1}

P = pressure, atm

Q = radiant flux, watts/cm^2

R = mean radius of a cylindrical flame, cm

T = temperature, °R

u = optical path length, g/cm^2

X = arbitrary path length, cm

α_λ = monochromatic transmittance

β_λ = monochromatic volume extinction coefficient, cm^{-1}

ϵ_c = emittance of globar

σ = Stephan-Boltzmann constant, 5.6699×10^{-5}, erg-sec $cm^2 °K^4$

λ = wavelength, micron

$\Delta\lambda$ = spectral slit width, micron

ρ = density, g/cm^3

ω = solid angle, steradian

θ = angle between normal to the surface and the central direction of solid angle, degrees

ζ = sweep angle, degrees

Φ = angle between central direction of the solid angle and target surface, degrees

SUBSCRIPTS

app = apparent

C = cavity

E = equivalent

H = opening

m,n = subdivision indices

N_2 = nitrogen

S = specimen

λ = monochromatic

BIBLIOGRAPHY

1. Allen, H. C., and Cross, P. C., Infrared Spectrum, New York, Wiley, 1963.

2. Babrov, H. J., and Tourin, R. H., "Methods for Predicting Infrared Radiance of Flames by Extrapolation from Laboratory Measurements," Journal of Quantitive Spectroscopic Heat Transfer, Vol. 3, Great Britain, Pergamon press, Ltd., 1963.

3. Baly, E. C. C., Spectroscopy, Vol. 1, Longmans, Green and Co. Ltd., 1927.

4. Barnes, R. B., Infrared Spectrum, New York, Reinhold Publishing Corporation, 1944.

5. Bell, E. E., Burnside, P. B., and Dickey, F. P., "Spectral Radiance of Some Flames and Their Temperature Determination," Journal of Optical Society of America, Vol. 50, No. 12, December, 1960.

6. Bone, W. A., and Townend, D. T. A., Flame and Combustion in Gases, Longmans, Green and Co., Inc., New York, 1927, Chapter II.

7. Breene, R. G., The Shift and Shape of Spectral Lines, Oxford, New York, Pergamon Press, 1961.

8. Broida, H. P., "Experimental Temperature Measurements in Flames and Hot Gases," Temperature; Its Measurement and Control in Science and Industry, Vol. II, Reinhold Publishing Corp., New York, 1955.

9. Burch, D. E., and Gryvnak, D. A., "Laboratory Investigation of the Absorption and Emission of Infrared Radiation," Journal of Quantitative Spectroscopy and Radiative Transfer, Vol. 6, No. 3, 1966.

10. Burch, D. E., Gryvnak, D. A., and Williams, D., "Total Absorption of Carbon Dioxide in the Infrared," Applied Optics, Vol. 1, No. 6, 1962.

11. Burch, D. E., France, W. L., and Williams, D., "Total Absorptance of Water Vapor in the Near Infrared," Applied Optics, Vol. 2, No. 6, 1963.

12. Chapman, D. L., London, Edinburgh and Dublin Philosophical Magazine and Journal of Science, Series 5, 47, 90, 1899.

13. Coblentz, W. W., Investigations of Infrared Spectra, Part I, Carnegie Institution of Washington, 1905.

14. Coward, H. F., and Greenwald, H. P., Propagation of Flame in Mixture of Natural Gas and Air, Washington, U. S. Government Printing Office, 1928.

15. Davis, M. M., Infrared Spectroscopy and Molecular Structures, New York, Elsevier Publishing Company, 1963.

16. Davy, H., Collected Works, Vol. VI, 1840.

17. Ellis, O. C. de C., A History of Fires and Flames, London, The Poetry Lover's Fellowship of Literature, Simpkin, Marshall, Limited, 1932.

18. Elsasser, W. M., Heat Transfer by Infrared Radiation in the Atmosphere, Second Edition, Milton, Mass., Harvard University, Blue Hill Meteorological Observatory, 1942.

19. Gubareff, G. G., Janssen, J. E., and Torborg, R. H., Thermal Radiation Properties Survey, Honeywell Research Center, Minneapolis-Honeywell Regulator Company, Minneapolis, Minnesota, 1960.

20. Fristrom, R. M., and Westenberg, A. A., Flame Structure, New York, McGraw-Hill, 1965.

21. Gaydon, A. G., Spectroscopy and Combustion Theory, London, Chapman and Hall Ltd., 1942.

22. Gaydon, A. G., The Spectroscopy of Flames, New York, Wiley, 1957.

23. Gaydon, A. G., and Wolfhard, H. G., Flames, Their Structure, Radiation and Temperature, London, Chapman and Hall, 1953.

24. Hollander, T., "Photometric Measurements on the Deviations from the Equilibrium State in Flames," AIAA Journal, Vol. 6, No. 3, 1968.

25. Hess, S. L., Introduction to Theoretical Meteorology, Henry Holt and Company, New York, 1959.

26. Hood, J. D., "A Method for the Determination of the Radiative Properties of Flames," Ph. D. Dissertation, The University of Oklahoma, 1966.

27. Huffman, K. G., "The Interaction and Merging of Flames from Burning Liquids," Ph. D. Dissertation, The University of Oklahoma, 1967.

28. Jamieson, J. A., Mcfee, R. H., Plass, G. N., and Grube, R. H., Infrared Physics and Engineering, McGraw-Hill Book Company, Inc., 1963.

29. Jenkins, F. A., and White, H. E., Fundamentals of Optics, McGraw-Hill Book Co., Inc., New York, 1957.

30. Kurlbaum, F., "Line Reversal Method for Temperature Measurement," Physikalische Zeitscrift, Vol. 3, 1902.

31. Lewis, B., and Elbe, G. V., Combustion, Flames and Explosions of Gases, New York, Academic Press, 1951.

32. Libby, P. A., and Economos, C., "A Flame Zone Model for Chemical Reaction in a Laminar Boundary Layer with Application to the Injection of Hydrogen-Oxygen Mixtures," International Journal of Heat and Mass Transfer, Vol. 6, 1963.

33. Lord, R. C., "Infrared Emission Spectra of Ammonia-Oxygen and Hydrogen Flames," Spectrochim. Acta., Vol. 8, 1959.

34. Love, T. J., Jr., Hood, J. D., Shahrokhi, F., and Tsai, Y. W., "A Method for the Prediction of Radiative Heat Transfer from Flames," ASME-AICHE Heat Transfer Conference and Exhibit, Seattle, Washington, August, 1967.

35. Love, T. J., Jr., Radiative Heat Transfer, to be published in 1968 by Charles E. Merrill Books, Inc., Columbus, Ohio.

36. Mallard, E., and Chatelier, H. L., "Combustion des Me'langes Gaseux Explosifs," Annales Mines, Vol. 4, 1883.

37. Markstein, G. H., Nonsteady Flame Propagation, New York, Macmillan, 1964.

38. Monk, G. S., Light Principles and Experiments, McGraw-Hill Book Co., Inc., New York, 1937.

39. Morris, J. C., "Comments on the Measurements of Emittance of the Globar Radiation Source," Journal of the Optical Society of America, Vol. 51, 1961.

40. Neil, D. T., "Heat Transfer from Uncontrolled Buoyant Diffusion Flames," Ph. D. Dissertation, The University of Oklahoma, 1968.

41. Penzias, G. J., and Tourin, R. H., "Method for Infrared Analysis of Rocket Flames in Situ," Combustion and Flames, Vol. VI, No. 3, London, Butterworths Scientific Publications, September, 1962.

42. Penzias, G. J., Liang, E. T., and Tourin, R. H., "Infrared Radiation and Temperature Measurements in Solid Propellant Flames," Part I: Technical Report No. 22, Contract NONR 3657(00), Advanced Research Projects Agency, Washington, D. C., 1962.

43. Plass, G. N., "The Theory of the Absorption of Flame Radiation by Molecular Bands," Applied Optics, Vol. 4, No. 2, 1965.

44. Rossi, B., Optics, Addison-Wesley Publishing Co., Inc., Mass., 1959.

45. Sato, T., Veda, K., Ohira, K., et al., "Radiant Heat Transfer from Luminous Flame," Transection of Japanese Society of Mechanical Engineers, Vol. 27, No. 7, 1961.

46. Schmidt, H., "The Radiation Law of the Bunsen Flame," Annalen der Physick, Vol. 29, 1909.

47. Shahrokhi, F., "Numerical Technique for Calculation of Radiant Energy Flux to Targets from Flames," Ph. D. Dissertation, the University of Oklahoma, 1965.

48. Silverman, J., "The Emissivity of Globar," Journal of Optical Society of America, Vol. 38, 1948.

49. Sokolik, A. S., "Self-ignition, Flame and Detonation in Gases," Translated from Russian by N. Kanor, Edited by R. Hardin, Jerusalem, Israel Program for Scientific Translations, Available from the Office of Technical Services, U. S. Department of Commerce, Washington, 1963.

50. Thompson, H. W., Advances in Spectroscopy, New York, Interscience Publishers, 1959.

51. Thring, M. W., "Luminous Radiation from Flames," Chemical Process Engineering, Vol. 46, No. 10, 1965.

52. Tourin, R. H., "Measurements of Infrared Spectral Emissivities of Hot Carbon Dioxide in the 4.3μ Region," Journal of the Optical Society of America, Vol. 51, No. 2, 1961.

53. Tourin, R. H., "Infrared Spectral Emissivities of CO_2 in the 2.7μ Region," Infrared Physics, Vol. 1, Great Britain, Pergamon Press, Ltd., 1961.

54. Venable, W. M., The Interpretation of Spectra, New York, Reinhold Publishing Corp., 1948.

55. Welker, J. R., and Sliepcevich, C. M., "Susceptibility of Potential Target Components to Defeat by Thermal Action," Quarterly Progress Report, Physical Research Laboratory, Edgewood Arsenal, Maryland, 1967.

56. West, T. S., "Atomic Analysis in Flames," Endeavour, Imperial Chemical Industries Ltd., Vol. 24, No. 97, 1967,

57. Williams, F. A., Combustion Theory, Addision-Wesley Publishing Company, 1965.

58. Wolfe, W. L., Handbook of Military Infrared Technology, Office of Naval Research Department of the Navy, Washington D. C., 1965.

APPENDIX A

RADIATIVE TRANSPORT PROPERTIES OF METHANOL, NATURAL GAS, ACETONE, N-HEXANE, CYCLOHEXANE AND BENZENE FLAMES

TABLE 5

TRANSPORT PROPERTIES OF METHANOL FLAME

Fuel: Methanol Series.: MF-(3)-1

Wavelength (microns)	Monochromatic Volume Extinction Coefficient (cm^{-1})			Monochromatic Volume Emission Coefficient (watts/cm^3-cm-steradian)		
	β_{λ_1}	β_{λ_2}	β_{λ_3}	J_{λ_1}	J_{λ_2}	J_{λ_3}
1.950	0.617	0.622	0.632	109.480	109.033	110.218
2.020	1.039	0.929	0.708	109.486	106.185	94.908
2.060	0.713	0.791	0.965	122.192	124.933	136.285
2.140	1.291	1.234	1.110	119.598	117.776	111.138
2.210	1.844	1.798	1.687	54.063	53.443	51.074
2.280	0.679	0.594	0.428	13.804	13.469	12.306
2.360	1.986	1.731	1.211	19.147	17.958	14.317
2.410	3.241	0.341	--	25.196	12.046	--
2.450	0.093	--	--	12.250	--	--
2.490	0.065	--	--	27.647	--	--
2.500	0.201	--	--	54.946	--	--
2.520	0.666	0.490	0.164	108.576	103.123	85.727
2.540	0.904	0.379	--	196.224	168.576	--
2.610	1.018	0.884	0.622	527.706	508.407	444.017
2.630	1.087	1.041	0.942	612.929	605.142	576.684
2.670	1.203	1.305	1.562	579.147	595.281	666.343
2.690	1.127	1.258	1.593	465.796	482.636	559.375
2.710	1.420	1.278	0.983	447.385	430.676	374.776
2.740	1.314	1.320	1.334	484.440	485.227	488.312
2.780	2.149	1.963	1.548	1212.326	1158.128	978.645
2.820	1.968	2.017	2.154	1435.962	1453.349	1529.751
2.860	2.220	2.230	2.260	1350.486	1353.833	1368.109
2.880	2.137	1.942	1.512	1227.536	1169.931	981.151
2.950	1.497	1.389	1.156	1010.481	981.972	882.835
2.990	1.324	1.271	1.155	874.197	861.872	816.702
3.080	1.300	1.139	0.817	532.735	510.009	435.650
3.170	0.997	0.988	0.967	246.377	245.736	243.302
3.270	1.207	1.067	0.785	139.460	134.215	116.748
3.310	0.995	1.150	1.548	93.462	97.547	116.611
3.390	0.693	--	--	48.148	--	--
3.430	0.380	--	--	35.055	--	--
3.510	0.620	--	--	33.657	--	--
3.590	0.826	--	--	25.550	--	--
3.720	0.882	--	--	15.528	--	--
4.020	0.882	--	--	8.096	--	--
4.160	1.229	1.067	0.746	10.887	10.416	8.878
4.180	1.229	1.067	0.746	10.907	10.434	8.894

TABLE 5 (continued)

Wavelength (microns)	Monochromatic Volume Extinction Coefficient (cm^{-1})			Monochromatic Volume Emission Coefficient (watts/cm^3-cm-steradian)		
	$\beta_{\lambda 1}$	$\beta_{\lambda 2}$	$\beta_{\lambda 3}$	$J_{\lambda 1}$	$J_{\lambda 2}$	$J_{\lambda 3}$
4.200	1.005	1.067	1.211	13.701	13.938	14.916
4.220	0.882	0.768	0.543	63.339	61.321	54.483
4.240	3.770	3.430	2.576	438.213	409.024	316.267
4.260	3.241	3.055	2.548	991.512	952.768	812.104
4.290	2.254	2.373	2.776	2434.818	2504.553	2864.513
4.330	1.916	1.862	1.730	4175.016	4118.758	3905.116
4.350	2.120	2.180	2.360	5243.082	5320.645	5674.305
4.370	2.586	2.520	2.336	6663.492	6561.977	6158.215
4.390	2.597	2.604	2.625	6644.168	6654.602	6700.949
4.410	3.084	2.795	2.114	7337.477	6884.430	5450.856
4.430	2.486	2.388	2.133	6746.492	6593.359	6015.766
4.460	2.482	2.415	2.233	7794.305	7672.441	7193.727
4.500	2.724	2.491	1.945	8981.430	8513.141	6980.871
4.550	2.767	2.367	1.557	7542.250	6875.395	5027.348
4.600	2.290	1.920	1.201	4611.742	4212.430	3100.751
4.650	2.017	1.684	1.066	2742.251	2528.000	1912.059
4.710	1.859	2.045	2.684	1659.396	1738.311	2174.235
4.830	1.127	1.067	0.939	1342.037	1319.899	1240.106
4.990	0.436	--	--	355.539	--	--
5.220	0.255	--	--	229.351	--	--
5.790	0.882	0.514	--	235.055	211.467	--

TABLE 6

TRANSPORT PROPERTIES OF NATURAL GAS FLAME

FUEL: NATURAL GAS SERIES NO.: NGF-1

WAVELENGTH MICRONS	MONO. VOL. EXT. COEF. /CM	MONO. VOL. EM. COEF. $WATTS/CM^4/STERADIAN$
1.230	1.696	38.598
1.290	0.592	69.732
1.360	0.814	72.292
1.420	1.082	103.901
1.500	1.014	65.637
1.650	1.364	29.469
1.720	0.235	15.355
1.780	0.235	14.412
1.850	0.306	58.992
1.950	0.538	102.111
2.020	0.472	95.289
2.060	0.684	111.940
2.140	0.387	66.820
2.210	0.368	26.056
2.280	0.625	19.334
2.360	0.306	15.065
2.410	0.327	17.242
2.450	0.292	26.962
2.490	0.251	63.796
2.500	0.711	121.118
2.520	0.261	155.556
2.540	0.558	247.478

TABLE 6 (continued)

WAVELENGTH MICRONS	MONO. VOL. EXT. COEF. /CM	MONO. VOL. EM. COEF. 4 WATTS/CM /STERADIAN
2.610	0.621	405.188
2.630	0.636	397.855
2.670	0.693	365.977
2.690	0.810	365.680
2.710	1.261	488.570
2.740	1.527	741.861
2.780	1.709	1287.161
2.820	1.523	1153.899
2.860	1.519	1035.054
2.880	1.244	935.422
2.950	0.994	746.741
2.990	0.783	563.226
3.080	0.364	287.802
3.170	0.327	162.093
3.270	0.472	83.599
3.310	0.947	72.806
3.390	0.563	58.313
3.430	0.527	47.608
3.510	1.107	54.133
3.590	1.082	39.399
3.720	0.768	20.441
4.020	0.235	10.437
4.160	0.472	10.053
4.180	0.966	21.417
4.200	1.928	70.075
4.220	1.811	202.086

TABLE 6 (continued)

WAVELENGTH MICRONS	MONO. VOL. EXT. COEF. /CM	MONO. VOL. EM. COEF. 4 WATTS/CM /STERADIAN
4.240	2.128	553.930
4.260	2.329	1179.948
4.290	1.840	1976.551
4.330	1.232	4075.042
4.350	1.295	5100.828
4.370	1.831	7167.934
4.390	2.385	8897.629
4.410	2.184	9023.840
4.430	2.851	10961.586
4.460	3.376	11056.613
4.500	3.783	11001.312
4.550	3.573	7998.605
4.600	3.476	5267.574
4.650	3.019	3101.207
4.710	2.766	1721.305
4.830	1.456	335.847
4.990	0.472	98.290
5.220	0.665	73.078
5.790	1.014	41.338

TABLE 7

TRANSPORT PROPERTIES OF ACETONE FLAME

FUEL: ACETONE SERIES NO.: AF-1-A

WAVELENGTH MICRONS	MONO. VOL. EXT. COEF. /CM	MONO. VOL. EM. COEF. 10^4 WATTS/CM /STERADIAN
0.850	1.462	716.781
0.862	0.910	607.933
0.874	1.260	765.469
0.886	0.910	713.153
0.899	0.297	692.719
0.911	0.240	602.280
0.924	0.310	786.410
0.938	0.465	1001.870
0.951	0.397	1021.620
0.964	0.353	1116.384
0.980	0.636	1280.056
0.990	0.430	1265.052
1.040	0.343	1192.719
1.080	0.636	1307.348
1.130	0.835	1366.082
1.180	1.390	1723.058
1.230	0.647	1260.516
1.290	1.234	1504.895
1.360	0.381	1089.240
1.420	0.910	1435.774
1.500	0.827	1189.163
1.650	0.484	904.880

TABLE 7 (continued)

WAVELENGTH MICRONS	MONO. VOL. EXT. COEF. /CM	MONO. VOL. EM. COEF. $WATTS/CM^4$ /STERADIAN
1.720	0.771	943.469
1.780	0.465	840.064
1.850	0.708	911.676
1.950	0.894	955.555
2.020	1.417	1056.785
2.060	0.580	838.794
2.140	1.208	959.965
2.210	1.377	886.077
2.280	1.382	770.324
2.360	0.570	543.220
2.410	0.682	554.238
2.450	0.740	556.259
2.490	0.799	560.402
2.500	0.713	578.615
2.520	0.615	611.826
2.540	0.649	700.657
2.610	0.934	1101.478
2.630	1.401	1365.044
2.670	1.571	1377.265
2.690	2.335	1579.302
2.710	1.771	1330.998
2.740	2.037	1695.126
2.780	3.169	3667.137
2.820	3.255	4117.516
2.860	2.917	3263.767
2.880	2.611	2804.792

TABLE 7 (continued)

WAVELENGTH MICRONS	MONO. VOL. EXT. COEF. /CM	MONO. VOL. EM. COEF. $WATTS/CM^4/STERADIAN$
2.950	1.464	1825.390
2.990	1.588	1657.347
3.080	1.108	948.857
3.170	1.020	601.678
3.270	0.924	411.902
3.310	0.943	356.323
3.390	0.869	280.780
3.430	0.531	232.113
3.510	0.812	229.389
3.590	0.424	174.598
3.720	0.484	139.172
4.020	0.812	122.858
4.160	1.312	135.080
4.180	1.312	135.326
4.200	1.556	122.813
4.220	2.301	317.755
4.240	0.802	400.024
4.260	0.673	840.738
4.290	1.947	4229.156
4.330	0.778	7274.949
4.350	0.891	9237.434
4.370	1.249	12350.152
4.390	2.724	14732.090
4.410	3.224	17908.312
4.430	3.812	20135.215
4.460	4.162	22036.637

TABLE 7 (continued)

WAVELENGTH MICRONS	MONO. VOL. EXT. COEF. /CM	MONO. VOL. EM. COEF. $WATTS/CM^4/STERADIAN$
4.500	3.042	17741.547
4.550	2.892	14227.367
4.600	2.921	10344.094
4.650	2.841	6799.344
4.710	2.568	3738.556
4.830	2.790	1369.791
4.990	1.580	336.339
5.220	0.910	135.484

TABLE 7 (continued)

FUEL: ACETONE SERIES NO.: AF-1-B

WAVELENGTH MICRONS	MONO. VOL. EXT. COEF. /CM	MONO. VOL. EM. COEF. $WATTS/CM^4/STERADIAN$
0.850	1.358	789.701
0.862	1.021	733.053
0.874	1.241	840.515
0.886	0.969	794.393
0.899	0.290	685.572
0.911	0.230	676.240
0.924	0.290	735.730
0.938	0.599	942.273
0.951	0.325	937.236
0.964	0.457	1066.828
0.980	0.745	1229.646
0.990	0.525	1200.907
1.040	0.735	1207.120
1.080	0.847	1224.940
1.130	0.450	1087.634
1.180	0.739	1252.412
1.230	0.684	1149.429
1.290	0.626	1097.057
1.360	0.889	1179.974
1.420	0.925	1326.547
1.500	0.555	1000.387
1.650	0.483	817.997

TABLE 7 (continued)

WAVELENGTH MICRONS	MONO. VOL. EXT. COEF. /CM	MONO. VOL. EM. COEF. WATTS/CM^4 /STERADIAN
1.720	0.563	785.387
1.780	0.566	754.272
1.850	0.808	818.103
1.950	0.325	717.879
2.020	0.585	746.944
2.060	0.262	700.129
2.140	0.620	731.047
2.210	0.430	553.024
2.280	0.603	539.794
2.360	0.308	433.875
2.410	0.684	480.460
2.450	0.546	465.380
2.490	0.421	471.850
2.500	0.483	483.673
2.520	0.401	510.573
2.540	0.766	677.204
2.610	1.846	1405.535
2.630	1.748	1475.465
2.670	1.513	1346.768
2.690	1.922	1410.325
2.710	2.414	1587.645
2.740	3.144	2199.919
2.780	3.300	3900.497
2.820	4.165	5185.469
2.860	3.424	3781.430
2.880	3.306	3389.866

TABLE 7 (continued)

WAVELENGTH MICRONS	MONO. VOL. EXT. COEF. /CM	MONO. VOL. EM. COEF. 10^4 WATTS/CM /STERADIAN
2.950	2.662	2542.135
2.990	2.130	1878.017
3.080	2.580	1355.572
3.170	2.526	872.919
3.270	1.547	471.508
3.310	1.832	449.866
3.390	1.437	318.919
3.430	0.684	230.318
3.510	1.026	238.540
3.590	0.440	176.027
3.720	0.364	131.682
4.020	0.684	111.758
4.160	0.796	109.811
4.180	0.796	110.010
4.200	1.769	168.985
4.220	1.034	231.306
4.240	2.569	606.684
4.260	1.275	994.804
4.290	0.989	3053.718
4.330	0.796	5980.773
4.350	0.837	6571.387
4.370	1.020	6182.930
4.390	1.600	12232.500
4.410	3.374	17910.227
4.430	3.910	20812.133
4.460	4.718	24598.777

TABLE 7 (continued)

WAVELENGTH MICRONS	MONO. VOL. EXT. COEF. /CM	MONO. VOL. EM. COEF. 4 WATTS/CM /STERADIAN
4.500	3.453	19155.242
4.550	3.057	14402.785
4.600	3.213	10709.895
4.650	4.507	9478.750
4.710	3.229	4387.563
4.830	1.595	919.629
4.990	0.635	258.895
5.220	0.925	156.471

TABLE 8

TRANSPORT PROPERTIES OF N-HEXANE FLAME

FUEL: N-HEXANE SERIES NO.: HF-1

WAVELENGTH MICRONS	MONO. VOL. EXT. COEF. /CM	MONO. VOL. EM. COEF. 4 WATTS/CM /STERADIAN
0.850	0.590	929.210
0.862	0.609	1449.118
0.874	0.426	1551.005
0.886	0.345	1710.060
0.899	0.289	1832.847
0.911	0.665	2635.546
0.924	0.551	2806.211
0.938	0.461	2560.200
0.951	0.603	3671.020
0.964	0.771	4215.301
0.980	1.137	5221.816
0.990	1.338	6184.246
1.040	1.874	7303.320
1.080	1.244	5691.602
1.130	1.121	5266.977
1.180	0.699	4357.820
1.230	0.590	3820.935
1.290	0.585	3605.844
1.360	0.307	3007.494
1.420	0.287	3279.736
1.500	0.345	2988.010
1.650	1.003	3804.262

TABLE 8 (continued)

WAVELENGTH MICRONS	MONO. VOL. EXT. COEF. /CM	MONO. VOL. EM. COEF. $WATTS/CM^4/STERADIAN$
1.720	0.986	3742.425
1.780	0.779	3380.399
1.850	1.207	3799.638
1.950	1.745	4498.930
2.020	1.305	3738.769
2.060	1.257	3607.600
2.140	1.044	3102.105
2.210	0.972	2787.522
2.280	1.006	2606.906
2.360	0.925	2338.367
2.410	0.850	2194.747
2.450	0.906	2195.077
2.490	1.113	2368.994
2.500	1.121	2382.066
2.520	1.215	2480.250
2.540	1.173	2449.539
2.610	1.463	2995.039
2.630	1.379	3023.251
2.670	1.178	2615.351
2.690	1.166	2446.759
2.710	0.661	1829.547
2.740	0.915	2117.946
2.780	1.868	3678.365
2.820	1.794	3532.182
2.860	1.276	2653.655
2.880	1.219	2414.719

TABLE 8 (continued)

WAVELENGTH MICRONS	MONO. VOL. EXT. COEF. /CM	MONO. VOL. EM. COEF. 10^4 WATTS/CM /STERADIAN
2.950	1.919	2825.824
2.990	2.048	2823.675
3.080	0.691	1319.659
3.170	0.824	1168.567
3.270	0.823	1024.430
3.310	1.253	1143.368
3.390	2.332	1499.934
3.430	2.556	1526.390
3.510	1.653	1036.774
3.590	0.514	492.610
3.720	0.461	472.333
4.020	0.239	317.972
4.160	1.224	461.447
4.180	1.044	424.659
4.200	1.044	425.431
4.220	0.978	521.870
4.240	1.370	739.364
4.260	1.162	1046.547
4.290	3.793	5478.750
4.330	3.318	9028.441
4.350	3.254	12238.137
4.370	3.851	15890.133
4.390	3.518	14216.934
4.410	3.876	14750.129
4.430	2.890	11907.668
4.460	2.205	10063.145

TABLE 8 (continued)

WAVELENGTH MICRONS	MONO. VOL. EXT. COEF. /CM	MONO. VOL. EM. COEF. $WATTS/CM^4/STERADIAN$
4.500	2.369	10607.742
4.550	4.738	15690.617
4.600	2.182	5711.426
4.650	1.865	3352.857
4.710	2.713	2923.709
4.830	1.613	763.322
4.990	1.085	296.696
5.220	0.426	151.782

TABLE 9

TRANSPORT PROPERTIES OF CYCLOHEXANE FLAME

FUEL: CYCLOHEXANE SERIES NO.: CF-1

WAVELENGTH MICRONS	MONO. VOL. EXT. COEF. /CM	MONO. VOL. EM. COEF. 10^4 WATTS/CM /STERADIAN
0.743	0.986	1584.868
0.850	0.651	2193.989
0.862	0.820	2662.194
0.874	0.954	3178.745
0.886	0.945	3485.315
0.899	0.840	3668.354
0.911	0.594	3599.570
0.924	0.408	3588.975
0.938	0.489	4071.423
0.951	0.597	4669.461
0.964	0.485	4891.387
0.980	0.455	5021.305
0.990	0.384	5248.687
1.040	0.433	5210.664
1.080	0.382	5023.430
1.130	0.731	5901.059
1.180	0.824	6745.914
1.230	0.763	6168.555
1.290	0.837	5943.313
1.360	0.920	5738.660
1.420	0.511	5106.480
1.500	0.421	3724.280

TABLE 9 (continued)

WAVELENGTH MICRONS	MONO. VOL. EXT. COEF. /CM	MONO. VOL. EM. COEF. $WATTS/CM^4/STERADIAN$
1.650	0.461	3648.180
1.720	0.397	3916.648
1.780	0.532	4093.722
1.850	0.612	4082.175
1.950	0.684	3828.424
2.020	0.733	3825.925
2.060	0.782	3905.601
2.140	0.805	3795.894
2.210	0.770	3574.118
2.280	0.761	3353.079
2.360	0.961	3452.211
2.410	1.086	3502.756
2.450	1.067	3330.783
2.490	1.059	3189.982
2.500	1.035	3099.156
2.520	1.020	3017.292
2.540	0.969	2894.609
2.610	1.766	4006.770
2.630	1.749	4240.687
2.670	2.000	4854.316
2.690	1.538	3644.228
2.710	1.025	2800.481
2.740	0.719	2511.622
2.780	1.428	3976.538
2.820	2.215	4103.324
2.860	2.221	4307.227

TABLE 9 (continued)

WAVELENGTH MICRONS	MONO. VOL. EXT. COEF. /CM	MONO. VOL. EM. COEF. $WATTS/CM^4/STERADIAN$
2.880	0.899	2411.824
2.950	1.430	2931.956
2.990	0.616	1870.874
3.080	0.328	1364.600
3.170	0.379	1161.933
3.270	0.167	925.921
3.310	0.264	934.809
3.390	0.208	821.763
3.430	0.196	782.838
3.510	0.259	759.866
3.590	0.221	691.981
3.720	0.173	603.479
4.020	0.219	455.971
4.160	0.313	431.404
4.180	0.152	399.693
4.200	0.200	408.834
4.220	1.202	721.122
4.240	0.176	540.785
4.260	0.251	729.788
4.290	1.194	2607.323
4.330	1.929	5907.355
4.350	1.844	6666.469
4.370	3.478	12580.719
4.390	2.645	10287.645
4.410	3.499	12608.770
4.430	3.010	12022.371

TABLE 9 (continued)

WAVELENGTH MICRONS	MONO. VOL. EXT. COEF. /CM	MONO. VOL. EM. COEF. 4 WATTS/CM /STERADIAN
4.460	2.314	10475.328
4.500	2.564	11174.520
4.550	2.520	8943.293
4.600	3.584	8590.281
4.650	2.505	4393.000
4.710	1.374	1852.067
4.830	1.098	694.181
4.990	0.294	293.619
5.220	0.214	197.294
5.790	0.471	123.101

TABLE 10

TRANSPORT PROPERTIES OF BENZENE FLAME

FUEL: BENZENE SERIES NO.: BF-1

WAVELENGTH MICRONS	MONO. VOL. EXT. COEF. /CM	MONO. VOL. EM. COEF. $WATTS/CM^4/STERADIAN$
0.850	0.386	830.614
0.862	0.344	1081.328
0.874	0.434	1186.130
0.886	0.309	1493.801
0.899	0.415	1785.465
0.911	0.481	2135.311
0.924	0.317	2383.791
0.938	0.438	2849.133
0.951	0.411	3113.184
0.964	0.421	3481.570
0.980	0.397	4251.816
0.990	0.537	4604.668
1.040	0.410	4471.828
1.080	0.426	4721.199
1.130	0.375	4651.719
1.180	0.351	5000.590
1.230	0.402	5230.699
1.290	0.594	5524.223
1.360	0.605	5539.219
1.420	0.491	6479.469
1.500	0.554	6230.703
1.650	0.910	6770.113

TABLE 10 (continued)

WAVELENGTH MICRONS	MONO. VOL. EXT. COEF. /CM	MONO. VOL. EM. COEF. 4 WATTS/CM /STERADIAN
1.720	1.117	7123.020
1.780	1.715	8406.742
1.850	2.076	8960.961
1.950	1.871	8469.824
2.020	1.369	7803.262
2.060	1.544	8272.293
2.140	1.647	8476.641
2.210	1.523	8138.797
2.280	1.553	7912.352
2.360	1.689	7793.238
2.410	1.652	7535.844
2.450	1.614	7286.254
2.490	1.560	7010.117
2.500	1.658	7116.480
2.520	1.759	7227.723
2.540	1.629	6888.047
2.610	1.474	7089.977
2.630	1.348	7482.070
2.670	1.757	9030.941
2.690	1.491	8032.660
2.710	1.158	7044.180
2.740	1.438	7469.520
2.780	1.338	7551.594
2.820	1.966	7780.906
2.860	1.915	6908.336
2.880	1.636	6078.449

TABLE 10 (continued)

WAVELENGTH MICRONS	MONO. VOL. EXT. COEF. /CM	MONO. VOL. EM. COEF. 10^4 WATTS/CM /STERADIAN
2.950	1.406	4935.738
2.990	1.662	4905.359
3.080	1.004	4129.902
3.170	0.670	3506.525
3.270	0.890	3498.371
3.310	0.945	3446.261
3.390	1.033	3250.337
3.430	1.040	3105.514
3.510	0.980	2994.796
3.590	0.859	2730.663
3.720	1.103	2471.323
4.020	1.433	2246.597
4.160	1.322	1976.573
4.180	0.969	1790.356
4.200	0.950	1775.039
4.220	2.793	2599.584
4.240	4.550	3820.099
4.260	4.550	4045.212
4.290	2.657	6265.531
4.330	3.190	13071.398
4.350	3.545	13965.211
4.370	3.219	13394.773
4.390	2.422	9964.887
4.410	1.957	7796.602
4.430	1.970	7498.145
4.460	1.744	7876.848

TABLE 10 (continued)

WAVELENGTH MICRONS	MONO. VOL. EXT. COEF. /CM	MONO. VOL. EM. COEF. 4 WATTS/CM /STERADIAN
4.500	2.133	9515.363
4.550	2.397	8516.516
4.600	2.059	5648.305
4.650	2.453	4266.441
4.710	1.549	2529.737
4.830	2.535	1615.708
4.990	2.109	1243.352
5.220	1.200	762.220
5.790	0.910	575.642

APPENDIX B

MONOCHROMATIC TRANSMITTANCE OF QUARTZ

TABLE 11

MONOCHROMATIC TRANSMITTANCE OF QUARTZ

Wavelength (microns)	Monochromatic Transmittance	Wavelength (microns)	Monochromatic Transmittance
0.743	0.980	2.690	0.879
0.850	0.980	2.710	0.879
0.862	0.980	2.740	0.921
0.874	0.980	2.780	0.921
0.886	0.980	2.820	0.929
0.899	0.980	2.860	0.932
0.911	0.980	2.880	0.919
0.924	0.980	2.950	0.926
0.938	0.980	2.990	0.992
0.951	0.980	3.080	0.924
0.964	0.980	3.170	0.931
0.980	0.980	3.270	0.944
0.990	0.980	3.310	0.933
1.040	0.980	3.390	0.926
1.080	0.980	3.430	0.899
1.130	0.980	3.510	0.858
1.180	0.980	3.590	0.743
1.230	0.980	3.720	0.673
1.290	0.980	4.020	0.528
1.360	0.980	4.160	0.503
1.420	0.980	4.180	0.467
1.500	0.980	4.200	0.484
1.650	0.980	4.220	0.497
1.720	0.980	4.240	o.452
1.780	0.980	4.260	0.434
1.850	0.980	4.290	0.367
1.950	0.985	4.330	0.300
2.020	0.979	4.350	0.278
2.060	0.973	4.370	0.264
2.140	0.956	4.390	0.261
2.210	0.948	4.410	0.253
2.280	0.949	4.430	0.244
2.360	0.946	4.460	0.236
2.410	0.946	4.500	0.254
2.450	0.946	4.150	0.287
2.490	0.946	4.600	0.307
2.500	0.943	4.650	0.279
2.520	0.977	4.710	0.213
2.540	0.933	4.830	0.027
2.610	0.922	5.990	0.0
2.630	0.929	5.220	0.0
2.670	0.902	5.790	0.0

APPENDIX C

COMPUTER PROGRAMS FOR RADIATIVE TRANSPORT PROPERTIES' CALCULATION AND TOTAL FLUX INTEGRATION FROM A CYLINDRICAL FLAME

```
C      VOLUME EMISSION AND VOLUME ABSORPTION COEFFICIENT CALCULATION
C      VOLUME EMISSION AND VOLUME ABSORPTION COEFFICIENT CALCULATION
C      BY CHANGING THE OPTICAL PATH LENGTH
       DIMENSION HAM%84<,DLAM%84<,CF%84<
       DIMENSION AA(3), QQ(3), HI(3), HJ(3)
       DIMENSION AB%84<,AJ%84<
       READ%1,3< %HAM%K<,DLAM%K<,CF%K<,K#1,84<
     3 FORMAT%3F10.3<
   200 CONTINUE
       READ %1,2< RATIO
     2 FORMAT %F8.3<
       READ(1,5000) Y,Z,AA
  5000 FORMAT(5F10.4)
       WRITE(3,5100) RATIO,Y,Z,AA
  5100 FORMAT(1H1,6F10.4)
       EPI #.001
       AO#0.0002455
       C2#25776.0
       D3 = 0.0
       DO 20 I#1,84
       READ(1,5200) QQ,D1
  5200 FORMAT(4F10.4)
       IF%D1<201,32,201
   201 CONTINUE
       D3#D1
    32 CONTINUE
       QT#QQ%1<&QQ%2<&QQ%3<
       IF%QT<299,299,1500
   299 AB%I<#.0
       GO TO 20
  1500  CONTINUE
       HI%1<#0.
       HI%2<#0.
       HI%3<#0.
       HJ%1<#0.
       HJ%2<#0.
```

```
      HJ%3<#0.
      CT#0.
      DO 150 J=1,2
      Q1=QQ(J)
      A1=AA(J)
      JJ=J+1
      DO 150 L=JJ,3
      Q2=QQ(L)
      A2=AA(L)
      M=J+L-2
      IF%Q1<150,150,21
   21 CONTINUE
      IF%Q2<150,150,25
   25 CONTINUE
      BN#ALOG%%A2*Q1</%A1*Q2<</%A2-A1<
      IF%BN<100,100,115
  115 CONTINUE
      BN#BN&BN/2.0
      K#0
  400 CONTINUE
      A#EXP%-BN*A1<*Q2
      B#EXP%-BN*A2<*Q1
      C#Q1-B
      D#Q2-A
      E#B*A2
      F#A*A1
      BNP1#BN-%C-D</%E-F<
      K#K&1
      DIFF#%BNP1-BN</BN
      IF%ABS%DIFF<-EPI<700,700,500
  500 CONTINUE
      IF%K-20<600,600,100
  600 CONTINUE
      BN#BNP1
      GO TO 400
  700 CONTINUE
```

```
      IF%BN< 100,100,109
  100 CONTINUE
      HI%M<#BN
      GO TO 150
  109 CONTINUE
      CT#CT&1.0
      HH=(Q2*D3)/(DLAM(I)*AO)
      BETA#BNP1
      HI(M)=BETA
      ALPHA# 1.0-EXP%-BNP1*A2<
      HJ(M)=(HH*BETA)/ALPHA
      IF%CF%I<<1001,1000,1001
1001  CONTINUE
      HJ(M)=HJ(M)/CF(I)
1000  CONTINUE
  150 CONTINUE
      HJT=0.0
      HIT=0.0
      DO 1100 J=1,3
      IF%HI%J<<1100,1100,1200
 1200 CONTINUE
      HJT=HJT+HJ(J)
      HIT=HIT+HI(J)
 1100 CONTINUE
      IF%CT<1300,1300,1400
 1400 CONTINUE
      AB%I<#HIT/CT
      AJ%I<#HJT/CT
 1300 CONTINUE
      WRITE%3,5300< HAM%I<,DLAM%I<,AB%I<,AJ%I<,QQ,HI,HJ
      WRITE%2,3< HAM%I<,AB%I<,AJ%I<
5300  FORMAT%1H ,3F8.4,F11.4,6F8.4,3F11.4<
   20 CONTINUE
      PP#0.0
      DO 29 M#1,84
      IF%AB%M<<179,29,179
```

```
  179 CONTINUE
      P#3.14159*AJ%M</AB%M<
      IF%M-1<73,74,73
   74 P#P*%HAM%M&1<-HAM%M<</2.
      GO TO 60
   73 IF%M-84< 1002,75,1002
   75 P#P*%HAM%M<-HAM%M-1<</2.
      GO TO 60
 1002 P#P*%HAM%M&1<-HAM%M-1<</2.
   60 PP#PP&P*.0001
   29 CONTINUE
      WRITE(3,5400) PP
5400  FORMAT%/,2X,4H PP#,F14.4<
      GO TO 200
      END
```

```
C       MONOCHROMATIC FLUX CALCULATION FROM CYLINDRICAL FLAMES
        DIMENSION AZ%82<,AW%82<,AJ%82<,AB%82<,CFR%82<,COSS%18<,COM%18<,
       1CFI%18<,CT%18<,DX%4<,CHC%82<
        WRITE%3,10<
        READ%1,179< %CHC%I<,I#1,82<
        READ%1,179<%CFR%I<,I#1,82<
  179 FORMAT%7F10.4<
  297 CONTINUE
        READ%1,199< %AZ%I<,AB%I<,AJ%I<,I#1,82<
  199 FORMAT%3F10.4<
   44 FORMAT%10F7.5<
        WRITE%3,7< %AZ%I<,AJ%I<,AB%I<,CFR%I<,CHC%I<,I#1,82<
  200 READ%1,6< DI,B
        N#2
        DI#DI*2.54
        B#B*2.54
        HL#12.7
        HU#B-HL
   99 FORMAT%I2<
        B#HU&HL
        WRITE %3,5< %B,DI,HL<
        R#DI/2.
        PI#3.141593
        PI2#PI/2.
        RR#R/3.
        WRITE %3,4<
        DX%1<#196.85
        DX%2<#270.50
        DX%3<#390.52
        DO 21 LL#1,3
        D#DX%LL<
        XPP#0.
        XRP#0.
        DO 29 L#1,N
        IF%L-1<80,80,90
   80 H#HU
```

```
      GO TO 81
   90 H#HL
   81 HM#H/6.
      FD#D&R
      I#0
      DO 22 J#1,6
      XJ#J
      FJ#%XJ-.5<*HM
      E2#FD*FD&FJ*FJ
      FI#ATAN%FJ/FD<
      DO 22 K#1,3
      XK#K
      FK#R-%XK-.5<*RR
      SI#ATAN%FK/SQRT%E2<<
      FIMN#ATAN%FJ/SQRT%FD*FD&FK*FK<<
      SOM#RR*HM*COS%SI<*COS%FI</%E2&FK*FK<
      SINB#FK/SQRT%FD*FD&FK*FK<
      SING#FD*SINB/R
      T#2.0*R*SQRT%1.-SING*SING</COS%FIMN<
      COSE#FD/SQRT%E2&FK*FK<
      I#I&1
      COM%I<#SOM
      CFI%I<#FI
      CT%I<#T
      COSS%I<#COSE
   22 CONTINUE
      PP#0.0
      RP#0.0
      DO 23 M#1,82
      P#0.0
      IF%AB%M<<60,60,61
   61 DO 24 I#1,18
   24 P#P&%COM%I<&COM%I<<*%AJ%M</AB%M<<*%1.0-EXP%-AB%M<*CT%I<<<*COSS%I<
      IF%CHC%M<<71,72,71
   71 CONTINUE
   72 IF%M-1<73,74,73
```

```
 74 P#P*%AZ%M&1<-AZ%M<</2.
    GO TO 60
 73 IF%M-82<1002,75,1002
 75 P#P*%AZ%M<-AZ%M-1<</2.
    GO TO 60
1002 P#P*%AZ%M&1<-AZ%M-1<</2.
 60 PP#PP&P*.0001
    RP#P*.0001*CFR%M<&RP
 23 CONTINUE
    XPP#XPP&PP
    XRP#XRP&RP
 29 CONTINUE
    WRITE %3,2< D,XPP,XRP
 21 CONTINUE
 10 FORMAT %1H1,4X,5H WAVE,7X,13H VOL EMISSION,3X,10H VOL EXTIN,
   15X,7H CORREC,6X,11H ABS.CORREC/3X,7H LENGTH,9X,6H  COEF,10X,
   25H COEF,8X,7H FACTOR,7X,7H FACTOR<
  9 FORMAT %10F7.4<
  8 FORMAT %10F7.1<
  7 FORMAT%/,2X,F5.3,10X,F11.3,4X,F7.5,6X,F7.6,7X,F6.4<
  6 FORMAT%2F7.3<
  5 FORMAT %1H1,2X,10H MEAN HT.#,F6.2,6X,9H MEAN D.#,F6.2,6X,4H RH#,
   1F6.2<
  4 FORMAT %//,3X,9H DISTANCE,14X,5H FLUX,15X,12H TRANS. FLUX<
  3 FORMAT %13,I2<
  2 FORMAT%/,5X,F5.1,12X,E14.8,8X,E14.8<
  1 FORMAT %10F7.6<
    GO TO 200
    END
```